A NON-CANONICAL ROLE OF ANGIOTENSIN-CONVERTING ENZYME IN SYNAPTIC PLASTICITY

A DISSERTATION
SUBMITTED TO THE FACULTY OF
UNIVERSITY OF MINNESOTA
BY

BRIAN HONG TRIEU

IN PARTIAL FULFILLMENT OF THE REQUIREMENTS
FOR THE DEGREE OF
DOCTOR OF PHILOSOPHY

ADIVSOR: PATRICK E. ROTHWELL

JUNE 2022

Acknowledgements

I would like to thank my adviser, Dr. Patrick Rothwell. We took a chance on each other, and I couldn't have wished for a better mentor, lab environment, and graduate experience. None of this work would be possible without you. I'll admit that I never thought my project was going to work since the start of the rotation until sometime in the middle - maybe that's normal, but your genuine commitment to science, teaching, mentorship, and constant enthusiasm helped me be more "cautiously optimistic" balanced with a healthy dose of skepticism, and ultimately helped me become the best scientist I could've hoped to be. You always answered my questions and entertained my ideas, no matter how silly they were. I am forever grateful for your support and for showing me what a conscientious scientist acts like.

Thank you to my thesis committee: Dr. Alfonso Araque, Dr. Suma Jacob, Dr. Esther Krook-Magnuson, and Dr. Swati More. Your guidance and support kept my PhD on track, helped me make the right decisions, and challenged me as a scientist. You're right, taking another year was quite worth it.

Thank you to the GPN and MSTP. These programs have made me feel like I belong. Thank you Dr. Yoji Shimizu for being the most incredible MSTP director. I am truly appreciative of your constant support.

Thank you to the Rothwell lab family, past and present, who certainly kept me sane throughout those bad patch days/weeks/months and the "It won't be *that* bad" mass spec experiments, which there was a lot of. Your scientific support, impromptu happy hours, and fun lab moments kept me going. Those 10 weeks of revision experiments was an absolute hurricane and I'm forever indebted to everyone. Thank you for being patient with me as I took up way more room than I needed and broke (but eventually fixed) almost everything in lab. Thank you Emilia and Cassie for letting me use your rigs when one just wasn't enough, I literally could not have finished this PhD without them.

Thank you to my GPN 2017 cohort and MSTP 2015 cohort. You all made Minnesota a home and I will forever cherish the friendships we've forged and the memories we've shared. I will sincerely miss how you've all let me be the biggest nerd possible and miss your company at the

state fair, breweries, Autumn Beer Review, D&D nights/Sundays, movie nights, boardgame nights, brewing sessions, pity parties, restaurant weeks, potluck nights, etc…

Thank you to Yingchun in the CCRB mass spectrometry lab. I never thought I'd be doing anything related to mass spec and it was wonderful learning this technique. Thank you to Manny and Anna who've helped me troubleshoot so many patch-related problems in the early days and who are always a welcoming source of information.

Last, but certainly not least, the biggest thank you to Thi, who has endlessly supported me and been a foundation for all my pursuits and ambitions. Thank you for putting up with all the past, current, and future craziness that comes with me being a "forever" student. Thank you to my family - Mom, Dad, Lynn, Justin, Oscar, and Tai - for your never-ending unconditional support and love. I love you all. Thank you to my friends back home - Sean, Scott, Dennis, Darrin, Rob, Ralph, and Lorenzo - who don't always know what I'm doing but nonetheless love and support me, and *always* keeps the group chat entertaining. Thank you to Turner and Stephanie who has enabled me to love [brewing] beer more than ever and who have been the most welcoming and productive soundboard ever, especially in the early days during our pandemic bubble.

I am grateful for funding support from UMN's MnDRIVE initiative and NIH grants and F30DA049476 and T32DA007234.

Dedication

To those who've helped me keep my head on straight, I promise I'm almost done.

Abstract

A diverse repertoire of endogenous opioid peptides are found within the brain, but because they are often co-expressed and co-released with other peptides, their role in synaptic plasticity remains elusive. These neuropeptides can have profound control over synaptic transmission upon binding to opioid receptors, particularly within the nucleus accumbens where converging signals are integrated to drive motivated behaviors. Neuropeptide effects are often terminated by extracellular degradation, but the mechanisms underlying this are also poorly understood. The identification of specific endogenous opioid peptides and insight into their extracellular regulation can reveal under-appreciated mechanisms that influence opioid receptor signaling to modulate the elaborate neuronal connectivity within this region. The studies presented in this dissertation show that an unconventional and potent endogenous opioid called Met-Enkephalin-Arg-Phe ("MERF"), an enkephalin heptapeptide, dose-dependently inhibited excitatory synaptic transmission onto medium spiny neurons (MSNs) in mouse brain slices. Angiotensin-converting enzyme (ACE) classically regulates blood pressure in the periphery and was found to non-canonically degrade endogenous MERF thereby regulating its effect in the nucleus accumbens. Liquid chromatography-tandem mass spectrometry analysis showed that a class of cardiovascular medications called ACE inhibitors selectively preserved extracellular MERF without affecting conventional enkephalins. ACE inhibitors alone unveiled cell type-specific depression of glutamate release onto MSNs expressing the Drd1 dopamine receptor (D1-MSNs), but not onto those expressing the Drd2 receptor (D2-MSNs). Glutamatergic synaptic depression was mediated by MERF binding to presynaptic μ-opioid receptors and was absent after conditional genetic deletion of ACE. Fiber photometry recordings of D1-MSNs *in vivo* demonstrated decreased sensitivity to optogenetic stimulation of excitatory medial prefrontal cortex following systemic administration of the ACE inhibitor captopril. Furthermore, mice given captopril displayed attenuated fentanyl-induced place preference and increased social behavior with other mice. Collectively, this dissertation defines an endogenous mechanism of synaptic plasticity induced by MERF and gated by ACE. We interpret this to be preclinical evidence for a class of safe and efficacious cardiovascular medications that could be repositioned or redesigned to mitigate brain conditions with underlying aberrant striatal pathophysiology characterized by an imbalance of D1- to D2-MSN synaptic activity.

Table of Contents

List of Tables

List of Figures

Chapter 3: Met-Enkephalin-Arg-Phe ("MERF") inhibits excitatory synaptic transmission

Chapter 4: Inhibition of angiotensin-converting enzyme boosts endogenous "MERF"

Chapter 5: Discussion, Future Directions, and Impact

List of Abbreviations

ACE - angiotensin-converting enzyme

APN - aminopeptidase N

D1-MSN - medium spiny neurons expressing the dopamine type-1 receptor

D2-MSN - medium spiny neurons expressing the dopamine type-2 receptor

DLS - dorsolateral striatum

DMS - dorsomedial striatum

DOR - δ-opioid receptor

EPSC - excitatory postsynaptic current

GPCR - G-protein coupled receptor

KOR - κ-opioid receptor

mEPSC - miniature excitatory postsynaptic current

MERF - Met-Enkephalin-Arg-Phe

MOR - μ-opioid receptor

mPFC - medial prefrontal cortex

NAc - nucleus accumbens

NEP - neprilysin

VTA - ventral tegmental area

Chapter 1: Introduction

The Nucleus Accumbens and Disease

Broadly, the basal ganglia consist of multiple nuclei that to connect to drive movement, motivation, decision-making, reward perception, goal-oriented behaviors, and habit formation [1-4]. As a framework it can be simplified into different, but related, circuits referred to as limbic, associative, or motor loops that drive different aspects of behavior. Pertinent differences within these loops relevant to this dissertation include the striatum which can be segregated into the dorsal and ventral aspects. The dorsal striatum in humans consists of the caudate nucleus and putamen which in rodents correspond to the dorsomedial striatum (DMS) and dorsolateral striatum (DLS), respectively. The ventral striatum consists of the nucleus accumbens (NAc) and olfactory tubercle in both humans and rodents. The "ascending spiral" [5] is a longstanding hypothesis which unites the basal ganglia loops and proposes that different stages of motivation and decision-making, and thus behavior, moves from the limbic to associative to motor loops (i.e. NAc to DMS to DLS) [6-8].

The striatum is anatomically unique in the brain in its cellular composition, afferent input, and efferent projections. The entire striatum consists of GABAergic medium spiny projection neurons (MSNs) and make up 95% of the total neuronal population. These MSNs can be further categorized into those expressing the Drd1 dopamine type-1 receptor (D1-MSN) or the Drd2 dopamine type-2 receptor (D2-MSN) [9]. Additionally, they can be differentiated based on neuropeptide expression with D1-MSNs expressing substance P and dynorphin and D2-MSNs expressing enkephalin. The remaining 5% of neurons consist of a variety of GABAergic and cholinergic interneurons. Although this cellular framework has been useful, it is quickly becoming apparent through high-resolution molecular analysis that there exists significant heterogeneity [10-13] and the functional implication of this remains a crucial area of study.

The dorsal striatum receives inputs from several cortical regions and thalamus, and dopaminergic inputs from midbrain nuclei [14]. Efferent projections from MSNs are often referred to as the "direct" pathway and "indirect" pathway and these projections often correspond to D1-MSNs and D2-MSNs, respectively. Dorsal striatal D1-MSNs project back to the midbrain toward basal ganglia output nuclei while D2-MSNs indirectly project to basal ganglia output nuclei via the globus pallidus.

Although the NAc resides in the broader striatum with somewhat similar cellular architecture to dorsal striatum, increasing evidence of distinct differences have challenged the notion that findings in the dorsal striatum can be assumed to be similar in the NAc. In contrast to

the dorsal striatum, the NAc receives a greater diversity of inputs from cortex, thalamus, hypothalamus, amygdala, hippocampus, pallidum, dorsal raphe, olfactory areas, and ventral tegmental area (VTA) [15,16]. Unlike the dorsal striatum where D1-MSNs and D2-MSNs have been synonymous with the direct and indirect pathway, respectively, NAc D1-MSNs have the expected "direct" projections to the VTA but also have projections to the ventral pallidum where "indirect" NAc D2-MSNs also project [17-19]. Differences between dorsal striatum and NAc have also been identified by spatial molecular markers, such as the presence or absence of μ-opioid receptors that define the "patch" and "matrix" found in the dorsal striatum [20]. Additional spatial analyses have identified distinctions within subregions of the NAc which are often compartmentalized into the core and the adjacent shell or along the rostral-caudal axis [21-23]. Beyond molecular boundaries, these subregions also display differences in afferent innervation [15,24] or synaptic mechanisms [25-27]. How these subregions contribute to behavior remains a large area of research.

Given its integrative role in reward and motivation, it is no surprise that the NAc has been implicated in several neuropsychiatric diseases. For instance, the effects of addiction of been found at the genetic, molecular, and cellular level within the NAc [28-39] which in turn affects the overall basal ganglia circuitry and manifests as the devastating symptoms and behaviors observed in people afflicted by this disease [40-43]. Several brain conditions including but not limited to: depression [44-52], chronic pain [53-55], obesity [56-60], and autism spectrum disorder [61-68] have also been linked to disruptions in striatal function. While the pathogenesis of these diseases affects several parts of the brain, the feed-forward nature of the basal ganglia and the integration of several afferents into the striatum make it an appealing target for therapeutics. However, our understanding of how exactly striatal activity affects behavior is continually evolving, thus complicating the endeavor to create novel therapeutics that target underlying striatal disruptions.

It is hypothesized that a dichotomy between D1- and D2-MSNs drives motivated behavior wherein D1-MSNs initiates or reinforces behavior while D2-MSNs opposes [69-74]. Dopamine released into the striatum from midbrain afferents bind to D1 or D2 receptors resulting in increased cellular activity in D1-MSNs or decreased activity in D2-MSNs which impact downstream nuclei [75]. Increasing evidence now suggests that D1- and D2-MSNs function in concert to produce behavior [76-82]. These paradigm shifts have highlighted the importance of understanding how D1-MSNs change relative to D2-MSNs following disease progression. Indeed, the last couple decades of addiction research have exemplified the need to identify cell type-specific differences which has been made possible using transgenic mice [25,44,62,83,84]. Several lines of evidence have supported hyperactive D1-MSN activity relative to D2-MSN activity, or other cell type-specific alterations,

as an underlying hallmark of addiction pathogenesis which may be susceptible to approaches that counter such changes [25,30,32,35,36,44,85-90]. Thus, hypothesizing that novel therapeutics aimed at restoring D1- to D2-MSN balance to reverse addiction pathophysiology is quite compelling.

The Endogenous Opioid System

The endogenous opioid system is widespread throughout the brain and is comprised of a multitude of opioid peptides and several receptors. The classical opioid receptors consist of μ- (MOR), δ- (DOR), and κ- (KOR) opioid receptors and are activated by families of peptides called endorphins, enkephalins, and dynorphins. More recently the nociceptin (orphanin FQ) peptide receptor and its ligand (nociceptin or orphanin FQ) have been of interest and is described as an opioid-like receptor [91,92]. The effects of opioid receptor activation are quite complex, particularly within the reward circuitry where ligands and receptors are broadly distributed and overlapping [93]. For instance, in addition to being a site of afferent integration, the striatum is also a region of dense MOR, DOR, and KOR expression as well as enkephalin and dynorphin expression. Genetic or pharmacological activation or inhibition of receptor subtypes throughout the basal ganglia or regionally within the striatum result in a myriad of behavioral phenotypes. Collectively, this enormous literature has supported a general framework for the role of opioid receptors in the reward circuitry: MOR activation is often associated with hedonic experience and euphoric states, DOR activation associated with anxiolytic properties and positive affective states, and KOR activation associated with dysphoria and negative affective states [94-96]. Indeed, insight into the substantial effects of opioid receptor activation can be demonstrated by the use of opium and morphine throughout history for analgesia and more recently the impact of synthetic opioid agonists on addiction [97,98].

Given the profound effects of opioid receptors on behavior, a greater understanding of endogenous opioid cellular physiology is needed. Opioid receptors are G-protein coupled receptors (GPCRs) and, when activated by a ligand, initiate signaling cascades mediated by the inhibitory $G_{i/o}$ pathway. Generally, downstream molecular effectors result in inhibition of adenyl cyclase which reduces cAMP production and inhibits PKA, inhibition of voltage-gated calcium channels, activation of G-protein gated inwardly rectifying potassium channels (GIRKs), and alteration of SNARE protein function to reduce neurotransmitter release [99-105]. Effects of receptor activation are further complicated by work demonstrating co-expression or heterodimerization of opioid receptor subtypes within neurons suggesting additional intricacies in regulating cellular activity [94,106-110].

Opioid signaling has long been shown to directly block synaptic transmission and plasticity throughout the brain making them powerful regulators of circuit activity [111-116].

The confluence of synaptic inputs and opioid receptor subtypes in the striatum suggest a region that is highly plastic to reflect the continual integration of diverse experience-dependent signals needed for behavioral adaptation; as such this region is highly sensitive to endogenous opioid disturbances caused by disease. Electrophysiology studies have been critical in understanding the diverse mechanisms underlying opioid-mediated synaptic plasticity in this region [117]. Work in the dorsal striatum by Brady Atwood and colleagues have demonstrated the nuances that delineate each receptor subtype and uncovered potential interactions with other synaptic mechanisms such as endocannabinoid-mediated plasticity [118]. Furthermore, MOR activation mediates long-term depression on specific presynaptic glutamatergic terminals that is dependent on striatal subregion [119-121]. While presynaptic activation of opioid receptors is a common mechanism, the type of presynaptic terminal can vary as is the case for KOR activation which produces differential effects that are afferent-specific as well as MSN cell type-specific [122], or DOR activation in dorsal striatum which can disinhibit D1-MSNs [27]. How these forms of opioid-dependent plasticity interact with GABA-mediated [123], endocannabinoid-mediated [124-129], or other forms of GPCR-mediated plasticity [130-133] in the NAc is unclear.

In order to activate opioid receptors, endogenous ligands must first be released. It is thought that the molecular processes involved in the exocytosis of neuropeptides into the synaptic cleft are inherently different compared to fast neurotransmitters like glutamate or GABA [134-136]. One major distinction is that neuropeptides are packaged into dense-core vesicles and require prolonged neuronal depolarization for their release [137,138]. This may be expressed as rapid and persistent action potentials arriving at the presynaptic terminal and has been recapitulated *in vitro* to varying extents using a combination of pharmacology and electrical stimulation [115,118,139-143]. More recently, cell type-specific optogenetic stimulation have been used to induce neuropeptide release *in vitro* and *in vivo* [144-146]. A major advantage of optogenetics is the circumvention of non-specific local stimulation which allows for better controlled mechanistic studies [147]. However, a remaining caveat remains in that individual cell types can co-express neuropeptides and co-release have been demonstrated [148-150]. This is especially true in the striatum where D1-MSNs can release several different dynorphin opioid peptides and substance P, and D2-MSNs can release several different enkephalin opioid peptides.

In general, endogenous opioid peptide ligands are categorized into three classical families called endorphins, enkephalins, and dynorphins, which originate from precursor peptides referred

to as POMC, proenkephalin, prodynorphin, respectively. Once processed, these opioid peptides bind with differing affinities to MOR, DOR, and KOR opioid receptors. Canonically, endorphins bind to MORs, enkephalins bind to DORs and somewhat less effectively to MORs, and dynorphins bind to KORs. However, decades of research have identified numerous subspecies of opioid peptides within these families [151]. Currently, there is a plethora of endogenous opioid peptides with a spectrum of binding affinities and potencies across opioid receptor subtypes.

While the presence of several ligands for opioid receptors can be interpreted as a form of molecular redundancy, this is likely not the case. Synthetic receptor ligands have demonstrated unique differences in downstream signal transduction often referred to as "biased agonism", such as the extent of G-protein activation or negative regulation by β-arrestin [152-154], and these intricacies have extended to endogenous peptide ligands as well [155-157]. Accentuating this complexity is the enkephalin peptide YGGFMRF (aka Met-Enkephalin-Arg-Phe or "MERF"). This heptapeptide contains two additional amino acids at the C-terminal which distinguishes it from the conventional Met-enkephalin peptide. It also appears to have high binding affinity to DOR and MOR (similar to conventional enkephalins) but additionally has high binding affinity to KORs similar to conventional dynorphins [151,158-160]. MERF has been found to be a powerful opioid receptor agonist with potential to regulate opioid-dependent circuits to influence nociception [161-163]. However, this contrasts with the overall sentiment that MERF functions most commonly as a precursor to Met-enkephalin, and thus a form of molecular redundancy.

The notion that MERF functions mainly as a precursor is sensical given that changes in biological activity because of enzymatic cleavage is common in the opioid peptide family. Indeed, all endogenous peptides are derived from a primary precursor and sometimes subsequent truncations of an opioid peptide are also biologically functional such as the κ-agonist Dynorphin A (1-17) which can be enzymatically cleaved into (1-13), (1-9), (1-8), (1-7), (1-6), and finally Leu-enkephalin - all have differing affinity at KORs [151,158,164,165]. While the various forms of peptides could also be precursors, this is unlikely given differential downstream signal transduction cascades once the various ligands bind to their receptor [155-157]. Similar to Dynorphin, it is unclear if MERF is indeed a precursor or if it itself participates in physiologically important mechanisms. This highlights the role of the several peptidase enzymes that exist to cleave specific amino acid motifs resulting in peptide activation or degradation. How these peptidases regulate synaptic function, or how they modulate neural circuits and thus behavior is largely unknown.

Several peptidases that target conventional Met-enkephalin (YGGFM or Tyr^1-Gly^2-Gly^3-Phe^4-Met^5) and Leu-enkephalin (YGGFL or Tyr^1-Gly^2-Gly^3-Phe^4-Leu^5) have been identified,

including specific sites of enzymatic cleavage [166,167]. Aminopeptidase N (APN) cleaves the Tyr^1-Gly^2 bond while Neprilysin cleaves the Gly^3-Phe^4 site in Met- and Leu-enkephalin. Interestingly, Angiotensin-Converting Enzyme (ACE) has also been proposed to cleave the Gly^3-Phe^4 bond, but also the Met^5-Arg^6 bond in MERF, thus participating as a degrader of Met-enkephalin as well as a paradoxical activator of Met-enkephalin (i.e. a degrader of MERF). However, the catalytic rate at the Met^5-Arg^6 bond is significantly higher than that of the Gly^3-Phe^4 bond [168] suggesting that there could be a difference in the physiological roles of Neprilysin and ACE, which may be the case in at least the amygdala [139] and a few small reports [169-175].

Angiotensin-Converting Enzyme (ACE)

ACE is a zinc-dependent dipeptidyl carboxypeptidase[1] and it is most known for its role in cleaving angiotensin I peptide into angiotensin II peptide which then binds to angiotensin II type I receptors (AT1R) in various organs to ultimately increase blood pressure. Teprotide was discovered in the 1960's from the venom of the *Bothrops Jararaca* pit viper and was found to be a potent inhibitor of ACE; this would eventually lead to a revolutionary medical discovery. This peptide was transformed into a medication called captopril and was the first in its class of ACE inhibitors. Since captopril's FDA approval in 1981 (as Capoten), there have been 15 newer ACE inhibitors[2] which are used for the treatment and prevention of hypertension, heart failure, nephropathy, and other cardiovascular and renal diseases. Since captopril, subsequent generations improve on its potency and efficacy with some being structurally unique. Collectively, their widespread use for several cardiovascular and renal diseases emphasizes its safety and utility as a medical tool [176-178].

In contrast to the seminal literature which focuses on ACE expression in the lungs, kidney, heart, blood vessels, and other peripheral organs [179,180], ACE was also found in the brain [181-186]. Radioligand and immunohistochemical studies showed high expression in the choroid plexus leading to the hypothesis that ACE participates in the maintenance of the blood-brain barrier due to its peptidase activity. Interestingly, ACE was also shown to have significant expression in the striatum and the role of this peptidase within this region is unclear. Similar to other peptidases, it was thought that ACE's enzymatic specificity was not limited to a singular substrate (i.e.

[1] Synonyms for ACE include: EC 3.4.15.1, CD143, peptidyl-dipeptidase A, Kininase II, Carboxycathepsin

[2] FDA-approved ACE inhibitors (www.fda.gov): Captopril (1981, Capoten), Enalapril/Enalaprilat (1984, Vasotec), Lisinopril (1987, Zestril and Prinivil), Benazepril (1991, Lotensin), Fosinopril (1991, Monopril), Quinapril (1991, Accupril), Ramipril (1991, Altace), Perindopril (1993, Aceon), Moexipril (1995, Univasc), Trandolapril (1996, Mavik). Other inhibitors used internationally: Cilazapril, Delapril, Imidapril, Spirapril, Temocapril, Zofenopril

angiotensin I). In agreement with this, ACE has been shown to cleave other peptides including but not limited to: Met-enkephalin, MERF, angiotensin 1-7, neurotensins, bradykinins, neurokinins, substance P, Ac-SDKP, HHL, GnRH, and amyloid-β [187-192]. However, several of these findings were made in the context of reduced *in vitro* preparations and presents a significant caveat when considering the role of ACE under physiological conditions. For example, there are several conflicting results regarding substance P degradation by ACE [193-195]. Furthermore, the potential enzymatic redundancy between ACE and Neprilysin at the Gly^3-Phe^4 site may be attributed to non-physiological conditions. Thus, it is entirely possible that ACE may have higher affinity toward specific substrates under physiological conditions.

Elucidating these mechanisms are particularly pertinent in the striatum where several endogenous opioid peptides and opioid receptors are expressed. Modulating neuropeptide longevity by altering how they are regulated extracellularly could have profound cellular effects that ultimately impact behavior. Indeed, this approach has been under investigation for the purposes of conferring analgesic effects for pain [196-201] without the clinical side effects and molecular adaptations induced by exogenous opioid agonists like morphine, oxycodone, or fentanyl [153,154,202-204]. Underlying this premise is the notion that within the repertoire of endogenous ligands there exists unique features, such as distinct signal transduction cascades, that can reveal novel cellular processes to inform therapeutic development.

Thus, there is an intriguing gap in our knowledge on how non-canonical neuropeptides may participate in synaptic transmission, how neuropeptides are regulated in the extracellular space, and how these mechanisms can impact synaptic plasticity to affect behavior and disease. This dissertation will examine the role of MERF in the nucleus accumbens and test the hypothesis that endogenous mechanisms of synaptic regulation can be leveraged to induce synaptic plasticity. Chapter 2 describes the methods used throughout this dissertation which integrates pharmacological and genetic manipulations across techniques of electrophysiology, mass spectrometry, and behavior. Chapter 3 explores the impact of exogenous Met-Enkephalin-Arg-Phe ("MERF") on synaptic transmission within the nucleus accumbens. Chapter 4 investigates how peptidase inhibitors can be used to reveal mechanisms that can gate synaptic plasticity. Finally, Chapter 5 discusses the broader context of these findings, highlights remaining questions of interest, and speculates on the potential impact of this work.

Chapter 2: Methods

This chapter contains work that was adapted with permission from the following article: Trieu et al., Science, 2022 [205]. Here, I describe the genetic, biochemical, molecular, electrophysiological, and behavioral approaches used to investigate the mechanisms underlying endogenous opioid peptide regulation and its role in regulating accumbal synaptic transmission and plasticity.

Subjects

All experiments were performed using comparable numbers of both female and male mice [206], at 5 to 12 weeks of age. For electrophysiology experiments, we crossed two BAC transgenic reporter lines: Drd1-tdTomato [84] (The Jackson Laboratory, stock #016204) and Drd2-eGFP [83] (Mutant Mouse Resource & Research Centers #036931-UCD). Hemizygous offspring used for experiments expressed tdTomato in D1-MSNs and/or eGFP in D2-MSNs (figure 3-1). Constitutive *Penk* knockout mice [207] (The Jackson Laboratory, stock #002880) were generated by crossing $Penk^{+/-}$ parents. Mice expressing channelrhodopsin-2 in D2-MSNs (figure 4-5) were generated by crossing homozygous Ai32 mice [208] (The Jackson Laboratory, stock #024109) with hemizygous Adora2a-Cre BAC transgenic mice [209] (KG139; Mutant Mouse Resource & Research Centers #036158-UCD). Floxed *Ace* mice [210] (Mutant Mouse Resource & Research Centers #043853-UNC) were crossed with Drd1-Cre BAC transgenic mice [211] (FK150; Mutant Mouse Resource & Research Centers #029178-UCD). To generate $Ace^{fl/fl}$ and $Ace^{wt/wt}$ littermates carrying Drd1-Cre for these experiments (figure 3-9), we crossed parents that were $Ace^{fl/wt}$, with one parent hemizygous for Drd1-Cre. Constitutive *Oprm1* knockout mice [212] (The Jackson Laboratory, stock #007559) were crossed with the Drd1-tdTomato reporter line. To generate $Oprm1^{-/-}$ and $Oprm1^{+/+}$ littermates for these experiments (figure 3-12), we crossed parents that were $Oprm1^{+/-}$, with one parent hemizygous for Drd1-tdTomato. All genetically modified strains were maintained on a C57BL/6J genetic background, and wildtype C57BL/6J mice were used for LC-MS/MS and behavior experiments except when noted otherwise. Experimental procedures were conducted between 0900h – 1700h. Mice were housed in groups of 2-5 per cage, on a 12 hour light cycle (0600h – 1800h) at ~23ºC with food and water provided ad libitum. All procedures conformed to the National Institutes of Health Guidelines for the Care and Use of Laboratory Animals, and were approved by the Institutional Animal Care and Use Committee at the University of Minnesota.

Electrophysiology

Mice were deeply anesthetized with isoflurane and perfused with 10 mL ice-cold sucrose cutting solution containing (in mM): 228 sucrose, 26 $NaHCO_3$, 11 glucose, 2.5 KCl, 1 NaH_2PO_4-H_2O, 7 $MgSO_4$-$7H_2O$, 0.5 $CaCl_2$-$2H_2O$. Mice were subsequently decapitated and brains were quickly removed then placed in ice-cold sucrose cutting solution. Coronal slices (240 µm thick) containing nucleus accumbens (NAc) or anterior cingulate cortex were collected using a vibratome (Leica VT1000S) and allowed to recover submerged in a holding chamber with artificial cerebral spinal fluid (aCSF) containing (in mM): 119 NaCl, 26 $NaHCO_3$, 11 glucose, 2.5 KCl, 1 NaH_2PO_4-H2O, 2.5 $CaCl_2$-$2H_2O$, 1.3 $MgSO_4$-$7H_2O$. Slices recovered in warm aCSF (33ºC) for 15 min and then equilibrated to room temperature for at least one hour before use. Slices were transferred to a submerged recording chamber and continuously perfused with aCSF at a rate of 2 mL/min at room temperature. All solutions were continuously oxygenated (95% O_2/5% CO_2).

Whole-cell voltage-clamp recordings from MSNs in the NAc core were obtained under visual control using IR-DIC optics from an Olympus BX51W1 microscope. D1-MSNs were distinguished from D2-MSNs by the expression of tdTomato or eGFP, respectively, and held at -70 mV. A subset of experiments (figure 3-9) used eYFP expression to distinguish D1-MSNs following transfection by AAVDJ-EF1a-DIO-eYFP. A subset of experiments (figure 4-7) measured responses from layer V pyramidal neurons in anterior cingulate cortex which were identified by resting membrane potential, capacitance, membrane resistance, and visual size, and held at -50 mV. Borosilicate glass electrodes (3-5 MΩ) were filled with (in mM): 120 $CsMeSO_4$, 15 CsCl, 10 TEA-Cl, 8 NaCl, 10 HEPES, 5 QX-314, 4 ATP-Mg, 1 EGTA, 0.3 GTP-Na (pH 7.2-7.3). Excitatory synaptic transmission was pharmacologically isolated using $GABA_A$ receptor antagonist picrotoxin (50 µM, Tocris). Excitatory postsynaptic currents (EPSC) were electrically evoked locally using bipolar stimulating electrodes (ISO-flex, AMPI) at 0.05 Hz. Miniature EPSCs (mEPSC) were obtained in the presence of tetrodotoxin (500 nM, Fischer Scientific) to block spontaneous activity. At least 200 events per treatment (e.g. "baseline") was acquired across 18 sec sweeps, filtered at 0.5 kHz, and detected using an amplitude threshold of 6 pA and a signal-to-noise ratio threshold of 4 standard deviations.

For current clamp recordings, borosilicate glass electrodes (3-5 MΩ) were filled with (in mM): 120 K-Gluconate, 20 KCl, 10 HEPES, 0.2 EGTA, 2 $MgCl_2$, 4 ATP-Mg, 0.3 GTP-Na (pH 7.2-7.3). Cells were injected with a series of current steps (0.5 sec duration) from 0 to +160 pA in 40 pA increments. Maximum firing rate was calculated as the average maximum firing rate over the 0.5 sec step that could be sustained without inducing a depolarization block, and multiplied by a factor of 2 to calculate Hz. Maximum firing rate was calculated in each cell before and after bath

application of each drug; captopril (10 μM), threshold MERF (100 nM), supra-threshold MERF (1 μM) and captopril + threshold MERF. All recordings were performed using a MultiClamp 700B (Molecular Devices), filtered at 2 kHz, and digitized at 10 kHz. Data acquisition and analysis were performed online using Axograph software. Series resistance was monitored continuously and experiments were discarded if resistance changed by >20%.

Drugs

Electrophysiology experiments used: captopril (Cayman Chemical) at 10 μM [118]; trandolaprilat (Cayman Chemical) at 1 μM; Met-enkephalin acetate salt (Bachem) at 0.01-10 μM [118]; Met-Enkephalin-Arg-Phe ("MERF", Bachem) at 0.01-10 μM; valsartan (BioVision) at 2-20 μM [213-216]; angiotensin I trifluoroacetate salt (Bachem) at 1 μM; naloxone hydrochloride dihydrate (Millipore Sigma) at 10 μM [115]; bestatin (Millipore Sigma) at 10 μM [115,118]; DL-thiorphan (Millipore Sigma) at 1 μM [118]; SDM25N hydrochloride (Tocris) at 500 nM [140,217]; nor-Binaltorphimine dihydrochloride ("norBNI", Tocris) at 100 nM [122,218]; and CTAP (Tocris) at 1 μM [112,115,118,120,219-223]. Standards for LC-MS/MS were purchased from Bachem and included: Met-enkephalin acetate salt, Leu-enkephalin acetate salt, Met-Enkephalin-Arg-Phe, Met-Enkephalin-Arg-Gly-Leu, Dynorphin A (1-8) acetate salt, Dynorphin B trifluoroacetate salt, Substance P acetate salt, Angiotensin II acetate salt, and Bradykinin acetate salt. Behavioral experiments used captopril (30 mg/kg i.p.), fentanyl (0.04 mg/kg s.c., Fagron), trandolapril (5 mg/kg s.c., Cayman Chemical) and sterile saline (5 mL/kg i.p. or s.c.).

Liquid Chromatography-Tandem Mass Spectrometry (LC-MS/MS)

Coronal slices (300 μm thick) were individually submerged in 100 μL aCSF ± peptidase inhibitors. Slices from wildtype mice were stimulated with KCl (50 mM) for 20 min. Slices from mice expressing channelrhodopsin-2 in D2-MSNs and their wildtype littermates lacking channelrhodopsin-2 were optogenetically stimulated for 10 min (470 nM, 20 Hz, 5 ms pulse width, ~40 mW light power at the tip). The extracellular fluid was collected after stimulation and samples were immediately stored at -80ºC. Samples underwent a modified desalting protocol [224] with C18-material stage tips (SP301, Thermo Scientific), was eluted with 200 μL solvent (40:60:0.1% water:acetonitrile:trifluoroacetic acid) and dried via speed vacuum overnight. Samples were reconstituted in 12 μL solvent (98:2:0.1% water:acetonitrile:formic acid).

Desalted concentrated samples underwent targeted proteomic identification and quantification based on selected reaction monitoring (SRM) and liquid chromatography-tandem mass spectrometry [225]. Samples (5 μL) were injected onto a home-packaged analytical C18 reverse

phase column (Phenomenex, Torrance, CA) and subsequently eluted with buffer A (0.1% FA in water) and buffer B (0.1% FA in ACN) with the following gradient profile: 0 – 5 min 2% buffer B flow rate at 1 µL/min; 5 – 5.5 min 2% B at 1 – 0.3 µL/min; 5.5 – 25 min 2 – 35% B at 0.3 µL/min; 25 – 26 min 35 – 90% B at 0.3 – 1 µL/min; 26 –29 min 90% B at 1 µL/min; 29 – 30 min 90 – 2% B at 1 µL/min; 30 – 35 min 2% B at 1 µL/min. Mass spectrometry detection was obtained on a TSQ Quantiva Triple Quadrupole (Thermo Scientific) in positive nanospray ionization mode. Mass spectrometry conditions were: spray voltage 2.0 kV, ion transfer tube temperature 350 °C, collision energy 4 – 29.2 V, and collision gas (argon) pressure 1 mTorr. Resolution settings were 0.7 Da (full width at half-maximum) for both quadrupoles and transition dwell times were 15 ms. Standards for absolute peptide quantification (10 pm, 50 pm, 100 pm, 500 pm, 1 nm, 5 nm, 10 nm) were injected after experimental samples and contained: Met-enkephalin, Leu-enkephalin, Met-Enkephalin-Arg-Phe (MERF), Met-Enkephalin-Arg-Gly-Leu (MERGL), Dynorphin A (1-8), Dynorphin B, Substance P, Angiotensin II, and Bradykinin. Although MERGL was included in the standards and detected reliably with comparable sensitivity, this peptide was not detected in experimental samples.

Skyline (MacCoss Lab) was used to empirically determine SRM transitions for all peptide standards and quantitative data processing. SRM transitions corresponding to the five largest integrated peaks were selected for targeted proteomic analysis and precursor / product transitions with the largest peak area was used for absolute peptide quantification as derived from calibration curves: Met-enkephalin (574.2330 / 278.1135), Leu-enkephalin (556.2766 / 278.1135), MERF (439.2049 / 714.3392), MERGL (450.7235 / 737.3763), Dynorphin A (1-8) (327.8591 / 409.7534), Dynorphin B (524.2999 / 627.3487), Substance P (674.3713 / 600.3378), Angiotensin II (523.7745 / 263.1390), Bradykinin (354.1944 / 419.2401). Peaks were manually inspected to ensure correct detection and integration for each peptide per sample.

Behavior

Place Conditioning: As previously described [44], activity test chambers (Med Associates, 11 x 11 x 11 in.) consisted of a single compartment with two types of removable floor tiles: transparent plastic with a rough texture and black plastic with a smooth texture. A five-day protocol was used which included a 20 min baseline session on day 1 that included both contexts; three conditioning days consisting of one 30 min saline (5 mL/kg s.c.) conditioning session in the morning (AM) paired to one context and one 30 min vehicle + fentanyl (0.04 mg/kg s.c.), captopril (30 mg/kg i.p.) + fentanyl, captopril, or vehicle conditioning session paired to the other context in the afternoon (PM); and finally a 20 min test session on day 5 containing both contexts.

Conditioning sessions were at least three hours apart. Captopril or vehicle was given 30 min and fentanyl was given 5 min prior to placement in activity chambers on conditioning days. Wildtype C57BL/6J mice were tested at 6 to 10 weeks of age and randomly assigned to either the control, captopril + fentanyl, or captopril group. All mice habituated to the procedure room for one hour prior to placement in activity chambers. Based on baseline preference as measured by time spent in either contexts, animals were assigned to either a smooth black or rough transparent context for saline and the opposite context for vehicle + fentanyl, captopril + fentanyl, captopril, or vehicle so that the group average baseline preference was approximately 50%. Individuals with a baseline preference greater than 75% for any one context was excluded. The total ambulatory distance in each activity chamber was recorded with Med Associates software during all tests and conditioning sessions. For experiments with trandolapril, trandolapril (5 mg/kg s.c.) or vehicle (3% DMSO in saline) was given once daily for 7 days prior to the first fentanyl exposure. On conditioning days for PM sessions, fentanyl was given normally and trandolapril or vehicle was given 45 min prior to placement in activity chambers.

Social Interaction Test: Evaluation of social interaction was performed as previously described [226]. All experiments were conducted at 60-70 luminosity, and at temperature conditions equal to those of the animal housing facility. Experimental sessions were video recorded and social interaction was hand scored by researchers blind to experimental conditions. Wildtype C57BL/6J mice were moved to an isolated testing room 1 hour before tests. Mice were tested at 6 to 8 weeks of age in an opaque white rectangular box with 1 cm of fresh corn cob bedding on the floor for 10 min. Both mice were novel social partners, age- and sex-matched, were not siblings or cage mates, and were both given either captopril (30 mg/kg i.p.) or vehicle. Video recordings of social behaviors exhibited by mice were hand scored by a blinded experimenter using Button Box 5.0 (Behavioral Research Solutions, LLC). Social behaviors were categorized into one of the following groups [227]: nose-nose interaction (direct investigation of orofacial region), huddling (stationary sitting next to partner), social exploration (anogenital investigation, social sniffing outside of orofacial region, social grooming), and following. The sum of these social behaviors was used for total "Interaction Time".

Fiber Photometry

Surgical Procedures: Drd1-Cre mice were anesthetized under ketamine/xylazine conditions (100/10 mg/kg) and surgical procedures were performed using a stereotaxic alignment system (Kopf Instruments, Tujunga, CA, USA). AAV9-FLEX-hSyn-jGCaMP8m (Addgene plasmid #162378; a gift from GENIE project) and AAVDJ-hSyn-ChrimsonR (Addgene plasmid

#59171; a gift from Ed Boyden) were infused unilaterally (500 nL at 100 nL/min) into the medial prefrontal cortex (AP: +1.65 mm, ML: -0.5 mm, DV: −2.4 from bregma) and nucleus accumbens core (10º from center, AP: +1.4 mm, ML: -1.5 mm, DV: −4.0 from bregma) regions, respectively. After infusion, the needle was left in place to allow for adequate viral diffusion, then gradually retracted. A 400 µm fiberoptic ferrule (Doric Lenses: MFC_400/430-0.48_6mm_MF1.25_FLT) was implanted unilaterally 0.05 mm above the targeted coordinates for viral infusions. Implants were secured to the skull with jeweler's screws and dual-cure resin (Geristore).

Data collection: Calcium changes in D1-MSNs were measured using a Tucker Davis Technologies RZ5P Fiber Photometry Processing System [228,229]. The RZ5P interfaced with an LED driver (ThorLabs) to modulate 470 (calcium-dependent) and 405 nm (isosbestic) LEDs at 531 and 211 Hz carrier frequencies, respectively, which was passed through a fluorescence minicube (Doric Lenses) and coupled to a fiber optic patch cord (400 µm, 0.48 NA, Doric Lenses) connected to the implanted fiberoptic ferrule. LED intensity at the distal end of the patch cord was a maintained within a range of 1.8-2.5 mW and emitted fluorescence was transmitted by dichroic and focused onto a photoreceiver (Newport, DC low mode). Animals received a session comprised of 2 phases: 1) saline injection followed 30 mins later by evoked recordings; and 2) captopril injection followed by 30 mins later by evoked recordings. For evoked recordings, a Master-8 (A.M.P.I.) was used to drive a 595 nm LED to generate 2, 10, and 40 pulses at 20 Hz to stimulate mPFC terminals in NAc, while simultaneously recording the response of jGCaMP8m.

Data Analysis: Recorded signals were saved for offline analysis using MATLAB. Changes in fluorescence, measured as dF/F, were calculated during saline and captopril conditions separately. First, a low-pass filter was applied, then the 405 nm calcium-independent signal was fit to the 470 nm calcium-dependent signal and dF/F was calculated as ([470 nm signal − fitted 405 nm signal] / [fitted 405 nm signal]). To correct for potential photobleaching, the 8th percentile value was subtracted over a 20-second rolling window over our signal. Stimulation onsets were transmitted to the RZ5P using TTL pulses from a MedAssociates System to drive the 595 nm LED. Data were grouped by pulse number (2, 10, or 40) and condition (saline, captopril) for averaging. Peak dF/F values were calculated as a 500 msec average of the evoked signal centered around 2.21 seconds for 2 pulses, 2.54 seconds for 10 pulses, and 3.28 seconds for 40 pulses. The peak response amplitude at each pulse number was used to construct an input-output curve for each mouse following injection of saline or captopril. We then quantified percent change in the slope of this optogenetic input-output curve following injection of captopril, relative to injection of saline.

RT-qPCR

Quantitative RT-PCR was performed on tissue punches containing the dorsal and ventral striatum, as previously described [228]. Tissue was snap frozen on dry ice and stored at -80°C. RNA was extracted and isolated using the RNeasy Mini Kit (Qiagen) according to manufacturer instructions. A NanoDrop One microvolume spectrophotometer (Thermo Fisher Scientific, Waltham, MA) was used to measure RNA concentration and verify that samples had A260/A280 purity ratio ≥ 2. Reverse transcription was performed using Superscript III (Invitrogen, Eugene, OR). For each sample, duplicate cDNA reactions and subsequent qPCR reactions were conducted in tandem on both samples. Mouse β-actin mRNA was used as the endogenous control to measure differences in expression of ACE mRNA. Primer sequences for detection of ACE mRNA were forward 5'-GCCTCCCAAGGAATTAGAAGAG-3' and reverse 5'-TGATGTACTCGGACCCATAGT-3'. Quantitative RT-PCR using SYBR green (BioRad, Hercules, CA) was carried out with a Lightcycler 480 II (Roche, Basel, Switzerland) using the following cycle parameters: 1 x (30 sec @ 95°C), 35 x (5 sec @ 95°C followed by 30 sec @ 60°C). Results were analyzed by comparing the C(t) values of the treatments tested using the ΔΔC(t) method. Expression values of target genes were first normalized to the expression value of β-actin. The mean of cDNA replicate reactions was used to quantify the relative target gene expression.

RNAscope

Fluorescent *in situ* hybridization via the RNAscope platform was performed as previously described [229]. Briefly, brains were collected from transgenic mice generated from a cross of Ai32 with Adora2a-Cre mice to generate genetically expressed channelrhodopsin-2 fused with eYFP within A2a-containing neurons. Brains were then frozen rapidly on dry ice in OCT embedding medium and stored at -80ºC until sectioning. Sections (10 µm thick) were collected at -20ºC using a cryostat (Leica CM3050s), placed immediately on positively charged glass slides, and stored at -80ºC until RNAscope assay was run. Protocols and reagents were provided by Advanced Cell Diagnostics (ACD) and used to conduct the RNAscope assay. Slides were post-fixed in 4% PFA for 15 min at 4ºC followed by ethanol dehydration by serial incubations of increasing concentrations of ethanol (50% > 70% > 100%) for 5 min each at room temperature (RT). Slides were left to air dry and a hydrophobic barrier was painted around the sections that would be used in the RNAscope assay. The provided protease IV was applied to applicable sections and let to sit for 30 min at RT. Slides were washed quickly twice in 1x PBS followed by application of hybridizing probes (eyfp 312131, drd1 406491-C2, drd2 406501-C3) to sections and incubated at 40ºC for 2 hours and then washed twice in RNAscope wash buffer for 2 min each. The following

steps were a series of amplification steps with provided AMP1-4 detection reagents. The reagents were applied sequentially and incubated for 15-30 min each at 40ºC as instructed with 1X RNAscope wash buffer washes between each reagent. After the final wash, mounting medium (Invitrogen Prolong Gold antifade reagent with DAPI) was applied before coverslips were placed on the slides. Images were taken at 40x using a Keyence fluorescence microscope. Images were imported into ImageJ software, overlaid, and hand-counted to determine the percent colocalization of Drd2 with eYFP-positive cells.

Immunohistochemistry

Transgenic mice expressing D1-tdTomato and D2-eGFP were deeply anesthetized using Beuthanasia (200 mg/kg, i.p.) and transcardially perfused with ice cold PBS followed by ice cold 4% paraformaldehyde in PBS. Brains were extracted and post-fixed overnight in 4% paraformaldehyde. Sagittal sections were collected bilaterally at 50 µm thickness between approximately 0.70 mm and 1.00 mm from the midline. Nonspecific binding was blocked with a solution containing 2% normal horse serum in PBS with 0.05% Tween-20 and 0.2% Triton-X100 for 1 hour at room temperature, followed by 48 hours in rabbit anti-ACE1 (Invitrogen, PA5-111652) diluted 1:500 in the same blocking solution at 4ºC. Sections were rinsed three times in PBS containing 0.1% Tween-20, then transferred to goat anti-rabbit IgG Alexa 647 (Invitrogen, A32733) diluted 1:1000 in blocking solution for 24 hours. Sections were rinsed three times in PBS with 0.1% Tween-20, mounted from PBS and coverslipped using ProLong Antifade mountant (Invitrogen, P36930).

Stained tissue sections were imaged on a laser-scanning confocal microscope (model TCS SPE, Leica Microsystems). The majority of MSN somata expressed variable abundance of ACE as immunoreactive puncta. We therefore applied a stringent threshold criterion to quantify the percentage of D1- and D2-MSNs with robust ACE expression; the cutoff value of 5 ACE immunoreactive puncta was used to define an MSN as ACE-immunoreactive. Cells containing fewer ACE puncta were qualified as ACE-negative. Three images of the nucleus accumbens core were collected from each of 5 sections at 40x and separate channels for tdTomato (D1-MSNs), eGFP (D2-MSNs), and Alexa 647 (ACE) were saved. These images were imported into ImageJ software, overlaid, and the cell counter plugin was used to quantify ACE-immunoreactive somata. Separate labels were used to count ACE-immunoreactive D1-MSNs and ACE-immunoreactive D2-MSNs and the percentage.

Evaluating ACE expression in published works

Three datasets (Table S1) were surveyed for ACE expression in D1- and D2-MSNs. Processed data were downloaded from DropViz.org [13] and GEO: GSE13776 [230] and GSE118020 [10]. Log-normalized expression of ACE gene in well-defined D1 and D2 populations were extracted and compared using default Wilcox tank-order test (R, v 4.1.0) to test the null hypothesis that ACE expression in D1-MSNs is not greater than that in D2-MSNs. P-values are reported in Table S1.

Statistical Analysis and Data Presentation

Female and male mice were used in all experiments, and sex was included as a variable in factorial ANOVA models analyzed using IBM SPSS Statistics v24 or GraphPad Prism 8. Significant interactions provided strong evidence that the effect of one variable depended on the level of another variable [231], and were decomposed by analyzing simple effects (i.e., the effect of one variable at each level of the other variable). Significant main effects were further analyzed using Fisher's LSD post-hoc tests. The Type I error rate was set to $\alpha=0.05$ (two-tailed) for all comparisons. In the figures, significant ANOVA effects and follow-up tests are denoted by black asterisks that indicate $*P<0.05$, $**P<0.01$, $***P<0.001$, $****P<0.0001$. All data are presented mean ± s.e.m., with open and closed circles indicating data points from female and male mice, respectively. Complete statistical information can be found in Appendix A.

Chapter 3: Met-Enkephalin-Arg-Phe ("MERF") inhibits excitatory synaptic transmission

This chapter contains work that was adapted with permission from the following article: Trieu et al., Science, 2022 [205].

Introduction

Enkephalin in the literature often refers to the conventional Met-enkephalin (amino acids YGGFM) and Leu-enkephalin (amino acids YGGFL) opioid peptides, and significant effort has been made to understand their biological properties and physiological roles. However, like dynorphin opioid peptides, there exists other enkephalins that have biological activity at opioid receptors. This includes the less studied Met-Enkephalin-Arg-Phe ("MERF", amino acids YGGFMRF), which is also produced from the proenkephalin polypeptide precursor. As the name implies, this peptide consists of Met-enkephalin plus amino acids RF at the C-terminus. Similar to Met- and Leu-enkephalin, MERF exhibits analgesic properties by activating opioid receptors [161-163]. While a potent agonist at MOR and DOR, MERF surprisingly binds to KOR with an affinity comparable to dynorphins [151,158-160]. Interestingly, investigations into the properties of MERF declined throughout the 1980's and its physiological properties have largely been unexplored. This could be due to its relative scarcity since the sequence for Met-enkephalin is present at four other sites within the proenkephalin polypeptide [232-235] and MERF itself is rapidly cleaved by ACE [168,170-175] suggesting that while MERF has biological activity, it may instead function as a precursor to Met-enkephalin. Despite this, the biological properties of MERF remain intriguing, and contrary to the assumption that it exists primarily as a precursor, the mechanisms regulating MERF may instead suggest a latent physiological role that remains to be examined. Therefore, this chapter discusses the impact of exogenous MERF application on excitatory synaptic transmission and following inhibition of its extracellular degradation within the NAc core.

Results

3.1 Effects of Exogenous MERF

Whole-cell recordings in voltage-clamp mode were taken from NAc core of transgenic mice expressing tdTomato or eGFP fluorescent protein in D1- or D2-MSNs, respectively, to investigate potential differences between cell types (figure 3-1). Miniature excitatory postsynaptic currents (mEPSCs) were measured in the presence of increasing concentrations of exogenously

applied MERF (10 nM, 100 nM, 1 μM, 10 μM) to form a dose-response curve for changes in mEPSC frequency and amplitude (figure 3-2). In both cell types, MERF dose-dependently decreased mEPSC frequency with minor alterations in amplitude which suggested a reduction of presynaptic glutamate release more so than postsynaptic effects. These findings were similar to exogenously applied Met-enkephalin (figure 3-3), however the potency of MERF (IC_{50} = 438 nm) was slightly higher than Met-enkephalin (IC_{50} = 993 nm).

Furthermore, exogenous application of 10 μM MERF robustly depressed electrically evoked excitatory postsynaptic currents (EPSCs) in D1- and D2-MSNs (figure 3-4 A-B) similar to previously published work using Met-enkephalin [118]. This depression was present at a lower concentration of MERF (1 μM) and was blocked by naloxone, a non-specific opioid receptor antagonist (figure 3-4 C-D). Perhaps not surprisingly, EPSC amplitude remained depressed during MERF application when recording from mice with constitutive deletion of MOR ($Oprm1^{-/-}$, figure 3-4 E-H), suggesting that relatively high concentrations of exogenous MERF may activate several opioid receptors to inhibit presynaptic glutamate release in accord with its strong affinity towards MOR, DOR, and KOR. Interestingly, MOR deletion had a greater effect on attenuating MERF-induced depression in D1-MSNs compared to wildtypes; this may suggest differential potency dependent on the specific receptor being activated and cell type recorded from, which is a hypothesis explored below (see Section 3.3, page 20).

Changes in paired-pulse ratio (PPR) can suggest alterations in vesicle release dynamics, for instance an increase in PPR in the context of depressed synaptic transmission is associated with a decrease in presynaptic release probability [129,236,237]. Thus, PPR is helpful in establishing the locus of synaptic change. However, it is often a variable measurement and requires a relatively large sample size to detect an effect if present. Demonstrating this, PPR tended to increase following 1 μM and 10 μM MERF application but only reached statistical significance when samples were pooled (figure 3-5 A). Due to variability in PPR measurements, additional evidence is often useful to support whether synaptic depression is expressed pre- or postsynaptically. To address this, spontaneous EPSCs were measured for ten seconds following electrical stimulation before and after 10 μM MERF application. A reduction in frequency was observed in agreement with the mEPSC and PPR findings that suggested MERF reduces presynaptic probability of glutamate release (figure 3-5 B-E).

3.2 Effects of Exogenous MERF in the Presence of an ACE Inhibitor

Once neuropeptides are release into the extracellular space, their actions on cognate receptors are terminated by degradation via enzymatic cleavage from peptidases. ACE has previously been identified as a peptidase with binding affinity towards MERF and while it is present in the striatum, it is unclear what physiological role it participates in. Intriguingly, work by Stephen Strittmatter and colleagues [181,184] observed ACE expression in the direct pathway (i.e. D1-MSNs) of the striatum in immunohistochemistry experiments and autoradiographic experiments using Captopril[3], a tritiated ACE inhibitor. We observed similar enriched expression in D1-MSNs compared to D2-MSNs using immunohistochemistry (figure 3-6) which aligns with previously published RNA sequencing datasets (table 3-1).

Thus, if MERF is negatively regulated by ACE via degradation, then it is reasonable to hypothesize that MERF can induce D1-MSN-specific effects under conditions that accentuate the difference in ACE expression between D1- and D2-MSNs, such as when ACE is inhibited. Because MERF depressed mEPSC frequency (figure 3.2) and electrically evoked EPSC amplitude (figure 3-4) in D1- and D2-MSNs to comparable levels at relatively high exogenous concentrations (1 - 10 μM), it is likely a lower concentration is required to reveal ACE-dependent regulation. Accordingly, a threshold concentration of MERF (100 nM) which had produced minimal effects on mEPSC frequency (figure 3-2) was used to test the hypothesis that ACE inhibition would enhance the potency of MERF in a cell type-specific manner. Under these conditions, 100 nM MERF application or ACE inhibition with 10 μM captopril separately did not alter mEPSC frequency or amplitude (figure 3-7). The latter finding with captopril is not surprising considering mEPSCs are recorded in the presence of tetrodotoxin to block action potentials, and prolonged terminal depolarization is often required to trigger neuropeptide release [137,138]. In contrast, combined 10 μM captopril and 100 nM MERF synergistically and potently depressed mEPSC frequency without affecting amplitude. This effect was notably absent in D2-MSNs.

The effect on synaptic transmission from combined ACE inhibition and MERF (100 nM) is particularly interesting because ACE inhibitors are usually combined with other peptidase inhibitors [112,115,118,139,166,199] and used as a pharmacological tool to study canonical enkephalins instead of MERF. As a carboxypeptidase, ACE is known to cleave 2 amino acids at the C-terminal of select substrates and the hypothesized cleavage site for MERF was at the Met^5-Arg^6 bond and the Gly^3-Phe^4 bond for Met- and Leu-enkephalin. The latter cleavage site is also cleaved by neprilysin (historically called "enkephalinase") and the Tyr^1-Gly^2 bond at the N-terminal is cleaved by Aminopeptidase N (APN). To test if synaptic depression by MERF can be modulated by these

other peptidases, baseline mEPSCs were recorded from D1- and D2-MSNs with consecutive infusions of the neprilysin inhibitor thiorphan (1 μM) plus the APN inhibitor bestatin (10 μM), followed by the addition of 100 nM MERF, which was then finally replaced by 100 nM Met-enkephalin (figure 3-8 A). Like captopril, mEPSC frequency or amplitude was not affected by bestatin or thiorphan, nor were they affected by the addition of 100 nM MERF. Instead, a threshold concentration of Met-enkephalin (100 nM) synergized with combined APN and neprilysin inhibition to reduce mEPSC frequency in D1- and D2-MSNs (figure 3-8 B-E). Three conclusions can now be drawn: 1) MERF is not regulated by APN or neprilysin despite being similar to Met-enkephalin, 2) Met-enkephalin is regulated by APN and neprilysin, and 3) inhibiting Met-enkephalin degradation impacts both MSN cell types while inhibiting MERF degradation with captopril affects only D1-MSNs.

3.3 MERF Signaling Mechanisms

A significant caveat of pharmacological experiments lies in a compound's specificity towards its target. Captopril is the prototypical ACE inhibitor for its class and was developed from the venom of the *Bothrops Jararaca* Brazilian pit viper; as such, captopril can mediate off-target effects independent of ACE inhibition [238]. To test if ACE is necessary to produce the synaptic effects following combined captopril and MERF application, we crossed mice that were both $Ace^{fl/wt}$ with one parent hemizygous for Drd1-Cre to produce control ($ACE^{wt/wt}$; Drd1-Cre) and conditional ACE knockout mice ($Ace^{fl/fl}$; Drd1-Cre) (figure 3-9 A, top). Knockout mice had significantly reduced ACE mRNA compared to wildtype controls (figure 3-9 B). We then injected AAVDJ-EF1a-DIO-eYFP into the NAc of these mice to visualize D1-MSNs for whole-cell recordings (figure 3-9 A, bottom). Under these conditions, excitatory mEPSC frequency was depressed following combined 10 μM captopril and 100 nM MERF application in control mice but the effect was significantly attenuated in $ACE^{fl/fl}$ mice (figure 3-9 C-H). This demonstrated the necessity of ACE expression in D1-MSNs and the sufficiency of captopril to induce a MERF-dependent effect.

As alluded to previously, the effect of MERF on synaptic transmission may be difficult to interpret considering its high affinity toward MOR, DOR, and KOR [151,158-160] and the relatively high concentration when applied exogenously (figures 3-2 and 3-4). However, captopril combined with nominal MERF (figure 3-7) allowed us to test what specific opioid receptor subtype is necessary for MERF-mediated inhibition of presynaptic glutamate release in D1-MSNs. Pretreatment of the MOR antagonist CTAP (1 μM) completely abolished the effect of combined captopril and 100 nM

MERF (figure 3-10) while the DOR antagonist SDM25N (500 nM) or the KOR antagonist NOR-BNI (100 nM) had no effect. Importantly, the concentrations of SDM25N and NOR-BNI used were effective at blocking opioid receptor activation by subtype-specific agonists (figure 3-11). To confirm the role of MOR, we tested the effect of combined captopril and MERF in constitutive MOR knockout mice ($Oprm1^{-/-}$) and wildtype littermates ($Oprm1^{+/+}$) (figure 3-12 A). Similar to the receptor antagonist manipulations, a reduction in excitatory mEPSC frequency in D1-MSNs following the application of synergistic captopril and threshold MERF was absent in $Oprm1^{-/-}$ mice but remained present in wildtype controls (figure 3-12 B-G). This is particularly striking considering that canonical enkephalins are often viewed primarily as endogenous DOR agonists.

Thus far, the focus has been on how MERF alters synaptic transmission at the presynaptic glutamatergic terminal. The findings that demonstrate MOR activation as the mediator of this change also highlight the observation that MOR is expressed postsynaptically by most D1-MSNs and fewer D2-MSNs [27,239]. Therefore, we tested if MERF can alter action potential firing via current-clamp recordings. MERF (1 μM) decreased action potential firing with increasing current steps in D1-MSNs, but not D2-MSNs, while 100 nM MERF had no effect compared to baseline in either cell types (figure 3-13). However, in combination with 10 μM captopril, 100 nM MERF was then able to decrease action potential firing in D1-MSN, but not D2-MSNs. These findings are reminiscent of the previously described voltage-clamp recordings in that supra-threshold concentrations of MERF can elicit synaptic changes while ACE inhibition by captopril can unveil cell type-specific effects that may more closely reflect endogenous concentrations of MERF under physiological conditions. Next, chapter 4 will explore how ACE inhibition can modulate endogenous MERF signaling to alter synaptic plasticity and murine behavior.

Table 3-1

Study	Species	Region	RNA Sequencing Method	ACE mRNA Expression	p-value
Saunders et al., 2018 (dropviz.org)	Mouse	Dorsal Striatum	Single Cell	D1 > D2	2.2e-16
Savell et al., 2020	Rat	Nucleus Accumbens	Single Nucleus	D1 > D2	5.9e-5
Chen et al., 2021	Mouse	Nucleus Accumbens	Single Cell	D1 > D2	2.1e-2

Table 3-1. ACE mRNA expression is enriched in D1-MSNs. Analysis of three published RNA sequencing studies that measured ACE mRNA expression in D1-MSNs and D2-MNS. All three data sets indicated ACE mRNA expression is greater in D1-MSNs; p-value come from a Wilcoxon rank-order test of the null hypothesis that ACE expression in D1-MSNs is not greater than that in D2-MSNs.

Figure 3-1

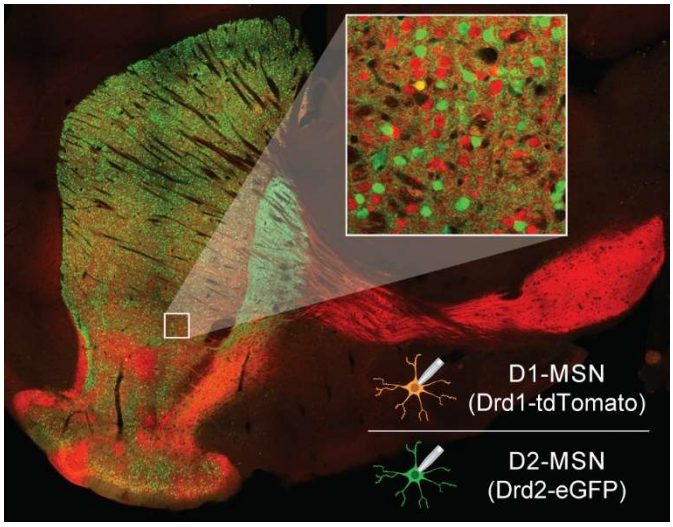

Figure 3-1. Immunohistochemical labeling of D1-MSNs and D2-MSNs in striatum. Mouse coronal section containing Drd1-tdTomato expression (red) in D1-MSNs and Drd2-eGFP expression (green) in D2-MSNs. All electrophysiology recordings, unless otherwise noted, were made in the nucleus accumbens core.

Figure 3-2

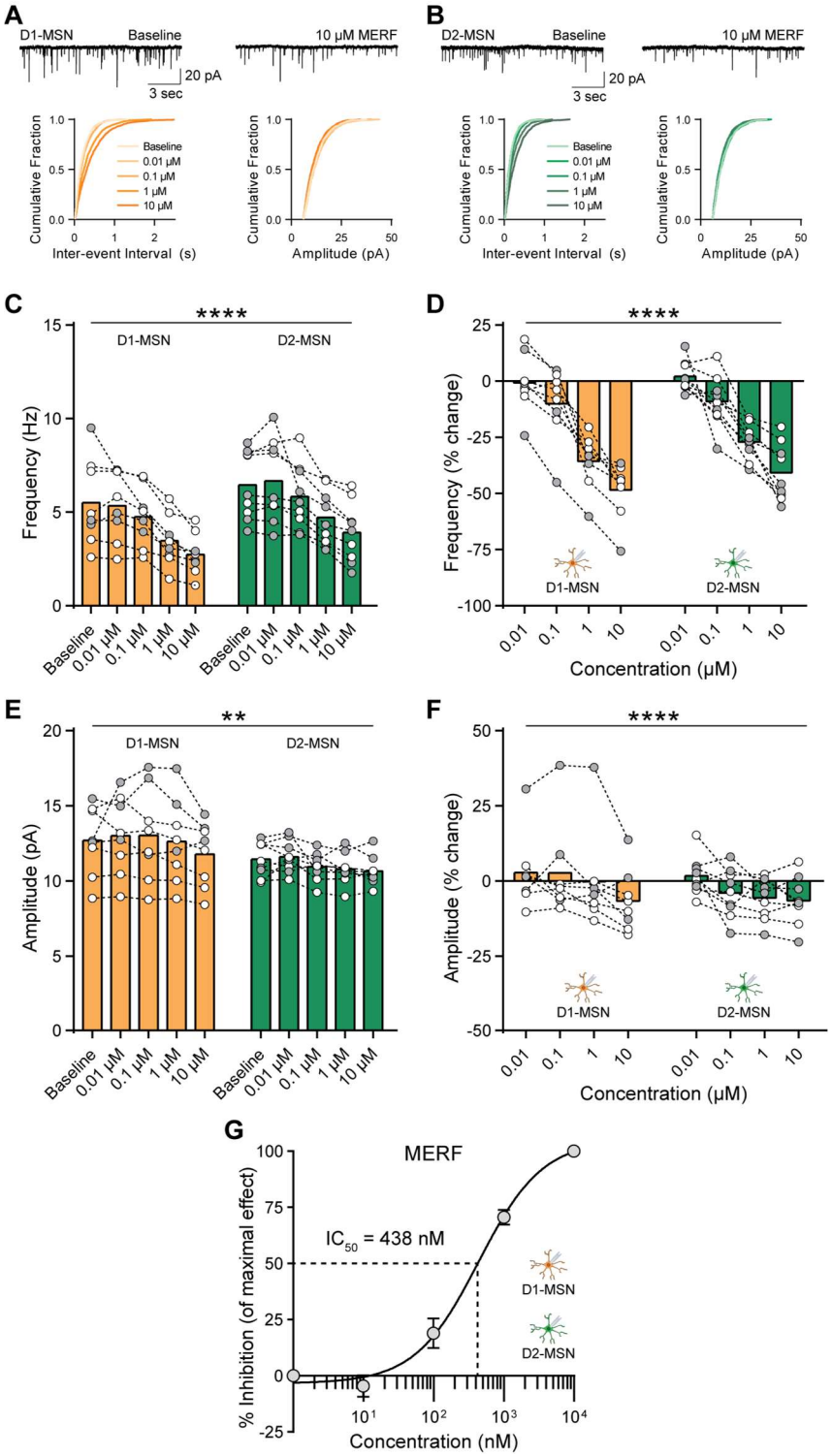
A
D1-MSN
Baseline
10 μM MERF
20 pA
3 sec
Cumulative Fraction
Baseline
0.01 μM
0.1 μM
1 μM
10 μM
Inter-event Interval (s)
Amplitude (pA)
B
D2-MSN
C
****
Frequency (Hz)
D
Frequency (% change)
Concentration (μM)
E
**
Amplitude (pA)
F
Amplitude (% change)
G
MERF
IC50 = 438 nM
% Inhibition (of maximal effect)
Concentration (nM)

Figure 3-2. Dose-dependent changes from exogenous MERF application. (**A, B**) Top, mEPSC traces from D1-MSNs (A) or D2-MSNs (B) before (left) and after (right) bath perfusion of MERF (10 μM). Bottom, cumulative fraction plots of mEPSCs from D1-MSNs (A) or D2-MSNs (B) for inter-event interval (left) and amplitude (right) at increasing MERF concentrations (0.01 - 10 μM). (**C, D**) MERF caused a dose-dependent decrease in mEPSC frequency in D1-MSNs (left, orange, *n*=8) and D2-MSNs (right, green, *n*=9) expressed as raw frequency (C) or percent change of baseline (D). (**E, F**) MERF did not cause a dose-dependent change in mEPSC amplitude in D1-MSNs (left, orange, *n*=8) or D2-MSNs (right, green, *n*=9) expressed as raw amplitude (E) or percent change of baseline (F). (**G**) Sigmoidal interpolation of MERF dose-response normalized to maximal frequency change at 10 μM (IC_{50}: 438 nM, 95% CI: 279 - 690 nM, *n*=17). Data are mean ± s.e.m. for all panels; open and closed circles indicate recordings from female and male mice, respectively. ***P*<0.01, *****P*<0.0001, ANOVA concentration main effect (C, D, E); see Appendix A for complete statistics.

Figure 3-3

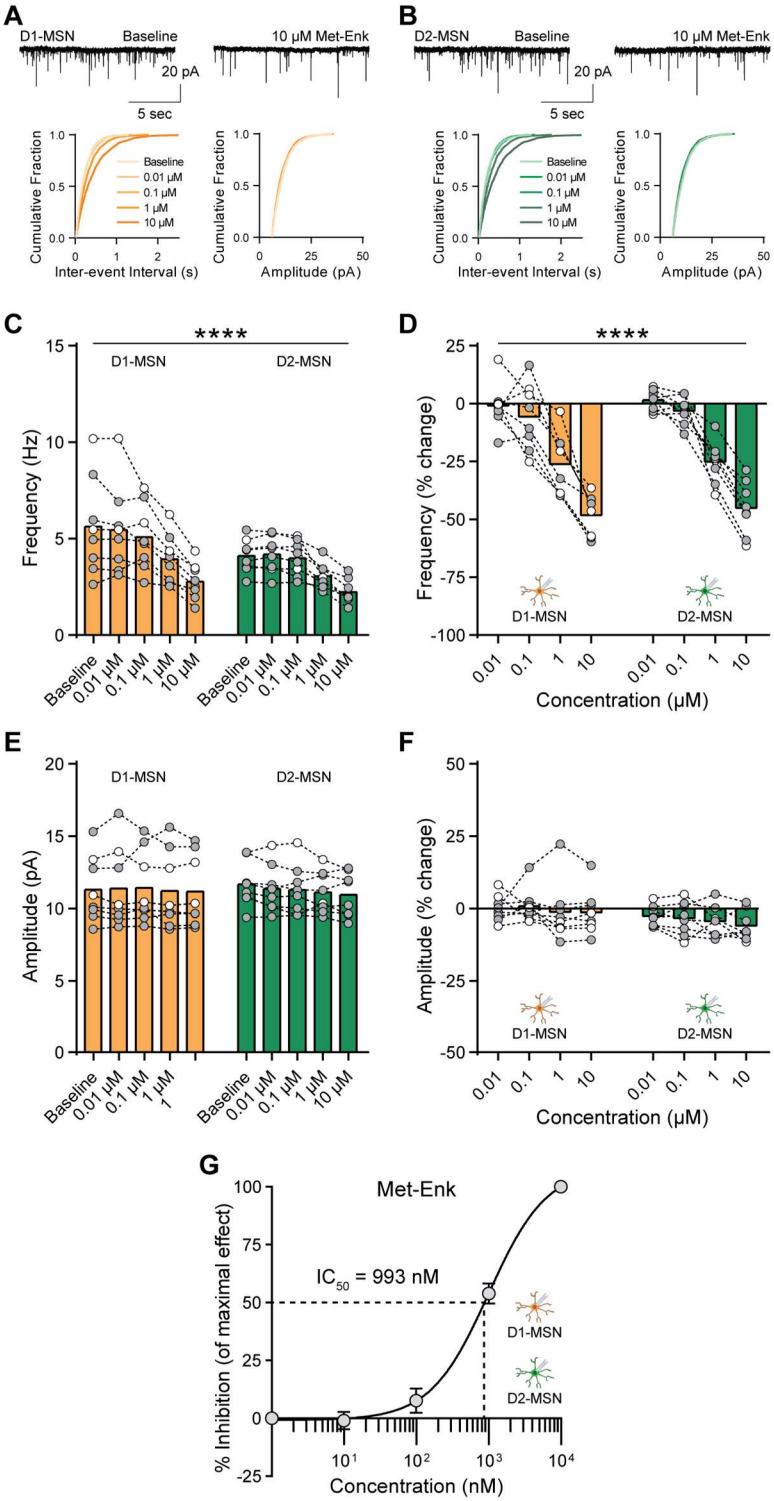
A
D1-MSN
Baseline
10 μM Met-Enk
20 pA
5 sec
Cumulative Fraction
Baseline
0.01 μM
0.1 μM
1 μM
10 μM
Inter-event Interval (s)
Amplitude (pA)
B
D2-MSN
C
****
D1-MSN
D2-MSN
Frequency (Hz)
D
Frequency (% change)
Concentration (μM)
E
Amplitude (pA)
F
Amplitude (% change)
G
Met-Enk
IC50 = 993 nM
% Inhibition (of maximal effect)
Concentration (nM)

Figure 3-3. Dose-dependent changes from exogenous Met-enkephalin application. (**A, B**) Top, mEPSC traces from D1-MSNs (A) or D2-MSNs (B) before (left) and after (right) bath perfusion of Met-Enk (10 μM). Bottom, cumulative fraction plots of mEPSCs from D1-MSNs (A) or D2-MSNs (B) for inter-event interval (left) and amplitude (right) at increasing Met-Enk concentrations (0.01 - 10 μM). (**C, D**) Met-Enk caused a dose-dependent decrease in mEPSC frequency in D1-MSNs (left, orange, n=8) and D2-MSNs (right, green, n=8) expressed as raw frequency (C) or percent change of baseline (D). (**E, F**) MERF did not cause a dose-dependent change in mEPSC amplitude in D1-MSNs (left, orange, n=8) or D2-MSNs (right, green, n=8) expressed as raw amplitude (E) or percent change of baseline (F). (**G**) Sigmoidal interpolation of Met-Enk dose-response normalized to maximal frequency change at 10 μM (IC_{50}: 993 nM, 95% CI: 669 - 1475 nM, n=16). Data are mean ± s.e.m. for all panels; open and closed circles indicate recordings from female and male mice, respectively. ****P<0.0001, ANOVA concentration main effect (C, D); see Appendix A for complete statistics.

Figure 3-4

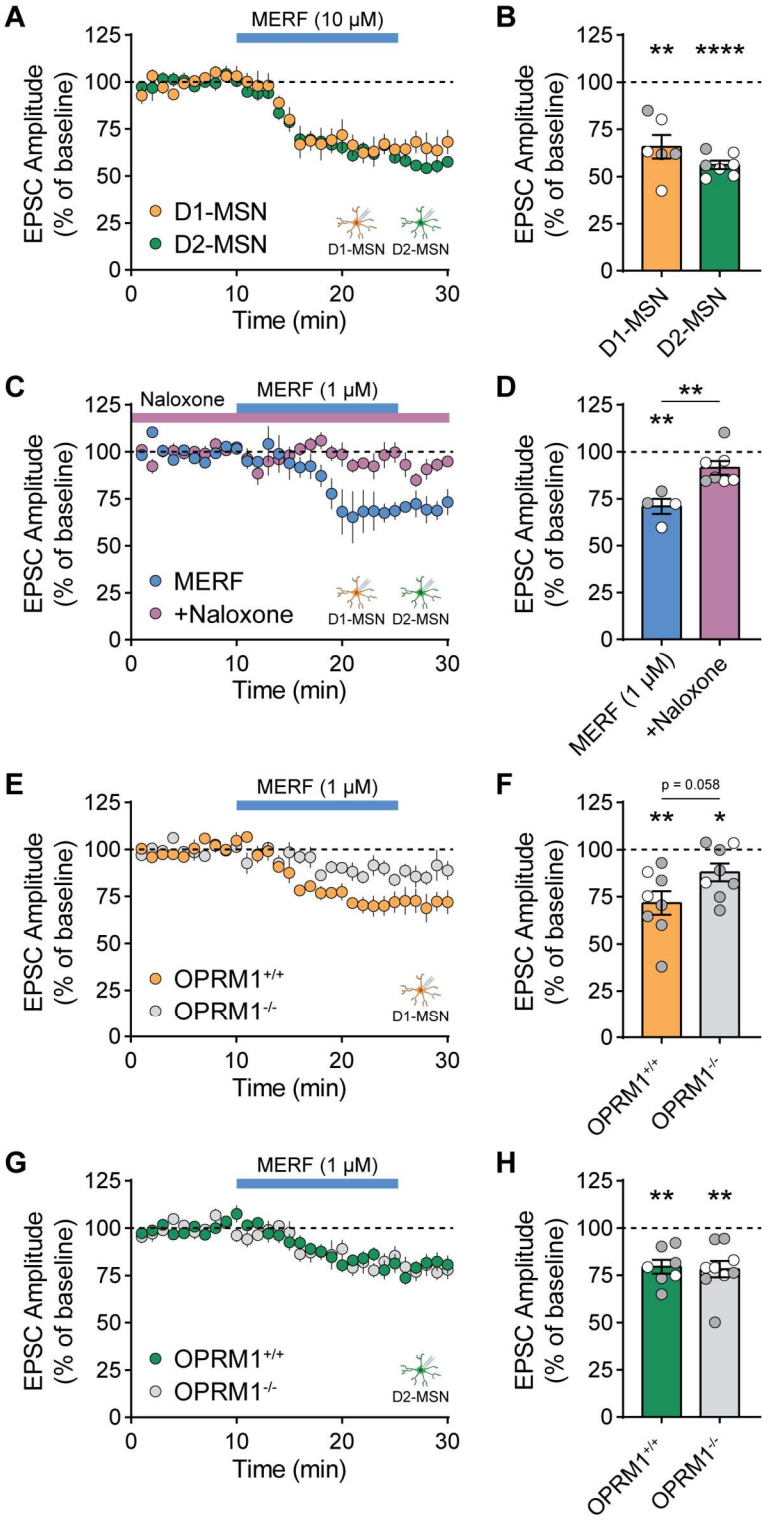
A
MERF (10 μM)
EPSC Amplitude (% of baseline)
D1-MSN
D2-MSN
Time (min)
B
**
****
D1-MSN
D2-MSN
C
Naloxone
MERF (1 μM)
MERF
+Naloxone
D
**
**
MERF (1 μM)
+Naloxone
E
MERF (1 μM)
OPRM1+/+
OPRM1-/-
F
p = 0.058
**
*
G
MERF (1 μM)
OPRM1+/+
OPRM1-/-
H
**
**

Figure 3-4. Exogenous MERF depresses electrically evoked EPSCs. (**A, B**) EPSC amplitude time course (A) or average amplitude during last 5 min (B) of MERF (10 μM) bath perfusion onto D1-MSNs (orange, n=6) and D2-MSNs (green, n=7). (**C, D**) EPSC amplitude time course (C) or average amplitude during last 5 min (D) of MERF (1 μM) bath perfusion onto D1-MSNs (blue, n=4) or while in the presence of the opioid receptor antagonist naloxone (10 μM, purple, n=7). (**E, F**) EPSC amplitude time course (E) or average amplitude during last 5 min (F) of MERF (1 μM) bath perfusion onto D1-MSNs in slices from Oprm1$^{-/-}$ mice (grey, n=8) or wildtype littermates (orange, n=8). (**G, H**) EPSC amplitude time course (G) or average amplitude during last 5 min (H) of MERF (1 μM) bath perfusion onto D2-MSNs in slices from Oprm1$^{-/-}$ mice (grey, n=7) or wildtype littermates (green, n=9). Data are mean ± s.e.m. for all panels; open and closed circles indicate recordings from female and male mice, respectively. *P<0.05, **P<0.01, ****P<0.0001, one-sample t-test (B, D, F, H), two-sample t-test (D, F); see Appendix A for complete statistics.

Figure 3-5

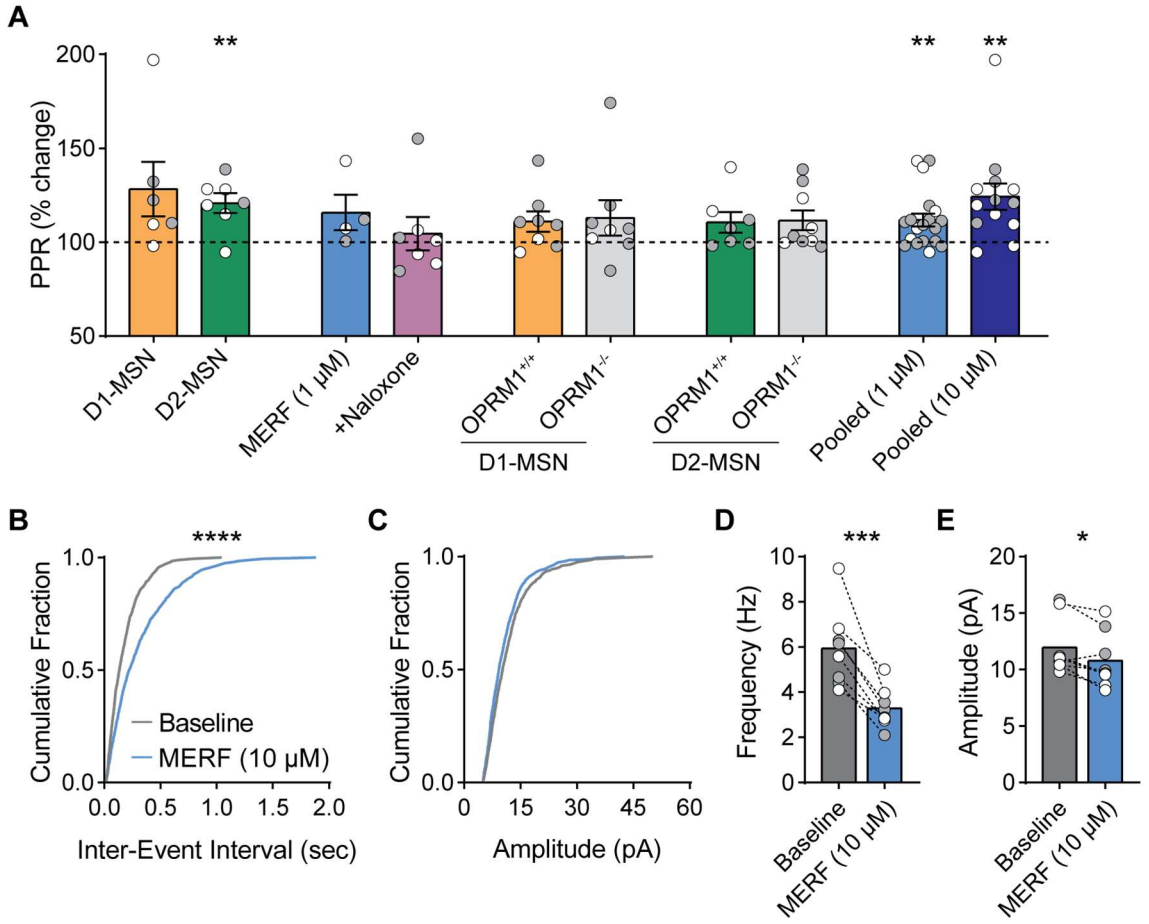

Figure 3-5. Exogenous MERF depresses presynaptic excitatory synaptic transmission. (**A**) Percent change in paired-pulse ratio after MERF bath perfusion relative to baseline for individual samples recorded in Figure 3-4 or pooled by concentration. (**B, C**) Cumulative fraction plots of inter-event interval (B) and amplitude (C) from spontaneous EPSCs before and after MERF (10 μM) bath perfusion. (**D, E**) Average spontaneous EPSC frequency (D) or amplitude (E) before and after MERF (10 μM) bath perfusion. Data are mean ± s.e.m. for all panels; open and closed circles indicate recordings from female and male mice, respectively. *$P<0.05$, **$P<0.01$, ***$P<0.001$, ****$P<0.0001$, one-sample *t*-test (A), Kolmogorov-Smirnov test (B), two-sample *t*-test (D, E); see Appendix A for complete statistics.

Figure 3-6

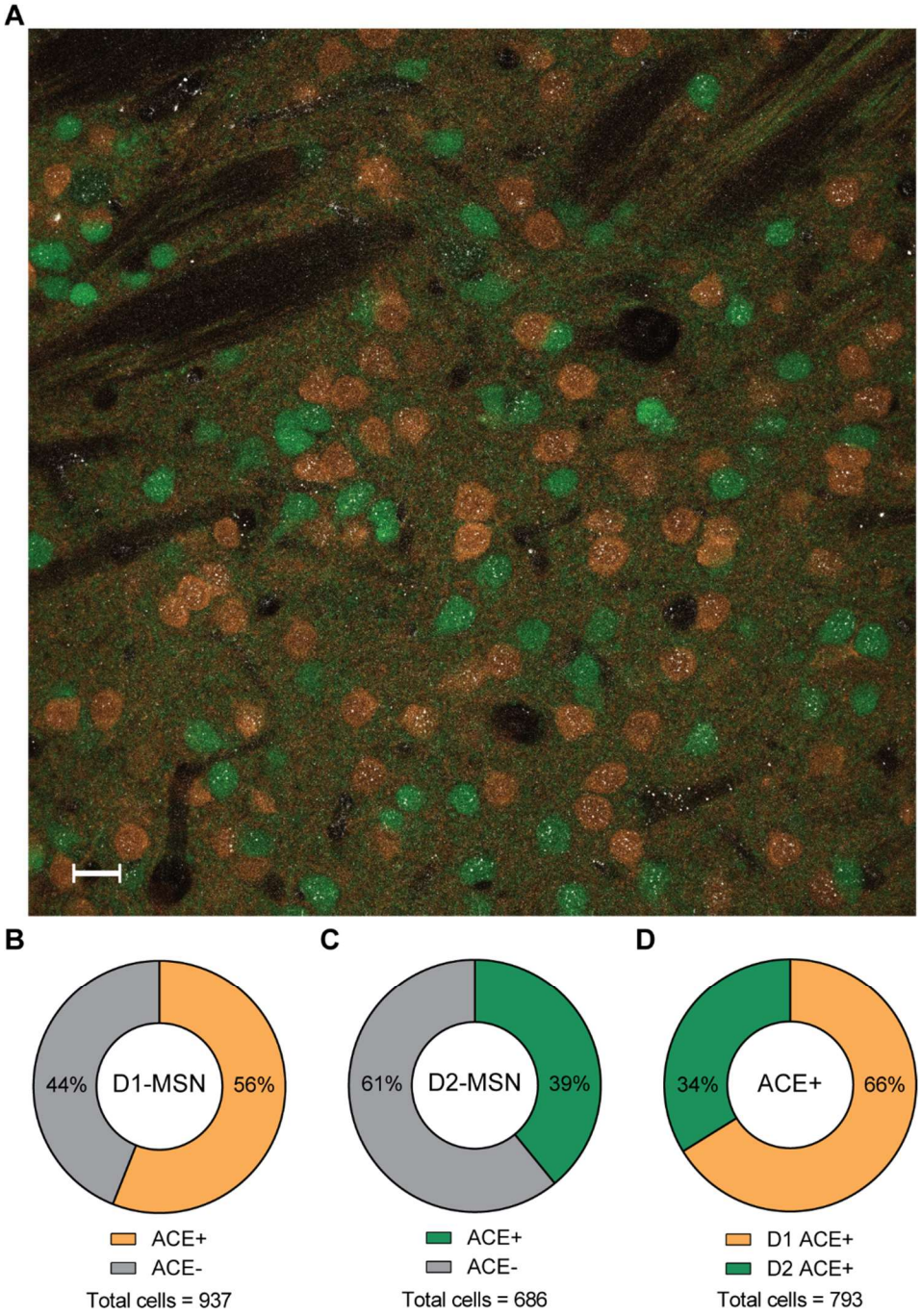
A
B
44%
D1-MSN
56%
ACE+
ACE-
Total cells = 937
C
61%
D2-MSN
39%
ACE+
ACE-
Total cells = 686
D
34%
ACE+
66%
D1 ACE+
D2 ACE+
Total cells = 793

Figure 3-6. Immunohistochemical labeling of ACE protein in nucleus accumbens. (**A**) Confocal image of ACE immunoreactive puncta (white) co-localized with tdTomato (orange) and eGFP (green) in nucleus accumbens core. Scale bar = 20 µm. (**B**) Quantification of ACE immunoreactive D1-MSNs (orange) as a percentage of total D1-MSNs. (**C**) Quantification of ACE immunoreactive D2-MSNs (green) as a percentage of total D2-MSNs. (**D**) Quantification of D1- and D2-MSNs containing ACE immunoreactivity as a percentage of all ACE-positive somata. Cell counts were conducted in tissue from three mice; the percentage of D1-MSNs that express ACE is significantly greater than for D2-MSNs, according to Fisher's exact test ($p < 0.001$).

Figure 3-7

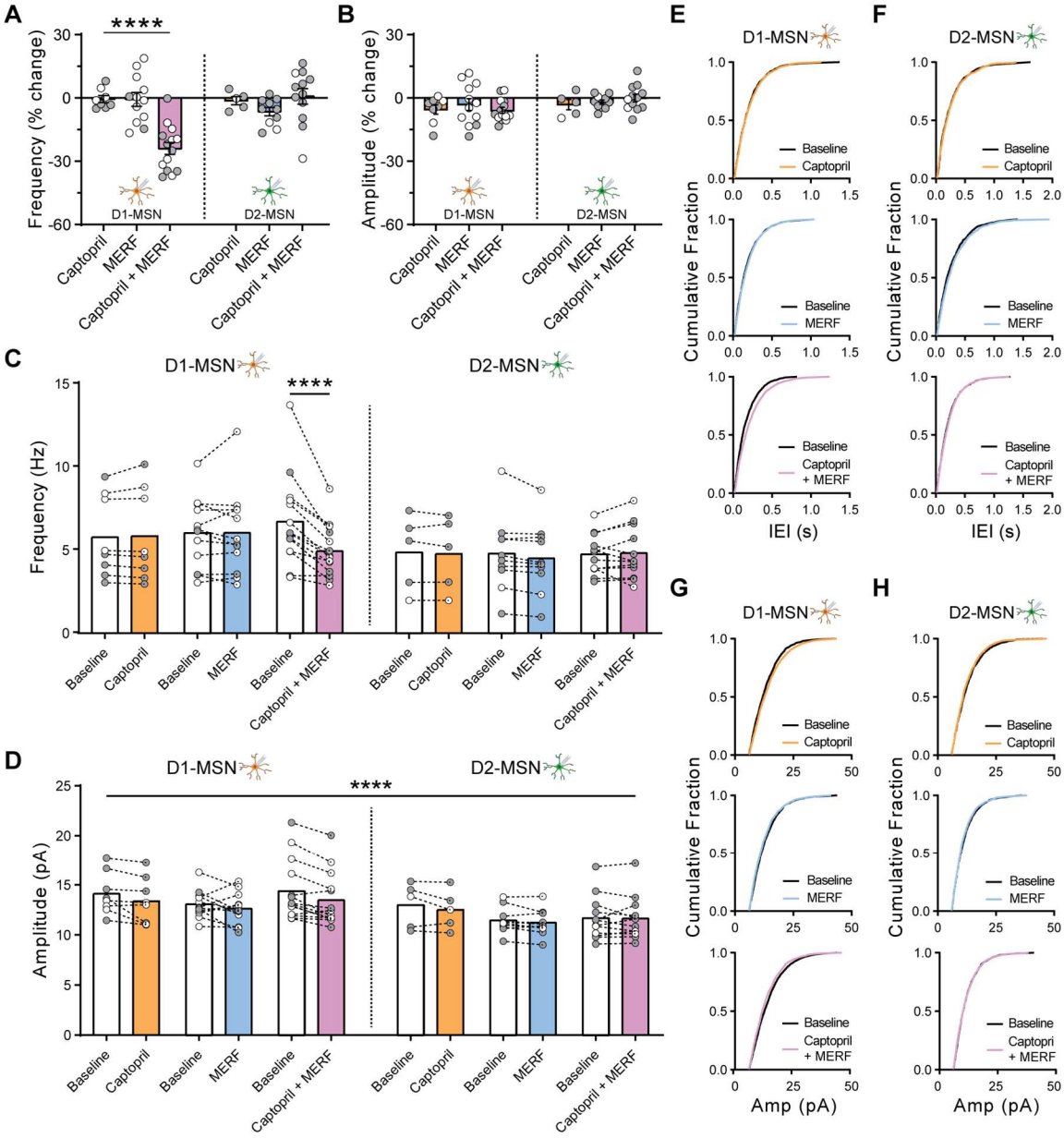
A
****
Frequency (% change)
30
0
-30
-60
D1-MSN
D2-MSN
Captopril
MERF
Captopril + MERF
B
Amplitude (% change)
C
D1-MSN
D2-MSN
****
Frequency (Hz)
15
10
5
0
Baseline
Captopril
MERF
Captopril + MERF
D
Amplitude (pA)
25
20
15
10
5
E
F
Cumulative Fraction
IEI (s)
G
H
Amp (pA)

Figure 3-7. Captopril synergizes with exogenous MERF to depress presynaptic glutamate release selectively in D1-MSNs. (**A, B**) mEPSC frequency (A) and amplitude (B) as a percent change relative to baseline after captopril (10 μM) and/or threshold MERF (100 nM) in D1-MSNs (left, *n*=14) and D2-MSNs (right, *n*=12). (**C, D**) Average mEPSC frequency (C) and amplitude (D) before and after captopril, MERF, or combined in D1-MSNs (left) and D2-MSNs (right). (**E, F**) Cumulative fraction plots of mEPSC inter-event interval in D1-MSNs (E) and D2-MSNs (F) before and after captopril, MERF, or combined. (**G, H**) Cumulative fraction plots of mEPSC amplitude in D1-MSNs (G) and D2-MSNs (H) before and after captopril, MERF, or combined. Data are mean ± s.e.m. for all panels; open and closed circles indicate recordings from female and male mice, respectively. ****$P<0.0001$, ANOVA treatment simple effect in D1-MSNs (A), ANOVA followed by Fisher's LSD post-hoc test (C), and ANOVA time main effect (D); see Appendix A for complete statistics.

Figure 3-8

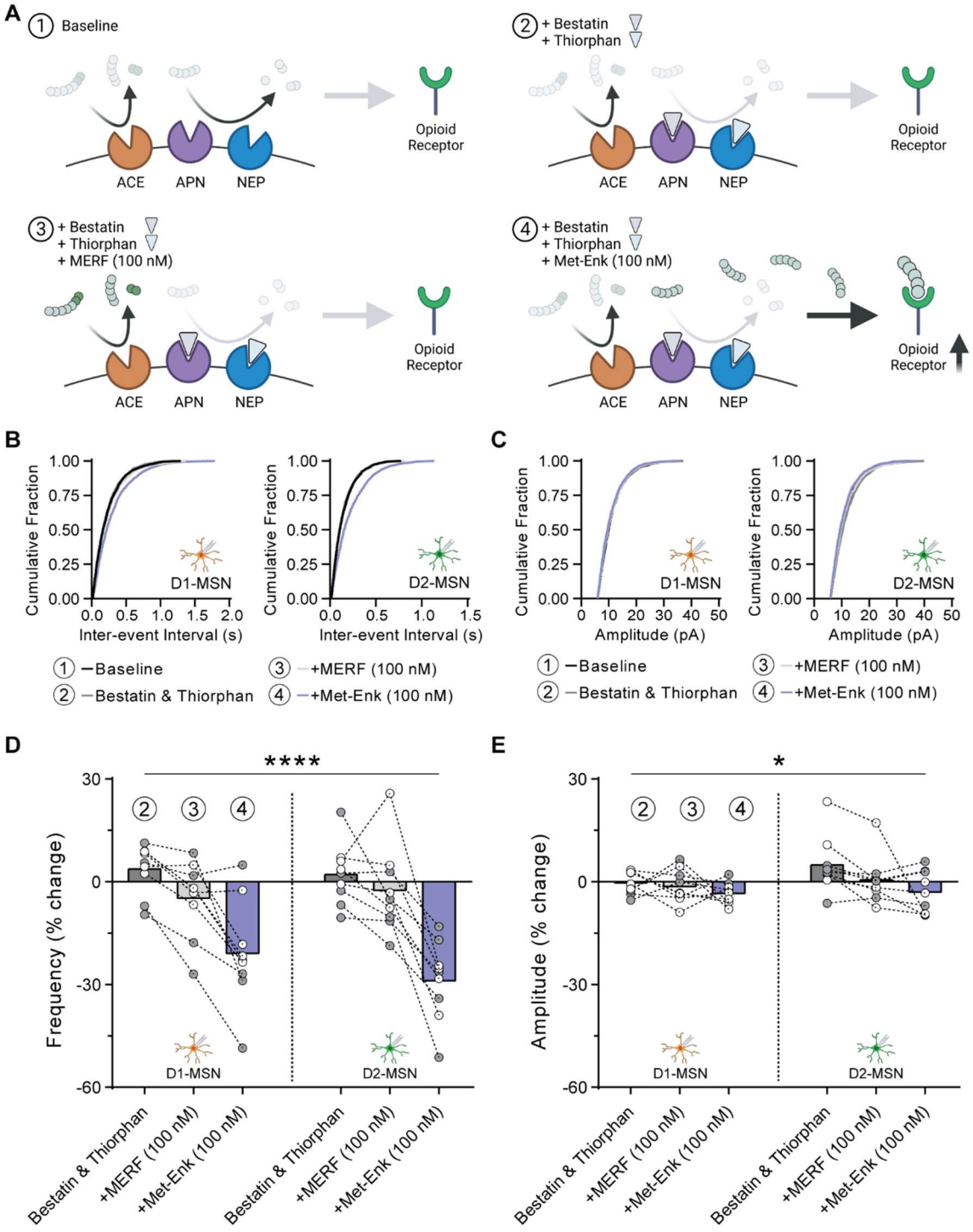
A
① Baseline
② + Bestatin
+ Thiorphan
③ + Bestatin
+ Thiorphan
+ MERF (100 nM)
④ + Bestatin
+ Thiorphan
+ Met-Enk (100 nM)
ACE
APN
NEP
Opioid Receptor
B
Cumulative Fraction
Inter-event Interval (s)
D1-MSN
D2-MSN
C
Amplitude (pA)
① —Baseline
② —Bestatin & Thiorphan
③ —+MERF (100 nM)
④ —+Met-Enk (100 nM)
D
****
Frequency (% change)
E
*
Amplitude (% change)
Bestatin & Thiorphan
+MERF (100 nM)
+Met-Enk (100 nM)

Figure 3-8. Exogenous Met-enkephalin synergizes with peptidase inhibitors of aminopeptidase N and neprilysin to depress glutamate release. (**A**) Conceptual schematic showing how peptidase inhibitors bestatin and thiorphan toward aminopeptidase N and neprilysin, respectively, affect opioid receptor signaling by MERF or Met-enkephalin. (**B, C**) Cumulative fraction plots from D1-MSNs (left, n=9) and D2-MSN (right, n=9) of mEPSC inter-event interval (B) and amplitude (C) following bath perfusion of combined bestatin (10 μM) and thiorphan (1 μM) plus MERF (100 nM) or Met-enkephalin (100 nM). (**D, E**) Met-enkephalin but not MERF synergizes with combined bestatin and thiorphan to depress mEPSC frequency in both cell types (D) without affecting amplitude (E). Data are mean ± s.e.m. for all panels; open and closed circles indicate recordings from female and male mice, respectively. *$P<0.05$, ****$P<0.0001$, ANOVA treatment main effect (D, E); see Appendix A for complete statistics.

Figure 3-9

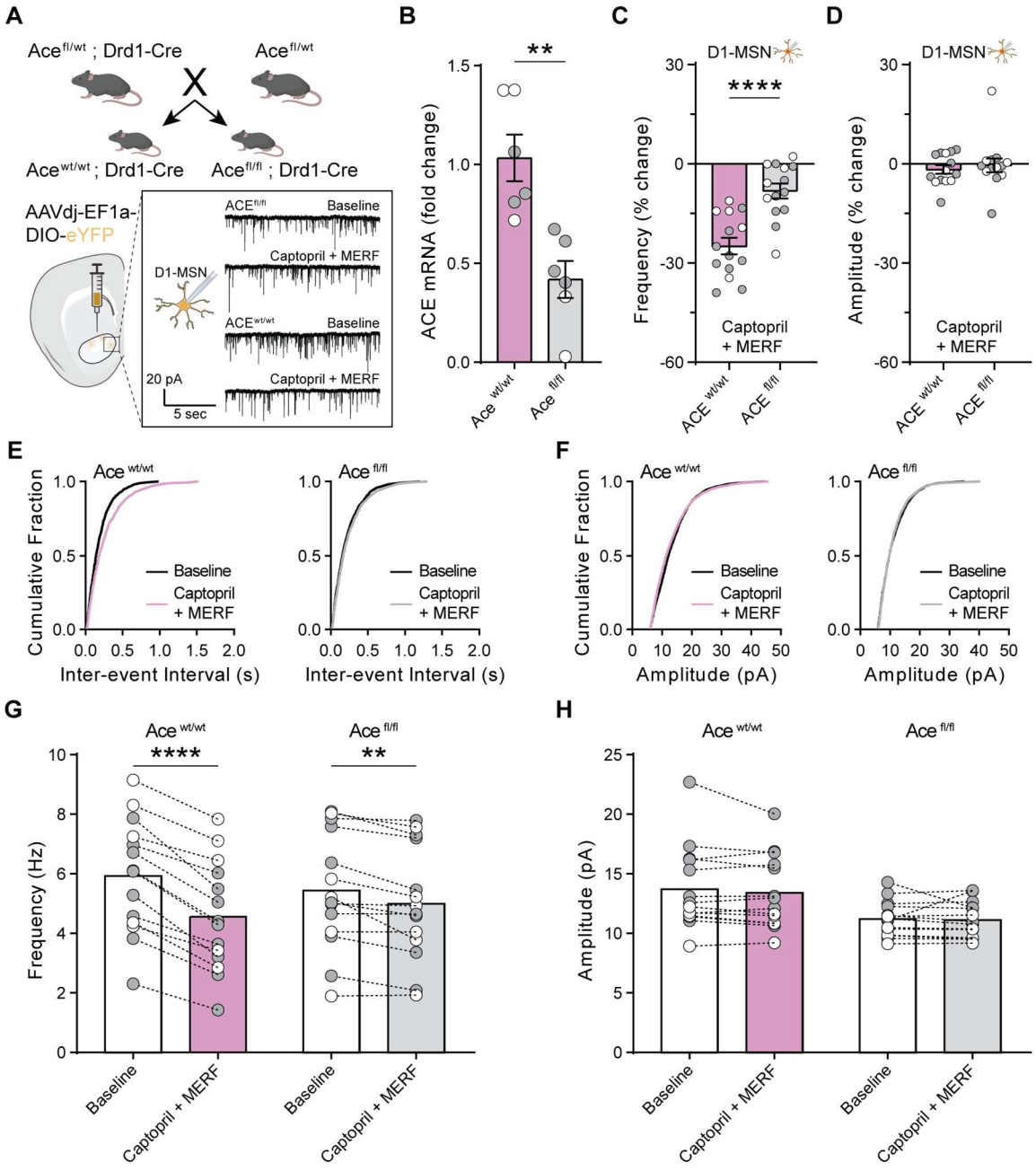
A
Ace fl/wt ; Drd1-Cre
Ace fl/wt
Ace wt/wt ; Drd1-Cre
Ace fl/fl ; Drd1-Cre
AAVdj-EF1a-DIO-eYFP
D1-MSN
ACE fl/fl
Baseline
Captopril + MERF
ACE wt/wt
Baseline
Captopril + MERF
20 pA
5 sec
B
**
ACE mRNA (fold change)
Ace wt/wt
Ace fl/fl
C
D1-MSN
****
Frequency (% change)
Captopril + MERF
ACE wt/wt
ACE fl/fl
D
D1-MSN
Amplitude (% change)
Captopril + MERF
ACE wt/wt
ACE fl/fl
E
Ace wt/wt
Ace fl/fl
Cumulative Fraction
Baseline
Captopril + MERF
Inter-event Interval (s)
F
Ace wt/wt
Ace fl/fl
Cumulative Fraction
Baseline
Captopril + MERF
Amplitude (pA)
G
Ace wt/wt
****
Ace fl/fl
**
Frequency (Hz)
Baseline
Captopril + MERF
H
Ace wt/wt
Ace fl/fl
Amplitude (pA)
Baseline
Captopril + MERF

Figure 3-9. ACE is necessary for synergistic effect of captopril and MERF. (**A**) Top, genetic cross to obtain control ($Ace^{wt/wt}$; Drd1-Cre) and conditional ACE knockout mice ($Ace^{fl/fl}$; Drd1-Cre). Bottom, stereotaxic injection of Cre-dependent eYFP reporter virus to identify NAc D1-MSNs for whole-cell recordings. Bottom-right inset show traces from control and ACE knockout mice. (**B**) mRNA quantification from striatal tissue punches (both nucleus accumbens and dorsal striatum) in control ($Ace^{wt/wt}$; Drd1-Cre, n=6) and conditional ACE knockout mice ($Ace^{fl/fl}$; Drd1-Cre, n=6). (**C-D**) Combined effect of captopril (10 μM) and MERF (100 nM) on mEPSC frequency (C) and amplitude (D) as percent change relative to pre-drug baseline after conditional deletion of ACE from D1-MSNs (grey, n=14) versus control (purple, n=14). (**E-H**) mEPSC parameters before and after combined captopril and MERF in $Ace^{wt/wt}$ (n=14) and $Ace^{fl/fl}$ (n=14) mice shown as cumulative fraction plots of inter-event interval (E), cumulative fraction plots of amplitude (F), and average frequency (G) and average amplitude (H). We note that the absence of ACE expression from D1-MSNs during development could lead to compensatory upregulation of other peptidases that contribute to MERF degradation, which may explain why genetic knockout of ACE expression does not cause the same effect as ACE inhibition. Data are mean ± s.e.m. for all panels; open and closed circles indicate samples or recordings from female and male mice, respectively. **P<0.01, ****P<0.0001, ANOVA genotype main effect (B, C) and ANOVA followed by Fisher's LSD post-hoc test (G); see Data S1 for complete statistics.

Figure 3-10

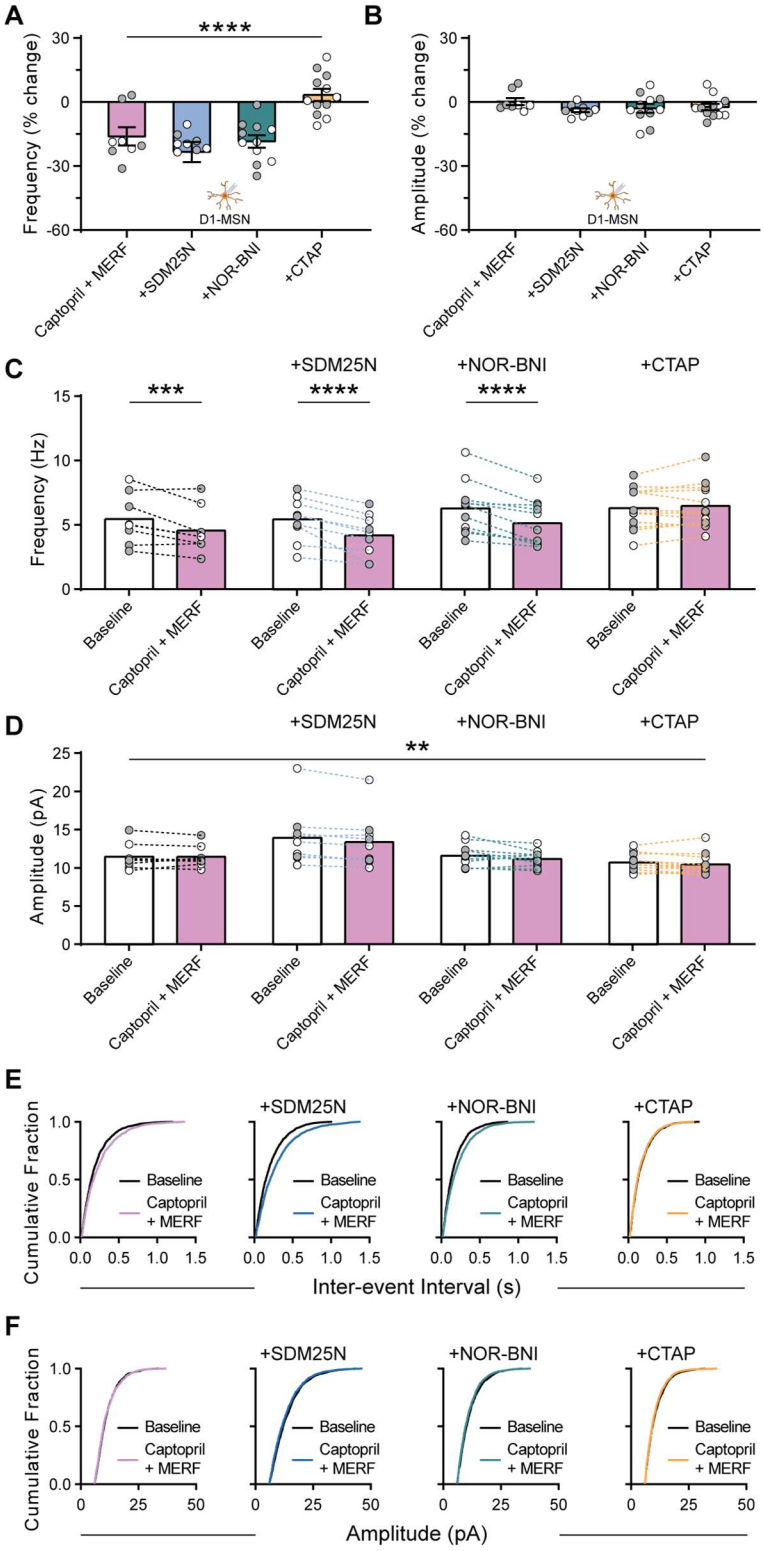
A
****
Frequency (% change)
30
0
-30
-60
D1-MSN
Captopril + MERF
+SDM25N
+NOR-BNI
+CTAP
B
Amplitude (% change)
30
0
-30
-60
D1-MSN
Captopril + MERF
+SDM25N
+NOR-BNI
+CTAP
C
+SDM25N
+NOR-BNI
+CTAP
***
****
****
Frequency (Hz)
15
10
5
0
Baseline
Captopril + MERF
D
+SDM25N
+NOR-BNI
+CTAP
**
Amplitude (pA)
25
20
15
10
5
0
Baseline
Captopril + MERF
E
+SDM25N
+NOR-BNI
+CTAP
Cumulative Fraction
1.0
0.5
0.0
Baseline
Captopril + MERF
0.0 0.5 1.0 1.5
Inter-event Interval (s)
F
+SDM25N
+NOR-BNI
+CTAP
Cumulative Fraction
1.0
0.5
0.0
Baseline
Captopril + MERF
0 25 50
Amplitude (pA)

Figure 3-10. μ-Opioid receptor antagonism blocks combined captopril and MERF synergy. (**A, B**) Change in frequency (A) or amplitude (B) of mEPSCs after combined effect of captopril and threshold MERF in the presence of selective antagonists to δ- (SDM25N, 500 nM, blue, *n*=9), κ- (NOR-BNI, 100 nM, green, *n*=11), or μ- (CTAP, 1 μM, orange, *n*=12) opioid receptors. (**C-F**) mEPSC parameters shown as average frequency (C), average amplitude (D), inter-event interval cumulative fraction (E), or amplitude cumulative fraction (F) before and after combined captopril and MERF with or without selective opioid receptor antagonists. The reduction in frequency (A and C) and rightward shift of inter-event interval (E) after combined captopril and threshold MERF was present in all conditions except when CTAP was present. Data are mean ± s.e.m. for all panels; open and closed circles indicate recordings from female and male mice, respectively. ***P*<0.01, ****P*<0.001, *****P*<0.0001, ANOVA treatment main effect (A), ANOVA followed by Fisher's LSD post-hoc test (C), ANOVA time main effect (D); see Appendix A for complete statistics.

Figure 3-11

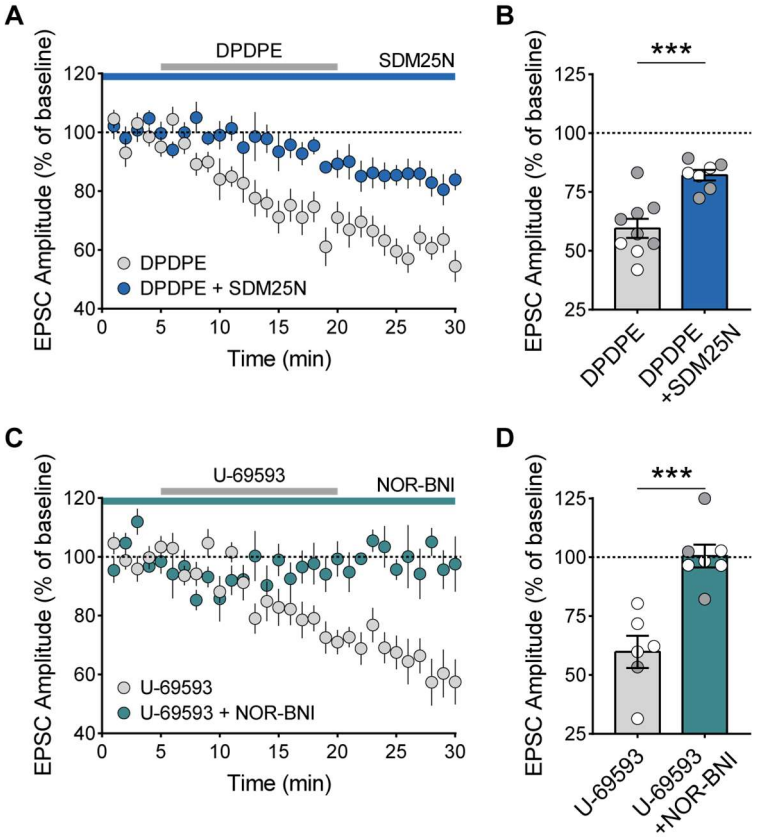

Figure 3-11. Confirmation that δ- and κ-opioid receptor antagonists have functional effects. (**A**) Time course of EPSC amplitude before, during, and after bath perfusion of DOR agonist DPDPE for 15 min (0.3-1 μM, grey, *n*=9) or DPDPE in the continuous presence of DOR antagonist SDM25N (500 nM, blue, *n*=7). (**B**) Average EPSC amplitude relative to baseline in last 5 min of (A). (**C**) Time course of EPSC amplitude before, during, and after bath perfusion of KOR agonist U-69593 for 15 min (300 nM, grey, *n*=6) or U-69593 in the continuous presence of KOR antagonist NOR-BNI (100 nM, green, *n*=7). (**D**) Average EPSC amplitude relative to baseline in last 5 min of (C). Data are mean ± s.e.m. for all panels; open and closed circles indicate recordings from female and male mice, respectively. ***P<0.001, Two-sample t-test (B, D); see Appendix A for complete statistics.

Figure 3-12

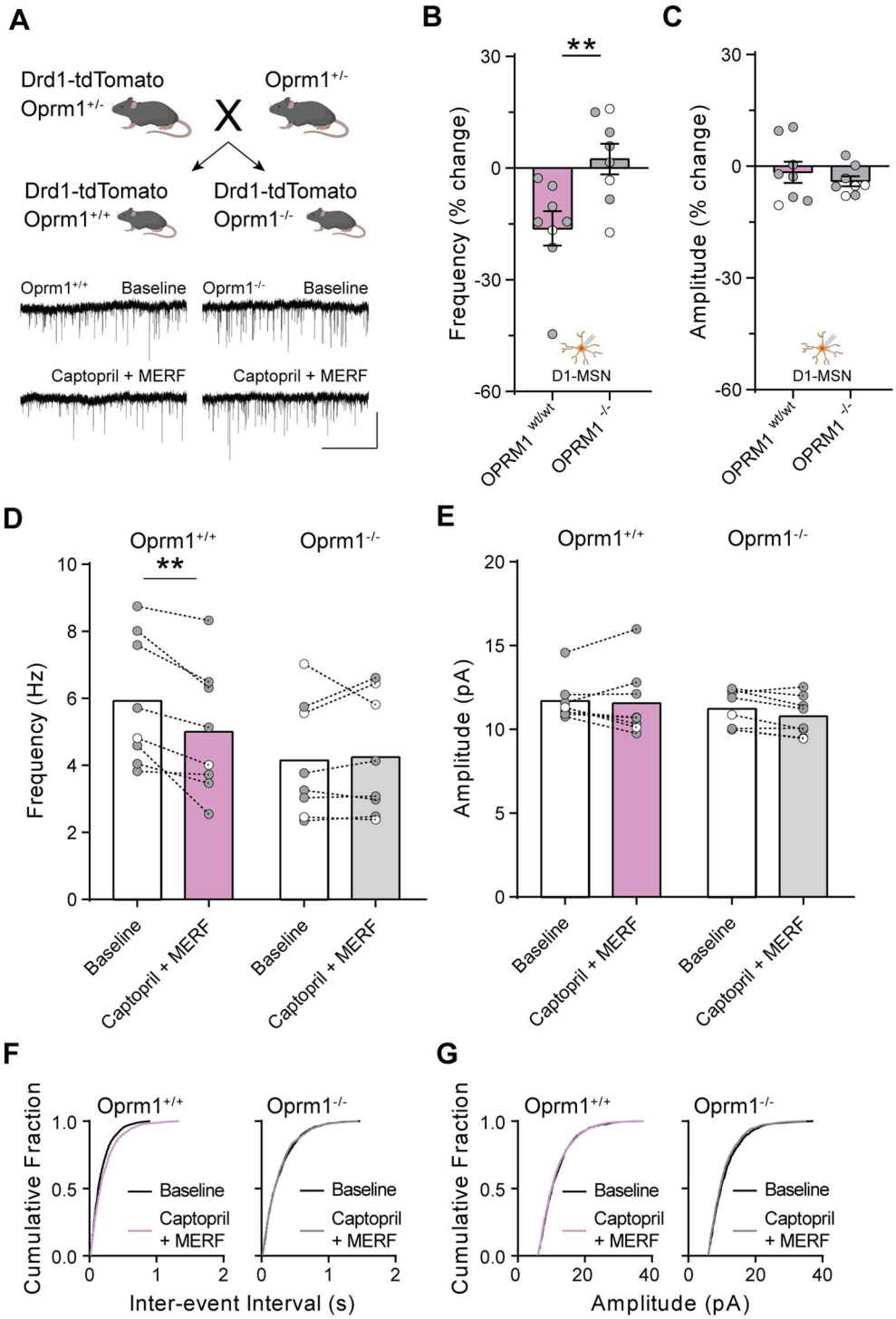
A
Drd1-tdTomato
Oprm1+/-
X
Oprm1+/-
Drd1-tdTomato
Oprm1+/+
Drd1-tdTomato
Oprm1-/-
Oprm1+/+
Baseline
Oprm1-/-
Baseline
Captopril + MERF
Captopril + MERF
B
**
Frequency (% change)
D1-MSN
OPRM1 wt/wt
OPRM1 -/-
C
Amplitude (% change)
D1-MSN
OPRM1 wt/wt
OPRM1 -/-
D
Oprm1+/+
Oprm1-/-
**
Frequency (Hz)
Baseline
Captopril + MERF
Baseline
Captopril + MERF
E
Oprm1+/+
Oprm1-/-
Amplitude (pA)
Baseline
Captopril + MERF
Baseline
Captopril + MERF
F
Oprm1+/+
Oprm1-/-
Cumulative Fraction
Baseline
Captopril + MERF
Baseline
Captopril + MERF
Inter-event Interval (s)
G
Oprm1+/+
Oprm1-/-
Cumulative Fraction
Baseline
Captopril + MERF
Baseline
Captopril + MERF
Amplitude (pA)

Figure 3-12. Constitutive deletion of μ-opioid receptors abolish synergy from combined captopril and MERF. (**A**) Top, genetic cross to obtain control (Oprm1$^{+/+}$; Drd1-tdTomato) and constitutive MOR knockout (Oprm1$^{-/-}$; Drd1-tdTomato) mice. Bottom, representative traces of mEPSCs in D1-MSNs from Oprm1$^{+/+}$ (left) and Oprm1$^{-/-}$ (right) mice during baseline and after combined captopril and MERF. (**B, C**) Frequency (B) and amplitude (C) percent change after combined captopril and threshold MERF in Oprm1$^{-/-}$ knockout mice (grey, n=8) and Oprm1$^{+/+}$ littermates (purple, n=8). (**D-G**) mEPSC parameters shown as average frequency (D), average amplitude (E), inter-event interval cumulative fraction (F), or amplitude cumulative fraction (G) before and after combined captopril and MERF in Oprm1$^{-/-}$ knockout mice and Oprm1$^{+/+}$ littermates. The reduction in frequency (B and D) and rightward shift of inter-event interval (F) after combined captopril and threshold MERF was absent in constitutive MOR-knockout mice. Data are mean ± s.e.m. for all panels; open and closed circles indicate recordings from female and male mice, respectively. **P<0.01, two-sample t-test (B), ANOVA followed by Fisher's LSD post-hoc test (D); see Appendix A for complete statistics.

Figure 3-13

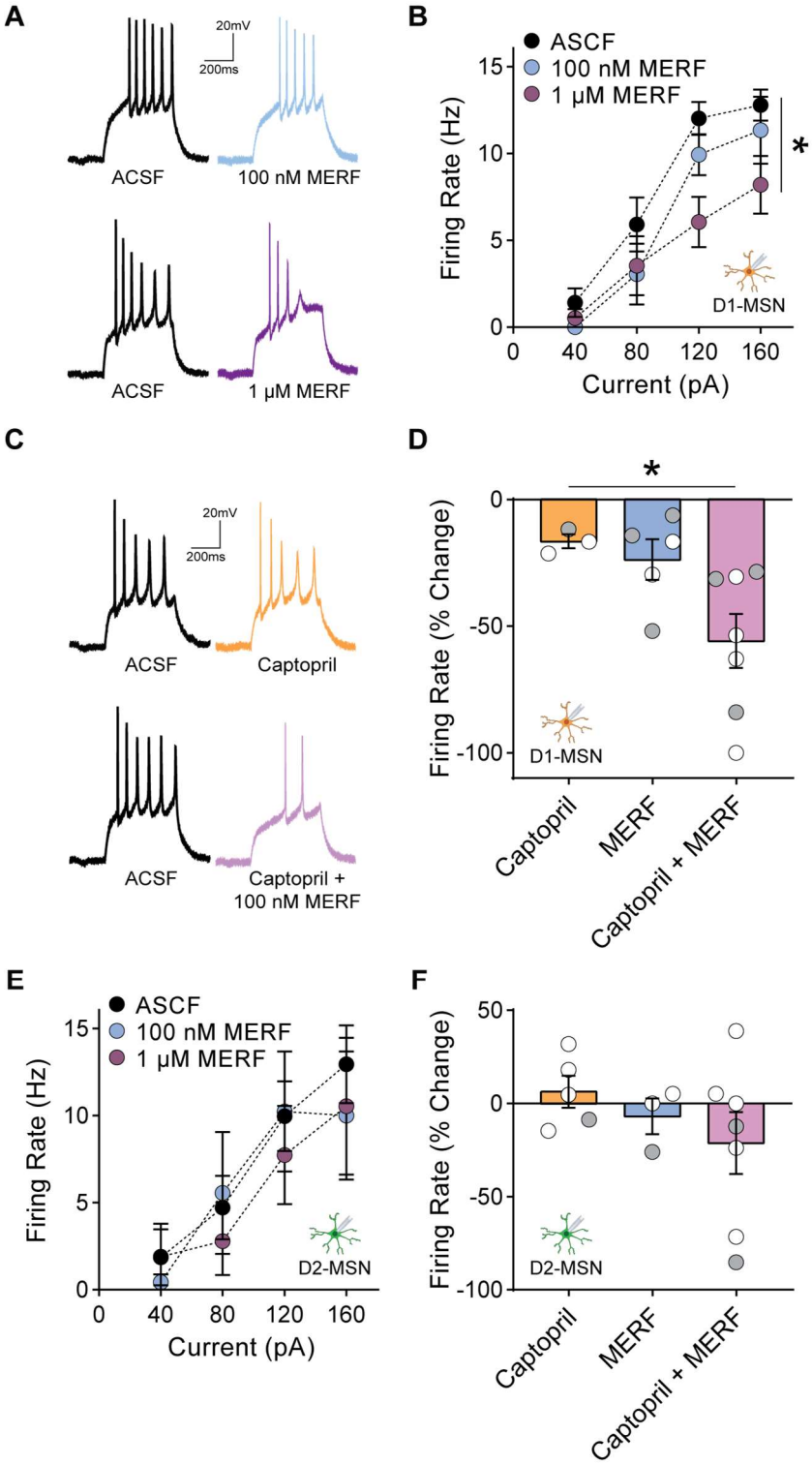
A
20mV
200ms
ACSF
100 nM MERF
ACSF
1 μM MERF
B
ASCF
100 nM MERF
1 μM MERF
Firing Rate (Hz)
Current (pA)
D1-MSN
*
C
20mV
200ms
ACSF
Captopril
ACSF
Captopril +
100 nM MERF
D
*
Firing Rate (% Change)
D1-MSN
Captopril
MERF
Captopril + MERF
E
ASCF
100 nM MERF
1 μM MERF
Firing Rate (Hz)
Current (pA)
D2-MSN
F
Firing Rate (% Change)
D2-MSN
Captopril
MERF
Captopril + MERF

Figure 3-13. Combined captopril and MERF reduces firing rate in D1-MSNs but not D2-MSNs. (**A, B**) Current clamp traces (A) and summary of action potential firing rate (B) in D1-MSNs (n=5-7) before and after exposure to MERF (0.1 - 1 μM). (**C, D**) Current clamp traces (C) and summary of action potential firing rate change in D1-MSNs (n=3-7) when injected with 120 pA after captopril (10 μM) and/or threshold MERF (100 nM). (**E**) Action potential firing rate in D2-MSNs (n=3-8) before and after exposure to MERF (0.1 - 1 μM). (**F**) Action potential firing rate change in D2-MSNs (n=3-7) when injected with 120 pA after captopril (10 μM) and/or threshold MERF (100 nM). Data are mean ± s.e.m. for all panels; open and closed circles indicate recordings from female and male mice, respectively. *P<0.05, ANOVA treatment main effect (K, L); see Appendix A for complete statistics.

Chapter 4: Inhibition of angiotensin-converting enzyme boosts endogenous "MERF"

This chapter contains work that was adapted with permission from the following article: Trieu et al., Science, 2022 [205].

Introduction

The detection and quantification of endogenous neuropeptides under physiological conditions have historically been a difficult task, particularly when considering the temporal and spatial dynamics of the brain and the availability of techniques that have varying sensitivity and specificity [240]. Complicating this is the fact that neuropeptides require prolonged synaptic depolarization to be released, are released at lower quantities into the synaptic cleft relative to small neurotransmitters, and are rapidly degraded by peptidases once released. This chapter will explore how ACE inhibitors modulate the interaction between ACE and endogenous MERF using 1) targeted proteomic analysis of several striatal neuropeptides by liquid chromatography-tandem mass spectrometry (LC-MS/MS), 2) electrophysiological investigation of the synaptic mechanisms affected by ACE inhibition, and 3) behavioral studies following systemic administration of ACE inhibitors.

Results

4.1 Liquid Chromatography-Tandem Mass Spectrometry

Targeted proteomic analysis using LC-MS/MS is frequently used in several fields and is a mainstay of proteomic research given the technique's high specificity for identifying numerous biochemical molecules simultaneously and continual advances in detection sensitivity [241,242]. However, its use in neuroscience research is relatively sparse [225,243,244]. Given the advantages of this technique, we employed nanoflow LC-MS/MS to detect low abundance endogenous neuropeptides in the striatum (figure 4-1 A). Several neuropeptides were screened, and standards were detected reliably with comparable sensitivity (figure 4-1 B-J).

Mouse brain slices containing the nucleus accumbens were then incubated in normal ACSF or ACSF containing high KCl (50 mM) to induce non-specific neuronal depolarization and subsequent release of vesicular contents. Neuropeptide concentrations were measured from the extracellular fluid by extrapolating from the standard curves. An increase in MERF, Met-enkephalin, Leu-enkepahlin, Dyn A (1-8), Dyn B, and substance P was observed following KCl

stimulation relative to slices incubated in normal ACSF (figure 4-2, table 4-1). Notably, angiotensin II and bradykinin (figure 4-3 A) were minimally detected under stimulated conditions suggesting that these striatal slices do not contain these classical ACE substrates or that they are not released under these conditions. Interestingly, regional tissue punches revealed significantly higher endogenous opioid peptides (MERF, Met-enkephalin, Leu-enkephalin, Dyn A (1-8)) in nucleus accumbens than dorsal striatum following KCl stimulation (figure 4-3 B-E). Furthermore, enkephalin signals were absent in constitutive knockout mice lacking the proenkephalin precursor gene *Penk* while dynorphin and substance P signals were preserved (figure 4-3 F-K), indicating *Penk* is the primary source of enkephalin in this preparation.

Although electrophysiology data in Chapter 3 showed that ACE inhibition by captopril synergizes with low concentrations of exogenous MERF (figure 3-7), it is unclear if ACE also participates in regulation of other neuropeptides in the nucleus accumbens. To test this, neuropeptides were measured from slices incubated in ACSF containing high KCl (50 mM) plus captopril (10 μM) and compared to slices stimulated by KCl alone. Captopril induced a robust and selective increase in MERF (figure 4-4 A) with no changes in other neuropeptides. Remarkably there were no changes in conventional Met-enkephalin or substance P, which were previously suggested as a substrates for ACE. The classical ACE substrates angiotensin II and bradykinin continued to be absent under these conditions. These effects were recapitulated using trandolaprilat, a newer ACE inhibitor (figure 4-4 B).

As mentioned previously, ACE inhibitors are often combined with other peptidase inhibitors [112,115,118,139,166,199] and used as a pharmacological tool to study conventional enkephalins. Bestatin (10 μM) and thiorphan (1 μM), which target aminopeptidase N and neprilysin, respectively, were used to investigate how inhibition of these other peptidases alter MERF concentrations. In contrast to captopril alone, extracellular levels of MERF were not affected by bestatin and thiorphan (figure 4-4 C). However, a cocktail of inhibitors toward all three peptidases blocked degradation of several neuropeptides and demonstrated a double dissociation between regulation of MERF and conventional enkephalins (figure 4-4 D).

One caveat of this experimental design lies in how the tissue was stimulated. Although high concentration KCl has been previously used to successfully induce neuronal depolarization for investigation of endogenous extracellular neuropeptide release [171,172,243,245], the experimental manipulation lacks specificity and is not physiological. Alternatively, an optogenetic approach allows for cellular specificity while maintaining physiological extracellular ion concentrations. Therefore, to address the potentially confounding effects of concentrated KCl, we bred mice with

genetic expression of channelrhodopsin-2 in D2-MSNs (figure 4-5 A-C) because these cells express high levels of Penk [13] and are likely the source of MERF. Optogenetic stimulation of acute brain slices from these mice increased extracellular levels of conventional enkephalins, but only MERF levels were elevated in the presence of captopril (figure 4-5 D-E, table 4.2).

4.2 Electrophysiology

To extend these findings of enhanced endogenous MERF presence after ACE inhibition, we next investigated the impact of captopril on synaptic responses which are in contrast to Chapter 3 which explored how exogenous MERF modulated glutamatergic synaptic transmission. Like before, D1-MSNs expressing tdTomato or D2-MSNs expressing eGFP were recorded under whole-cell voltage-clamp configuration from acute brain slices containing nucleus accumbens (figure 3-1). Brief exposure to captopril (10 μM) caused long-term depression (captopril-LTD) of electrically evoked EPSCs solely onto D1-MSNs without altering responses in D2-MSNs (figure 4-6 A). This corroborates previously presented data demonstrating lower ACE expression in D2-MSNs (figure 3-6) and depression of miniature EPSCs only in D1-MSNs after a combination of captopril plus exogenous 100 nM MERF (figure 3-7). There was also no effect of captopril at excitatory synapses onto layer V pyramidal neurons in the anterior cingulate cortex, where ACE expression is low [13,181], while those same synapses were sensitive to exogenous MERF (1 μM) application (figure 4-7).

Captopril and other ACE inhibitors canonically block conversion of angiotensin I to angiotensin II, preventing activation of the angiotensin II type 1 receptor (AT1R) and increasing levels of angiotensin I (figure 4-8). While our LC-MS/MS results showed minimal extracellular angiotensin II in the striatum with no changes after captopril exposure, it is still possible that captopril could cause an increase in angiotensin I or hypoactivation of AT1R under these electrophysiology conditions. However, LTD was not observed in D1-MSNs exposed to valsartan (2-20 μM), an AT1R antagonist, or exogenous angiotensin I peptide (1 μM) (figure 4-6 B). In contrast, captopril-LTD in D1-MSNs was blocked in the continuous presence of naloxone (10 μM), an opioid receptor antagonist, but was not reversed by chasing captopril with naloxone (figure 4-6 C) suggesting only brief opioid receptor activation by MERF subsequent to ACE inhibition is necessary to induce LTD.

Captopril-LTD in D1-MSNs was associated with an increase in PPR and a decrease in $1/CV^2$ (figure 4-6 D-F), two changes that indicate decreased presynaptic probability of glutamate release [236] similar to the effects of exogenous MERF application. These effects were more evident after pooling all electrically evoked experiments in D1-MSNs where captopril was applied (figure

4-9). Inhibition of ACE by trandolaprilat (1 μM) recapitulated effects similar to captopril-LTD (figure 4-10).

As mentioned previously, MOR activation was necessary to observe the synergistic effect of captopril and exogenous MERF (figures 3-10 and 3-12). Those findings in addition to the absence of captopril-LTD in the presence of naloxone supports an opioid receptor-dependent mechanism. Indeed, captopril-LTD was abolished in mice lacking MOR ($Oprm1^{-/-}$) and preserved in wildtype littermates ($Oprm1^{+/+}$) (figure 4-11).

4.3 In Vivo Approaches

Thus far, results from LC-MS/MS and electrophysiology experiments have demonstrated that ACE inhibition reduces excitatory synaptic input onto D1-MSNs in a MERF-dependent manner mediated through MOR activation. To complement these analyses, we used *in vivo* fiber photometry to evaluate calcium activity in accumbal D1-MSNs in response to optogenetic stimulation of medial prefrontal inputs before and after systemic captopril administration (30 mg/kg, i.p.; figure 4-12 A-B). There was a dose-response effect of light pulse number on D1-MSN GCaMP responses (figure 4-12 C-E) that was modulated by captopril as seen by a decrease in fluorescence signal, and ultimately a decrease in slope of the optogenetic input-output curve following captopril injection relative to saline baseline (figure 4-12 F-I).

Since the rewarding effects of additive drugs are driven by D1-MSN activity and strengthening of excitatory synaptic input [32,35,89,246], we used an unbiased place conditioning assay to determine if systemic captopril administration can counteract the rewarding properties of fentanyl (figure 4-13 A). Mice exhibited robust conditioned place preference (CPP) for a fentanyl-paired context (0.04 mg/kg, s.c.), but the magnitude of CPP on test day was significantly attenuated when captopril (30 mg/kg, i.p.) was injected prior to fentanyl during the three preceding conditioning days (figure 4-13 B-C). A similar effect was observed in a separate cohort of mice that received trandolapril (5 mg/kg, s.c.), the prodrug form of trandolaprilat, prior to fentanyl conditioning days (figure 4-14). Captopril itself was not rewarding or aversive when probing for preference on test day after mice were given either saline or captopril (30 mg/kg, i.p.) throughout conditioning (figure 4-15). Similarly, captopril, whether delivered prior to fentanyl or alone, did not acutely alter locomotion during conditioning or have a lasting impact on locomotion on test day (figure 4-16).

Altered MOR signaling in the NAc has been shown to modulate social behavior in mice [226]. Because ACE inhibition enhances MOR signaling via MERF, we tested if systemic

administration of captopril can also impact mice behavior in a social interaction test between two freely moving mice. Captopril increased the overall amount of social interaction including instances of reciprocal huddling and nose-to-nose interactions as well as social exploration of each other (figure 4-17). These findings are consistent with enhanced MOR signaling in the NAc [247] and rules out a general disruption of motivated behavior.

In summary, these findings from LC-MS/MS and electrophysiology studies demonstrated that ACE inhibition increased endogenous MERF levels which underlies enhanced MOR signaling at presynaptic glutamatergic terminals specifically onto accumbal D1-MSNs. This mechanism can be extended to behavioral studies that show attenuated fentanyl-conditioned place preference and increased social interaction without a general disruption in motivation. Next, we will conclude with a discussion on these results, future directions, and the potential impact of these findings.

Table 4-1

	CONCENTRATION (pM)				
PEPTIDE	*aCSF*	*+KCl*	*+Captopril*	*+Bestatin +Thiorphan*	*+Bestatin +Thiorphan +Captopril*
MERF	291 ± 52	446 ± 28	1142 ± 138	737 ± 188	1994 ± 578
Met-Enk	775 ± 311	9001 ± 2389	6297 ± 958	15016 ± 4683	17252 ± 4882
Leu-Enk	295 ± 112	4087 ± 878	3123 ± 433	13586 ± 3242	13015 ± 3150
Dynorphin A (1-8)	519 ± 8	692 ± 35	812 ± 47	1066 ± 89	1055 ± 78
Dynorphin B	509 ± 34	734 ± 62	905 ± 78	1677 ± 165	1599 ± 155
Substance P	259 ± 64	1709 ± 245	1606 ± 242	6840 ± 1645	7082 ± 1313

Table 4-1. Peptidase inhibitors reveal double dissociation between MERF and conventional enkephalins using LC-MS/MS. Absolute quantification of neuropeptides from Figure 2B-C (n=8) showing elevated levels of MERF only when the ACE inhibitor captopril (10 μM) is present and elevated levels of Met- and Leu-Enkephalin only when the aminopeptidase N inhibitor bestatin (10 μM) plus neprilysin inhibitor thiorphan (1 μM) are present. Data are mean ± s.e.m.

Table 4-2

	CONCENTRATION (pM)			
	Cre-		**ChR2**	
PEPTIDE	*aCSF*	*+Captopril*	*aCSF*	*+Captopril*
MERF	173 ± 2	183 ± 7	182 ± 4	270 ± 15
Met-Enk	205 ± 30	218 ± 31	614 ± 91	710 ± 110
Leu-Enk	122 ± 14	127 ± 12	391 ± 49	452 ± 52
Dynorphin A (1-8)	340 ± 3	344 ± 3	326 ± 12	333 ± 10

Table 4-2. Captopril selectively increases extracellular MERF levels following optogenetic stimulation of D2-MSNs. Absolute quantification of neuropeptides from Figure 2E-F in control (Cre-, *n*=4) and ChR2-expressing slices (*n*=7) following 10 min optogenetic stimulation (20 Hz, 5 ms pulse width) in the presence or absence of captopril (10 μM). Data are mean ± s.e.m.; each mean is comprised of 4-7 biological replicates; each biological replicate is calculated by averaging quantified neuropeptides from 4 individually stimulated slices per brain hemisphere (i.e. 4 technical replicates).

Figure 4-1

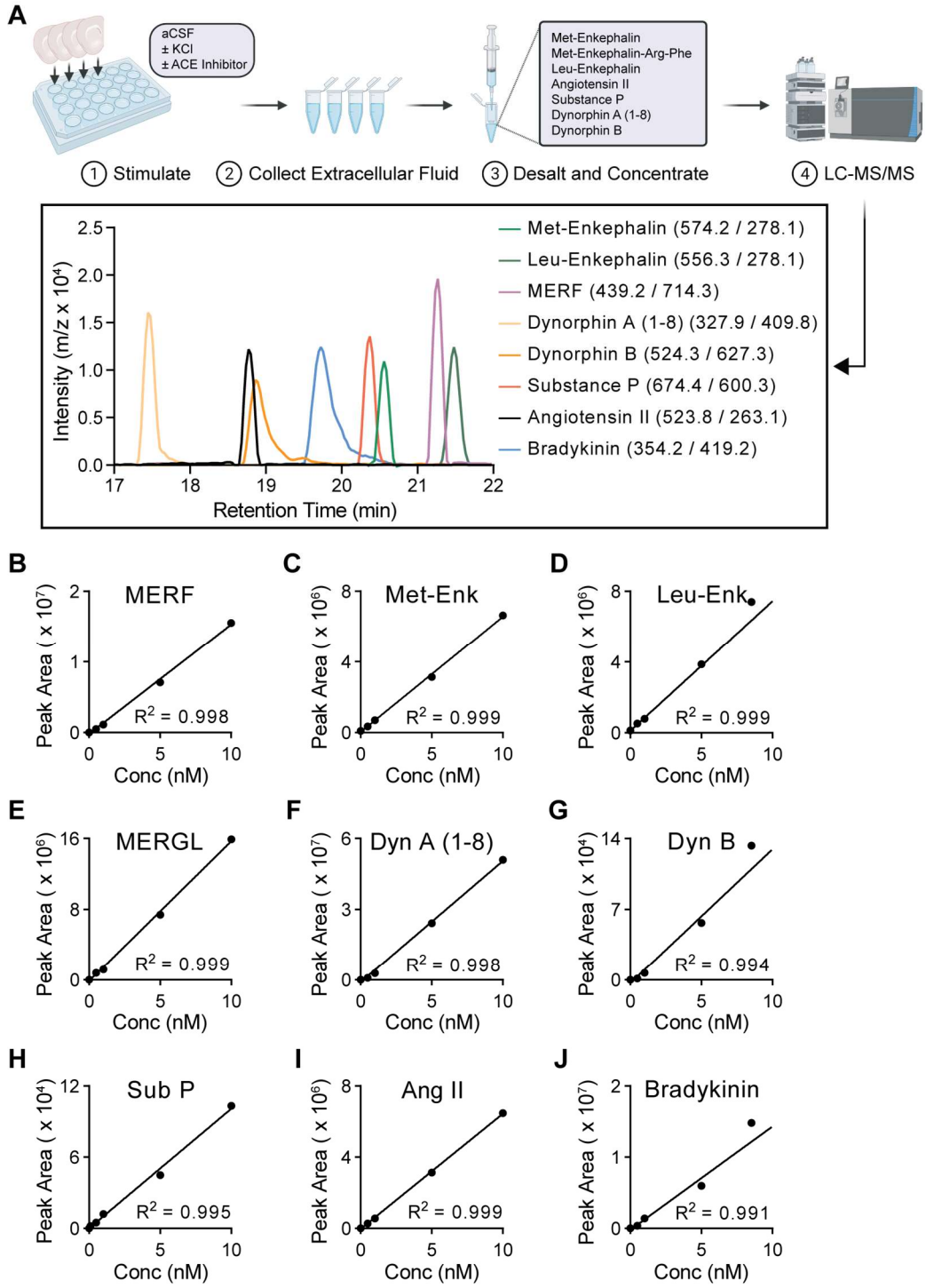
A
aCSF
± KCl
± ACE Inhibitor
Met-Enkephalin
Met-Enkephalin-Arg-Phe
Leu-Enkephalin
Angiotensin II
Substance P
Dynorphin A (1-8)
Dynorphin B
1 Stimulate
2 Collect Extracellular Fluid
3 Desalt and Concentrate
4 LC-MS/MS
Intensity (m/z x 10⁴)
Retention Time (min)
Met-Enkephalin (574.2 / 278.1)
Leu-Enkephalin (556.3 / 278.1)
MERF (439.2 / 714.3)
Dynorphin A (1-8) (327.9 / 409.8)
Dynorphin B (524.3 / 627.3)
Substance P (674.4 / 600.3)
Angiotensin II (523.8 / 263.1)
Bradykinin (354.2 / 419.2)
B MERF R² = 0.998
C Met-Enk R² = 0.999
D Leu-Enk R² = 0.999
E MERGL R² = 0.999
F Dyn A (1-8) R² = 0.998
G Dyn B R² = 0.994
H Sub P R² = 0.995
I Ang II R² = 0.999
J Bradykinin R² = 0.991
Peak Area
Conc (nM)

Figure 4-1. Nanoflow liquid chromatography-tandem mass spectrometry can be used for targeted neuropeptide identification and quantification. (**A**) Top, experimental workflow to quantify neuropeptide release from brain slices using LC-MS/MS. Bottom, example reconstructed chromatogram showing typical retention time and SRM transition (precursor / product) that produces the largest integrated peak area (out of five different transitions per peptide, not shown) which is used for peptide quantification. (**B-J**) Calibration curves for each peptide (10 pM, 50 pM, 100 pM, 500 pM, 1 nM, 5 nM, and 10 nM, black dots) extrapolated from standards containing mixture of all peptides.

Figure 4-2

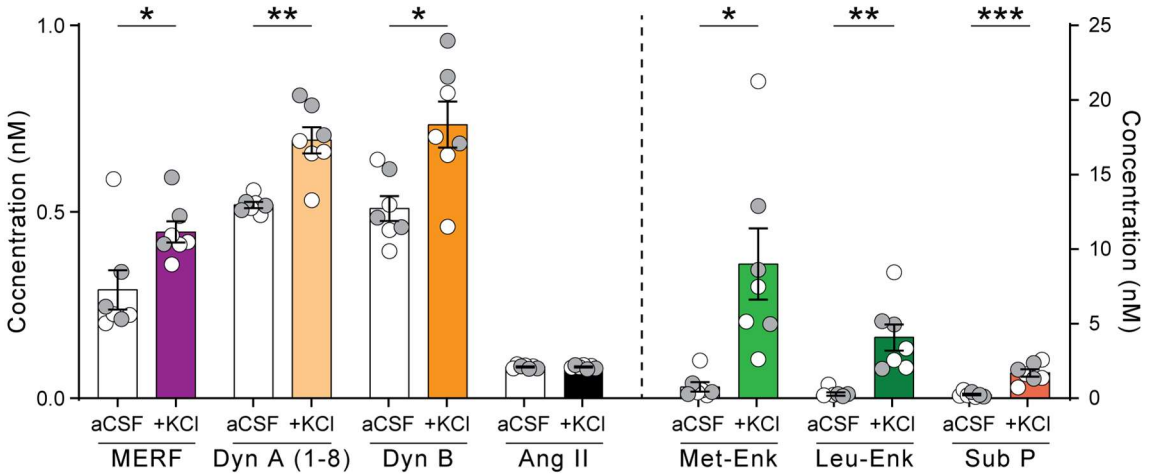

Figure 4-2. High extracellular [K+] induces release of endogenous neuropeptides. Quantification of extracellular neuropeptide concentrations from slices submerged in normal aCSF or aCSF with 50 mM KCl. Data are mean ± s.e.m. for all panels; open and closed circles indicate samples from female and male mice, respectively. **P*<0.05, ***P*<0.01, ****P*<0.001, ANOVA followed by simple effect test (B); see Appendix A for complete statistics.

Figure 4-3

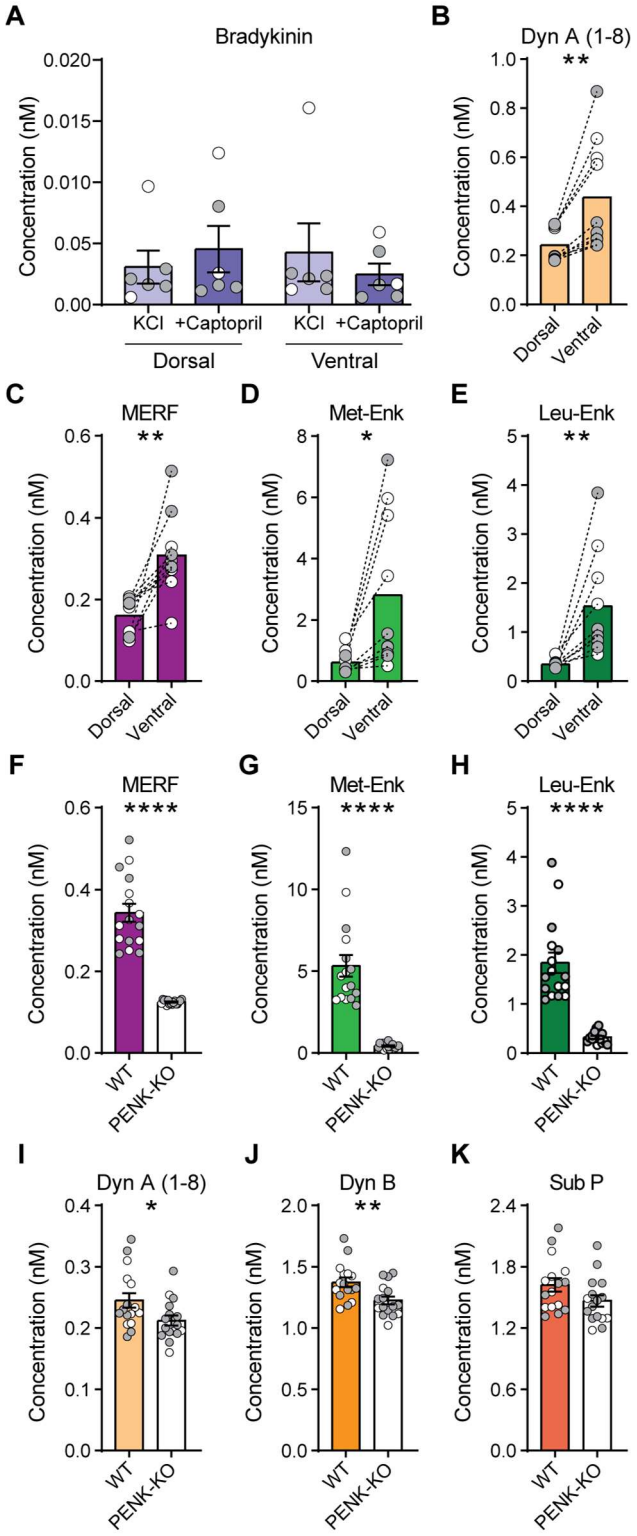
A
Bradykinin
Concentration (nM)
0.020
0.015
0.010
0.05
0.00
KCl
+Captopril
KCl
+Captopril
Dorsal
Ventral
B
Dyn A (1-8)
**
Concentration (nM)
1.0
0.8
0.6
0.4
0.2
0.0
Dorsal
Ventral
C
MERF
**
Concentration (nM)
0.6
0.4
0.2
0.0
Dorsal
Ventral
D
Met-Enk
*
Concentration (nM)
8
6
4
2
0
Dorsal
Ventral
E
Leu-Enk
**
Concentration (nM)
5
4
3
2
1
0
Dorsal
Ventral
F
MERF
****
Concentration (nM)
0.6
0.4
0.2
0.0
WT
PENK-KO
G
Met-Enk
****
Concentration (nM)
15
10
5
0
WT
PENK-KO
H
Leu-Enk
****
Concentration (nM)
5
4
3
2
1
0
WT
PENK-KO
I
Dyn A (1-8)
*
Concentration (nM)
0.4
0.3
0.2
0.1
0.0
WT
PENK-KO
J
Dyn B
**
Concentration (nM)
2.0
1.5
1.0
0.5
0.0
WT
PENK-KO
K
Sub P
Concentration (nM)
2.4
1.8
1.2
0.6
0.0
WT
PENK-KO

Figure 4-3. Neuropeptide quantification by LC-MS/MS is sensitive to regional and genetic effects. (**A**) Quantification of extracellular bradykinin from dorsal and ventral striatum (nucleus accumbens) tissue punches (*n*=6) after submersion in aCSF containing 50 mM KCl with and without captopril (10 μM). (**B-E**) Extracellular levels of Dynorphin A (1-8), MERF, Met-enkephalin, and Leu-enkephalin from ventral striatum and dorsal striatum tissue punches after submersion in aCSF with 50 mM KCl (*n*=10). (**F-K**) Quantification of neuropeptides after KCl stimulation of individual striatal slices from constitutive Penk knockout mice ($Penk^{-/-}$, *n*=16, white bars) compared to wildtype littermates ($Penk^{+/+}$, *n*=16, color bars) to validate specificity and sensitivity of SRM-based targeted proteomic quantification for endogenous enkephalin peptides. Data are mean ± s.e.m. for all panels; open and closed circles indicate samples from female and male mice, respectively. *P<0.05, **P<0.01, ****P<0.0001, two-sample t-test (B-K); see Appendix A for complete statistics.

Figure 4-4

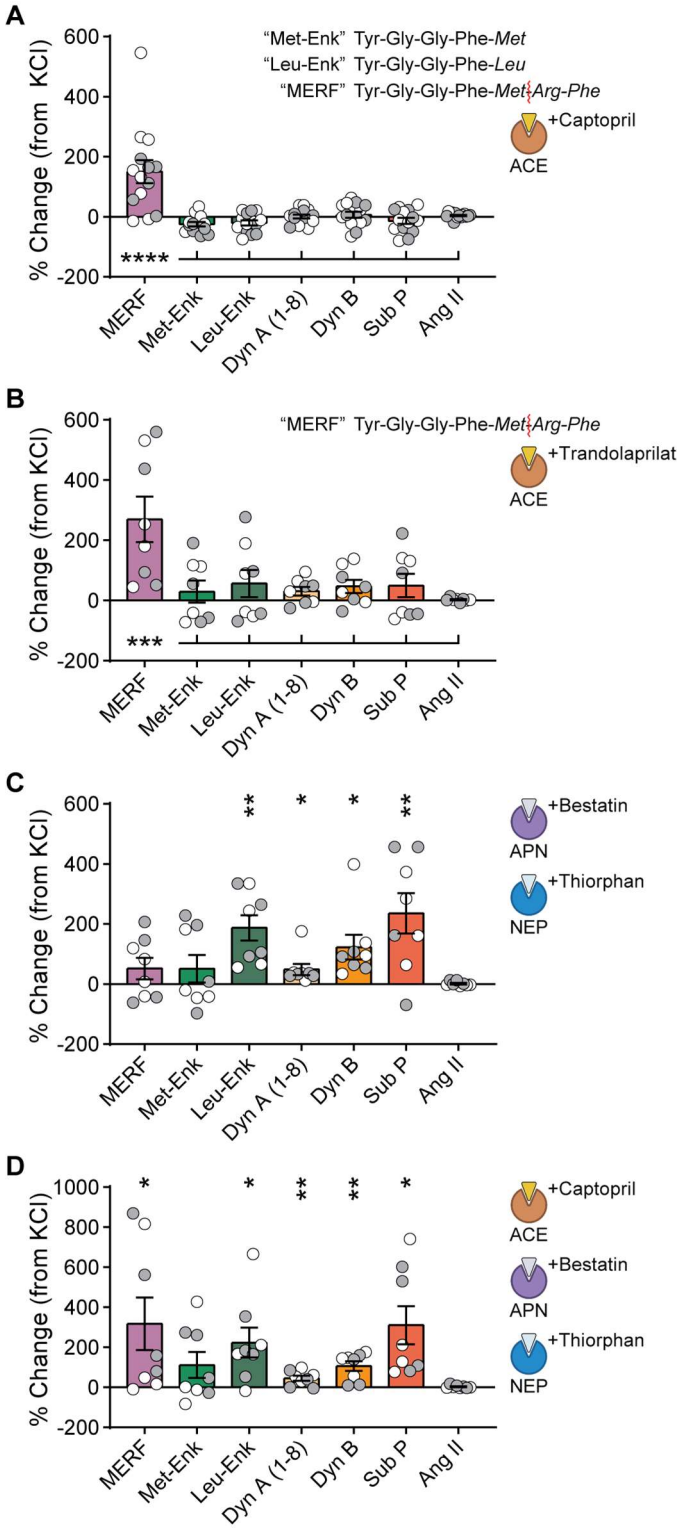
A
"Met-Enk" Tyr-Gly-Gly-Phe-Met
"Leu-Enk" Tyr-Gly-Gly-Phe-Leu
"MERF" Tyr-Gly-Gly-Phe-Met-Arg-Phe
+Captopril
ACE
% Change (from KCl)
600
400
200
0
-200
****
MERF
Met-Enk
Leu-Enk
Dyn A (1-8)
Dyn B
Sub P
Ang II
B
"MERF" Tyr-Gly-Gly-Phe-Met-Arg-Phe
+Trandolaprilat
ACE
***
C
+Bestatin
APN
+Thiorphan
NEP
D
1000
800
+Captopril
ACE
+Bestatin
APN
+Thiorphan
NEP

Figure 4-4. Peptidase inhibitors reveal double dissociation between MERF and conventional enkephalins using LC-MS/MS. (**A-D**) Percent change in extracellular neuropeptide levels after KCl stimulation in presence versus absence of 10 μM captopril (A), 1 μM trandolaprilat (B, the active form of the lipophilic ACE inhibitor trandolapril), 10 μM bestatin plus 1 μM thiorphan (C), or a cocktail of captopril, bestatin, and thiorphan (D). A cocktail of all peptidase inhibitors demonstrates additive effects from samples exposed to captopril alone in (A) and combined bestatin plus thiorphan in (C). Inset shows enkephalin amino acid sequences and site of enzymatic cleavage of MERF by ACE (red line). Data are mean ± s.e.m. for all panels; open and closed circles indicate samples from female and male mice, respectively. *P<0.05, **P<0.01, ***P<0.001, ****P<0.0001, ANOVA followed by Fisher's LSD post-hoc test (A, B) or one-sample *t*-test (C, D); see Appendix A for complete statistics.

Figure 4-5

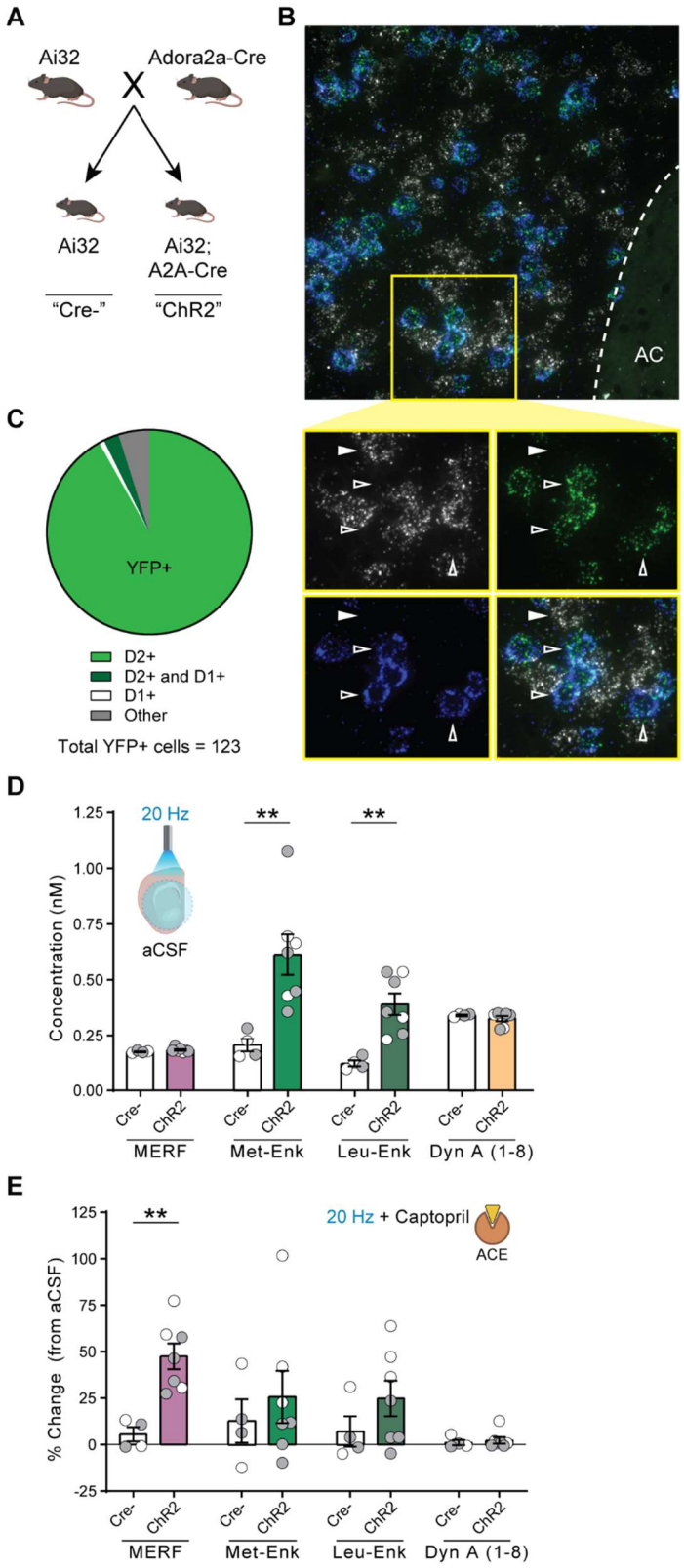
A
Ai32
Adora2a-Cre
X
Ai32
Ai32;
A2A-Cre
"Cre-"
"ChR2"
B
AC
C
YFP+
D2+
D2+ and D1+
D1+
Other
Total YFP+ cells = 123
D
20 Hz
aCSF
Concentration (nM)
1.25
1.00
0.75
0.50
0.25
0.00
**
**
Cre-
ChR2
MERF
Met-Enk
Leu-Enk
Dyn A (1-8)
E
20 Hz + Captopril
ACE
% Change (from aCSF)
125
100
75
50
25
0
-25
**
Cre-
ChR2
MERF
Met-Enk
Leu-Enk
Dyn A (1-8)

Figure 4-5. Captopril selectively increases extracellular MERF levels following optogenetic stimulation of D2-MSNs. (**A**) Breeding strategy to generate mice expressing channelrhodopsin-2 in D2-MSNs. (**B**) Top, fluorescent *in situ* hybridization image of nucleus accumbens core with hybridizing probes against Drd1 (white, D1-MSNs), Drd2 (green, D2-MSNs), and eYFP (blue, fused to ChR2 in the Ai32 allele). Abbreviation: AC, anterior commissure. Bottom, zoomed image of area shown in yellow box. ChR2-positive cells (blue) colocalize with Drd2-positive cells (green, open arrows) but not Drd1-positive cells (white, closed arrows). (**C**) Quantification of cells in nucleus accumbens core colocalized with eYFP. Cell counts were conducted in tissue from two mice. (**D**) Extracellular neuropeptide levels from slices following optogenetic stimulation at 20 Hz. (**E**) Percent change in extracellular neuropeptide levels after optogenetic stimulation in presence versus absence of captopril (10 μM). Data are mean ± s.e.m. for all panels; open and closed circles indicate samples from female and male mice, respectively. $^{**}P<0.01$, ANOVA followed by simple effect test (D, E); see Appendix A for complete statistics.

Figure 4-6

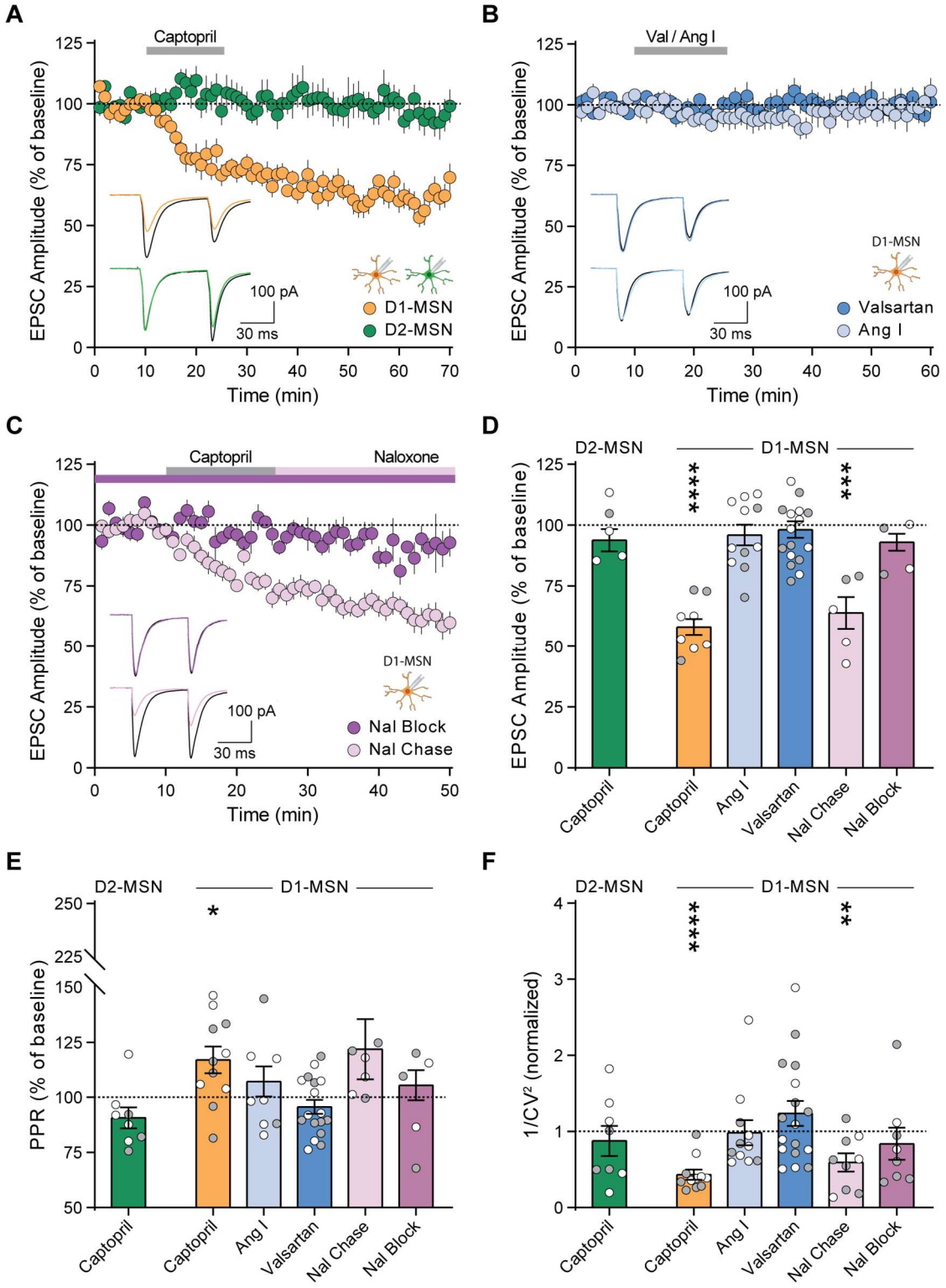
A
Captopril
EPSC Amplitude (% of baseline)
Time (min)
100 pA
30 ms
D1-MSN
D2-MSN
B
Val / Ang I
D1-MSN
Valsartan
Ang I
C
Captopril
Naloxone
D1-MSN
Nal Block
Nal Chase
D
D2-MSN
D1-MSN
****
***
Captopril
Captopril
Ang I
Valsartan
Nal Chase
Nal Block
E
PPR (% of baseline)
*
F
1/CV² (normalized)
**

Figure 4-6. ACE inhibition reduces excitatory input to D1-MSNs via endogenous opioid signaling. (**A-C**) EPSC amplitude before, during, and after 15 min bath perfusion (grey bar) of 10 μM captopril in D1-MSNs (orange, *n*=11) or D2-MSNs (green, *n*=8) (A); AT1R antagonist valsartan (dark blue, 2 μM *n*=8 and 20 μM *n*=9) or angiotensin I peptide (1 μM, light blue, *n*=11) in D1-MSNs (B); or captopril (10 μM) in continual presence of opioid receptor antagonist naloxone (10 μM, dark purple, *n*=8) or chased by naloxone (10 μM, light purple, *n*=9) in D1-MSNs (C). Bottom-left insets show traces before (black lines) and after (last 5 min of recording, colored lines). (**D-F**) EPSC parameters during the last 5 min of each recording, expressed as percentage of baseline prior to drug application: EPSC amplitude (D), paired-pulse ratio (E), and $1/CV^2$ (F). Data are mean ± s.e.m. for all panels; open and closed circles indicate recordings from female and male mice, respectively. **P*<0.05, ***P*<0.01, ****P*<0.001, *****P*<0.0001, ANOVA followed by one-sample *t*-test versus baseline; see Appendix A for complete statistics.

Figure 4-7

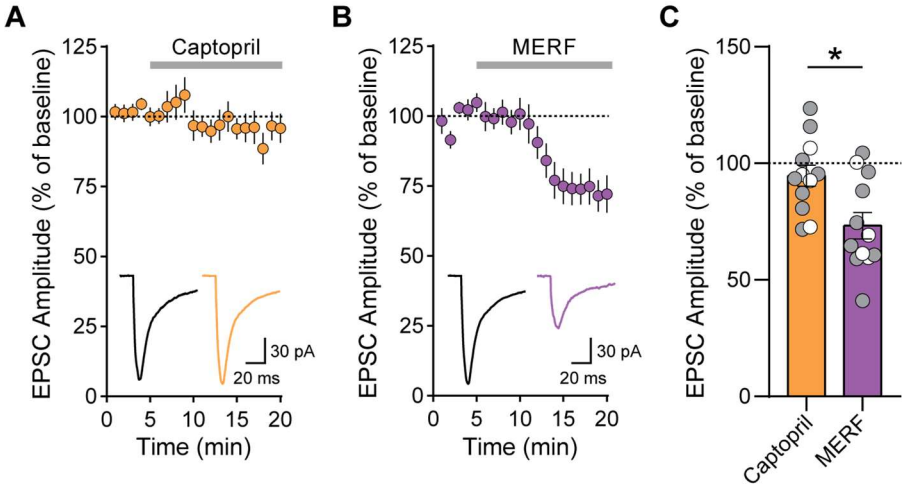

Figure 4-7. Excitatory input to layer V pyramidal neurons in anterior cingulate cortex is reduced by MERF but not captopril. (**A-B**) Time course of evoked ESPC amplitude before and during 15 min bath perfusion (grey bar) of 10 µM captopril (A) and 1 µM MERF (B) from the same cell (*n*=12). Inset show traces during baseline, captopril, and MERF bath perfusion. (**C**) Average EPSC amplitude in the last 5 min of each drug perfusion. Data are mean ± s.e.m. for all panels; open and closed circles indicate recordings from female and male mice, respectively. **P*<0.05, ANOVA treatment main effect (C); see Appendix A for complete statistics.

Figure 4-8

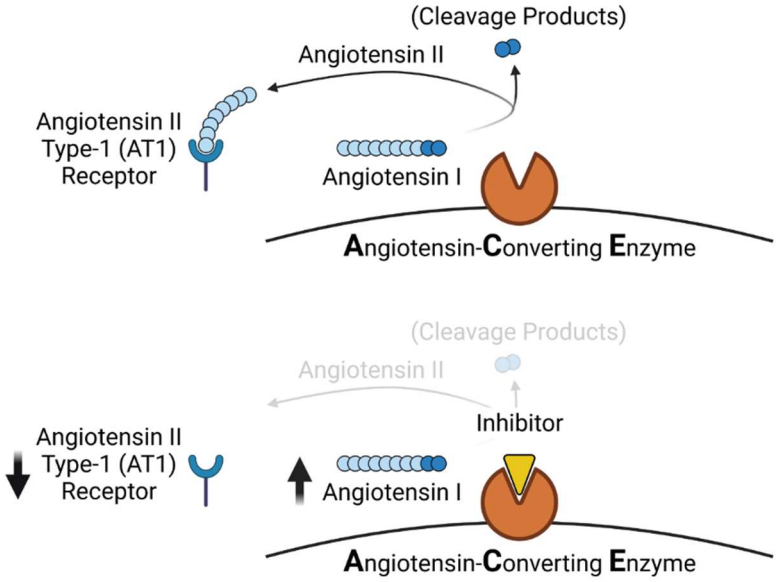

Figure 4-8. Schematic of angiotensin regulation by ACE. (**A**) ACE converts Angiotensin I peptide into Angiotensin II peptide which activates AT1R. (**B**) ACE inhibitors block Angiotensin II conversion resulting in elevated Angiotensin I peptide levels and hypoactivation of AT1R.

Figure 4-9

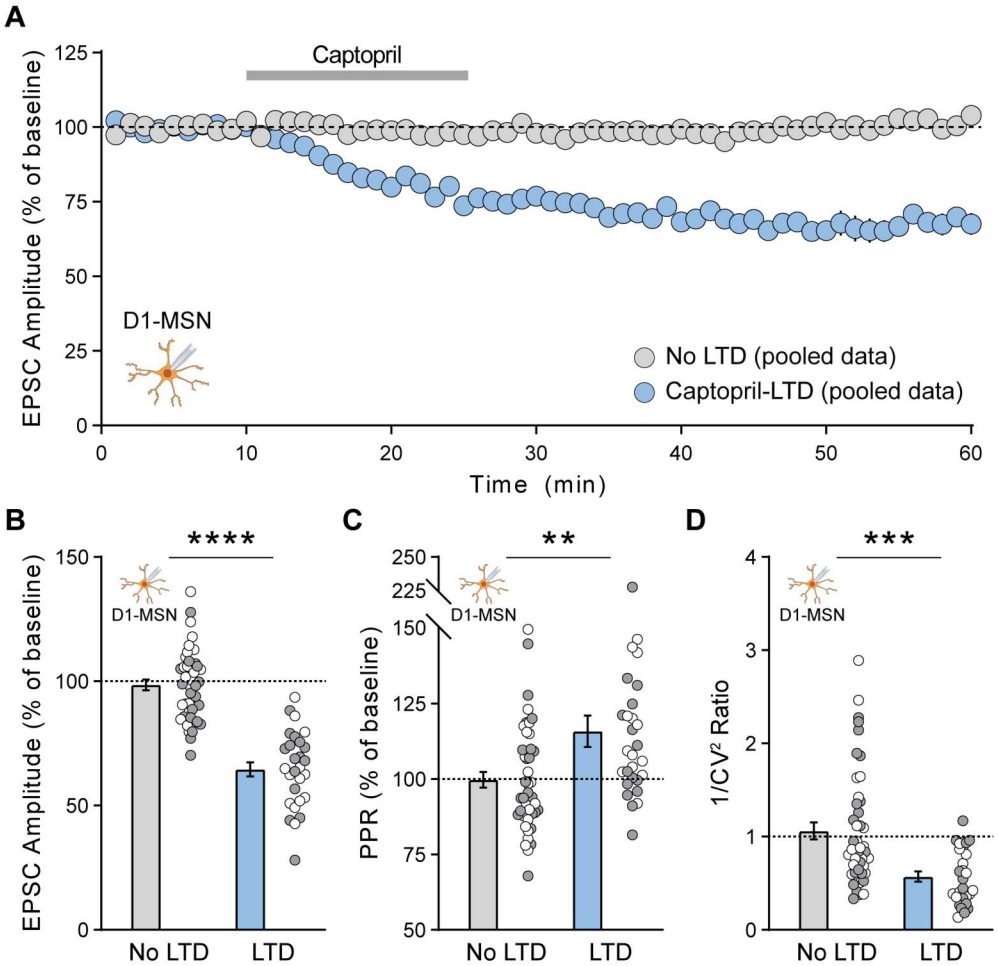

Figure 4-9. Captopril-LTD in D1-MSNs occurs via a presynaptic mechanism. (**A**) Time course of captopril-LTD from pooled LTD (*n*=28) and control (*n*=45) data sets. (**B-D**) EPSC parameters averaged in the last 5 min of each recording: EPSC amplitude (B)**,** paired-pulse ratio (C)**,** and inverse of squared-coefficient of variation (D). Pooled data includes recordings from D1-MSNs seen in Figure 4-6 and Figure 4-11. Data are mean ± s.e.m. for all panels; open and closed circles indicate recordings from female and male mice, respectively. ***P*<0.01, ****P*<0.001, *****P*<0.0001, ANOVA LTD main effect (B, C, D); see Appendix A for complete statistics.

Figure 4-10

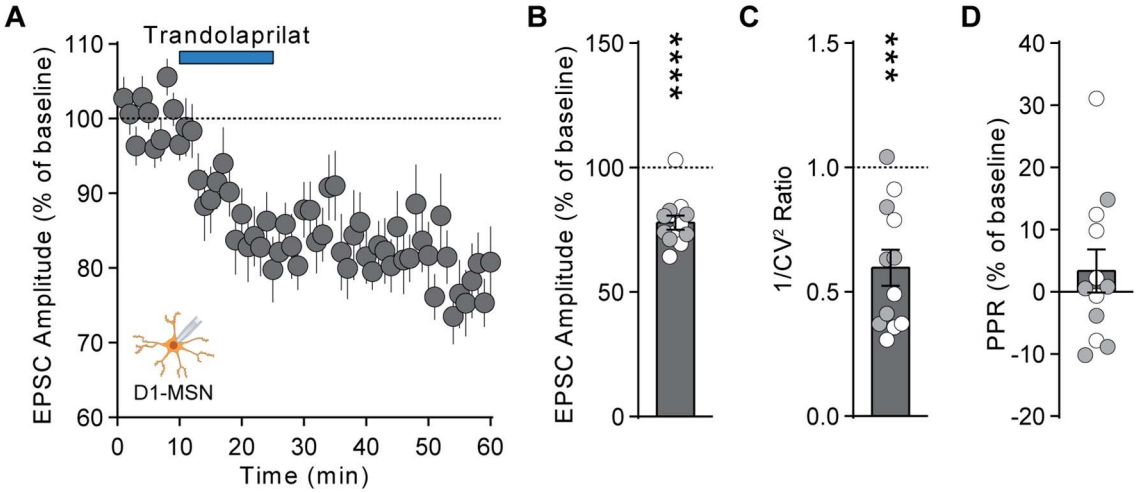

Figure 4-10. Trandolaprilat causes long-term depression of presynaptic excitatory synaptic transmission onto D1-MSNs. (**A**) Time course of EPSC amplitude before, during, and after 15 min bath perfusion (blue bar) of 1 μM trandolaprilat in D1-MSNs (*n*=12). (**B-D**) EPSC parameters during last 5 min of recording in (A) expressed as percentage of baseline prior to drug application: EPSC amplitude (B), $1/CV^2$ (C), and paired-pulse ratio (D). Data are mean ± s.e.m. for all panels; open and closed circles indicate recordings from female and male mice, respectively. ***P<0.001, ****P<0.0001, one-sample *t*-test (B, C); see Appendix A for complete statistics.

Figure 4-11

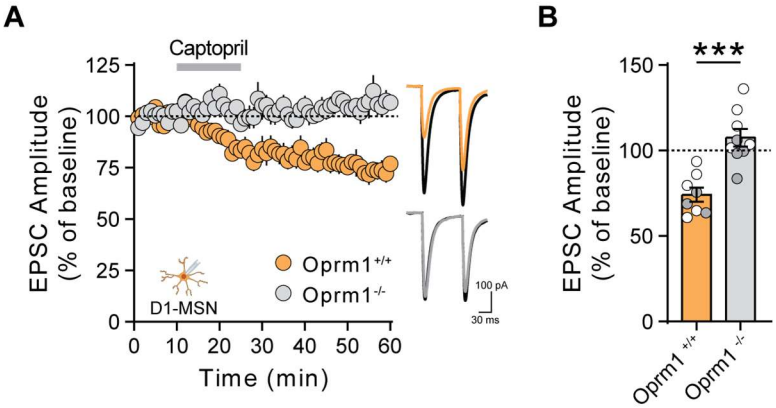

Figure 4-11. μ-Opioid receptors are necessary for Captopril-LTD. (**A, B**) EPSC amplitude time course (A) or average during last 5 min (B) of captopril-LTD in constitutive MOR knockout mice (Oprm1$^{-/-}$, grey, *n*=9) and wildtype littermates (Oprm1$^{+/+}$, orange, *n*=8). Inset show traces before captopril (black lines) and during last 5 min (color lines). Data are mean ± s.e.m. for all panels; open and closed circles indicate recordings from female and male mice, respectively. ***P<0.001, ANOVA genotype main effect (B); see Appendix A for complete statistics.

Figure 4-12

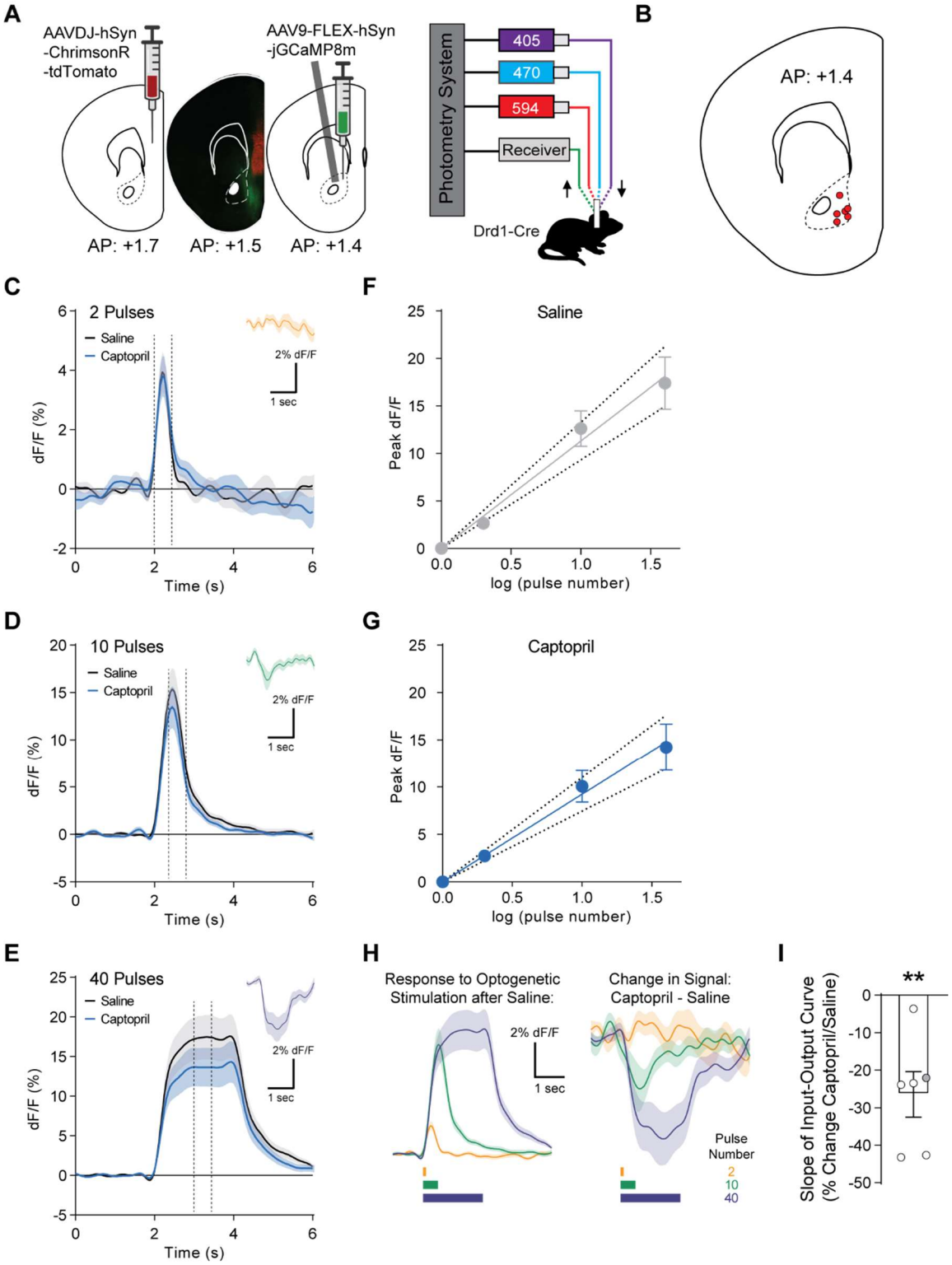
A
AAVDJ-hSyn
-ChrimsonR
-tdTomato
AAV9-FLEX-hSyn
-jGCaMP8m
AP: +1.7
AP: +1.5
AP: +1.4
Photometry System
405
470
594
Receiver
Drd1-Cre
B
AP: +1.4
C
2 Pulses
Saline
Captopril
2% dF/F
1 sec
dF/F (%)
Time (s)
D
10 Pulses
Saline
Captopril
2% dF/F
1 sec
dF/F (%)
Time (s)
E
40 Pulses
Saline
Captopril
2% dF/F
1 sec
dF/F (%)
Time (s)
F
Saline
Peak dF/F
log (pulse number)
G
Captopril
Peak dF/F
log (pulse number)
H
Response to Optogenetic
Stimulation after Saline:
2% dF/F
1 sec
Change in Signal:
Captopril - Saline
Pulse
Number
2
10
40
I
Slope of Input-Output Curve
(% Change Captopril/Saline)
**

Figure 4-12. Captopril reduces GCaMP signal from D1-MSNs in response to optogenetic stimulation of medial prefrontal cortex inputs *in vivo*. (**A**) Left, schematic showing viral injection of ChrimsonR-tdTomato in mPFC and Cre-dependent GCaMP8m in NAc, separated by fluorescent image showing viral expression. Right, setup for simultaneous optogenetic stimulation (594 nm) and fiber photometry recording (405/470 nm). (**B**) Placement of fiberoptic ferrule in mice (*n*=6) used for photometry experiments. (**C-E**) Traces showing average evoked GCaMP response (*n*=6) to 2 (C), 10 (D), and 40 pulses (E) of red light at 20 Hz after injection of saline (black) or captopril (blue, 30 mg/kg, i.p.). Dotted lines demarcate the time window for analysis of peak dF/F. Inset shows average change in response after captopril relative to saline. (**F-G**) Input-output curve for optogenetic stimulation pulse number against average peak dF/F (%) of evoked responses following saline injection (F) and captopril injection (G). (**H**) Traces showing average response to 2, 10, and 40 pulses of red light at 20 Hz after injection of saline (left), and average change in response following injection of captopril (right). (**I**) Percent change in slope of the input-output curve following injection of captopril versus saline (*n*=6). Data are mean ± s.e.m. for all panels; open and closed circles in (I) indicate female and male mice, respectively. **P<0.01, one-sample t-test (I); see Appendix A for complete statistics.

Figure 4-13

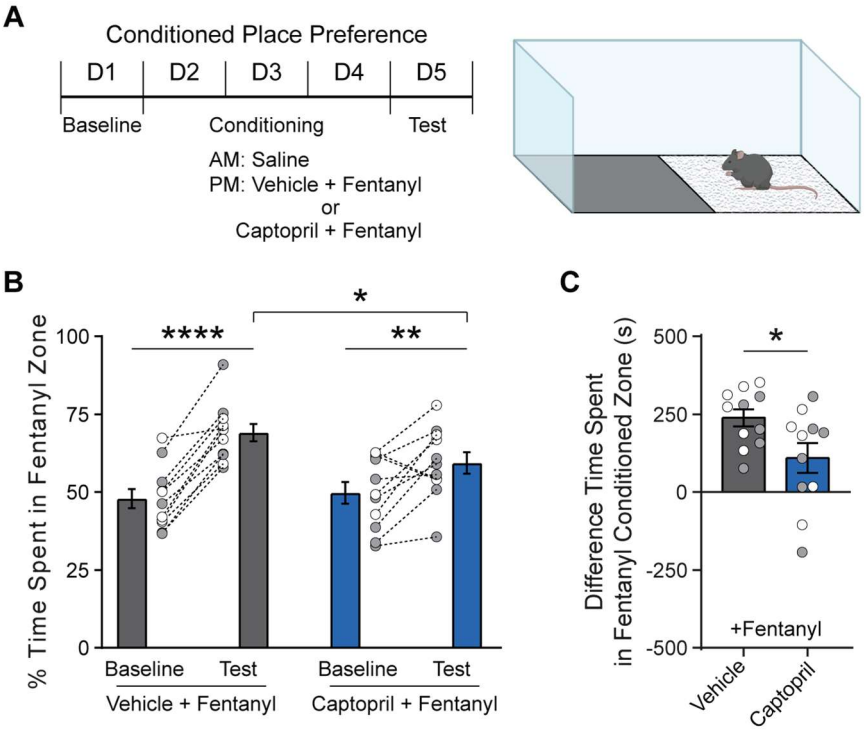

Figure 4-13. Captopril attenuates fentanyl-conditioned place preference. (**A**) Schematic of unbiased place conditioning procedure. (**B**) Percent time in fentanyl zone on Day 1 (baseline) and Day 5 (test) for groups receiving fentanyl (0.04 mg/kg, s.c.) preceded by vehicle (*n*=11, dark grey) or fentanyl preceded by captopril (30 mg/kg, i.p.; *n*=11, dark blue). (**C**) CPP score calculated as time spent in fentanyl zone on Day 5 minus Day 1. Data are mean ± s.e.m. for all panels; open and closed circles indicate female and male mice, respectively. *P<0.05, **P<0.01, ****P<0.0001, ANOVA followed by simple effect test of session and treatment (B), and ANOVA treatment main effect (C); see Appendix A for complete statistics.

Figure 4-14

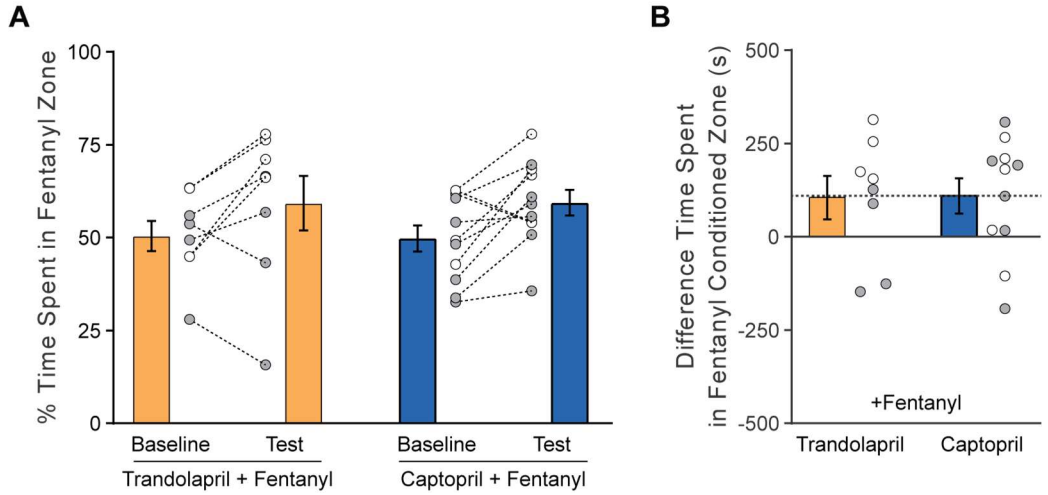

Figure 4-14. Trandolapril and captopril attenuate fentanyl CPP to a similar extent. (**A-B**) Percent time in fentanyl zone during baseline and test sessions (A) and CPP score (B) for groups receiving fentanyl (0.04 mg/kg, s.c.) preceded by the lipophilic ACE inhibitor trandolapril (5 mg/kg, s.c.; *n*=8, orange) or prototypical ACE inhibitor captopril (30 mg/kg, i.p.; *n*=11, blue). Captopril data from Figure 4-13 are reproduced here for comparison with the effect of trandolapril. Data are mean ± s.e.m. for all panels; open and closed circles indicate female and male mice, respectively.

Figure 4-15

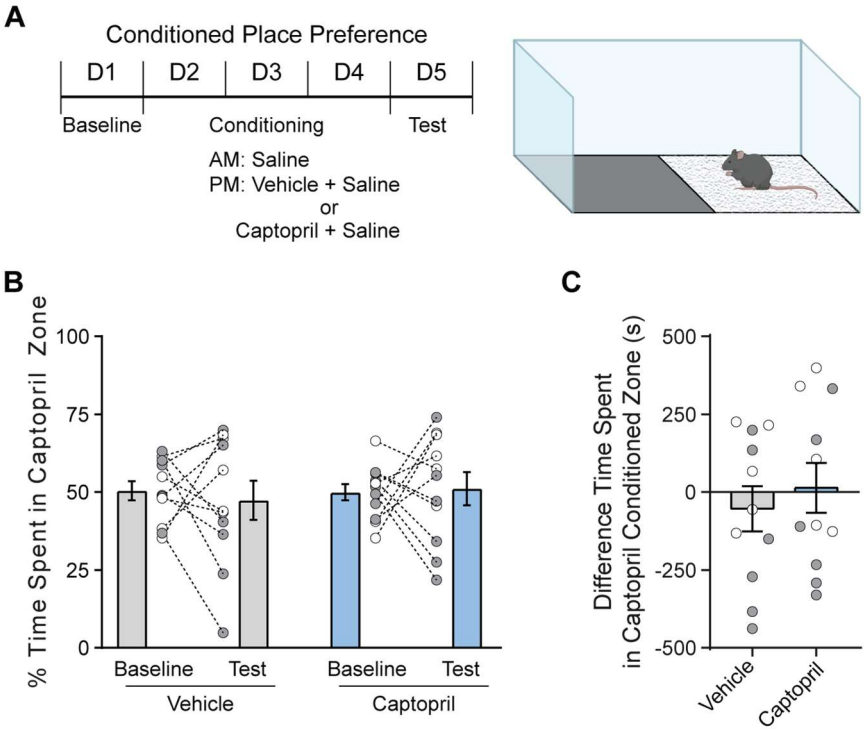

Figure 4-15. Captopril does not induce conditioned place preference or aversion. (**A**) Schematic of unbiased place conditioning procedure. (**B**) Percent time in captopril zone on Day 1 (baseline) and Day 5 (test) for groups receiving saline preceded by vehicle (*n*=11, grey) or saline preceded by captopril (30 mg/kg, i.p.; *n*=11, blue). (**C**) CPP score calculated as time spent in captopril zone on Day 5 minus Day 1. Data are mean ± s.e.m. for all panels; open and closed circles indicate female and male mice, respectively. See Appendix A for complete statistics.

Figure 4-16

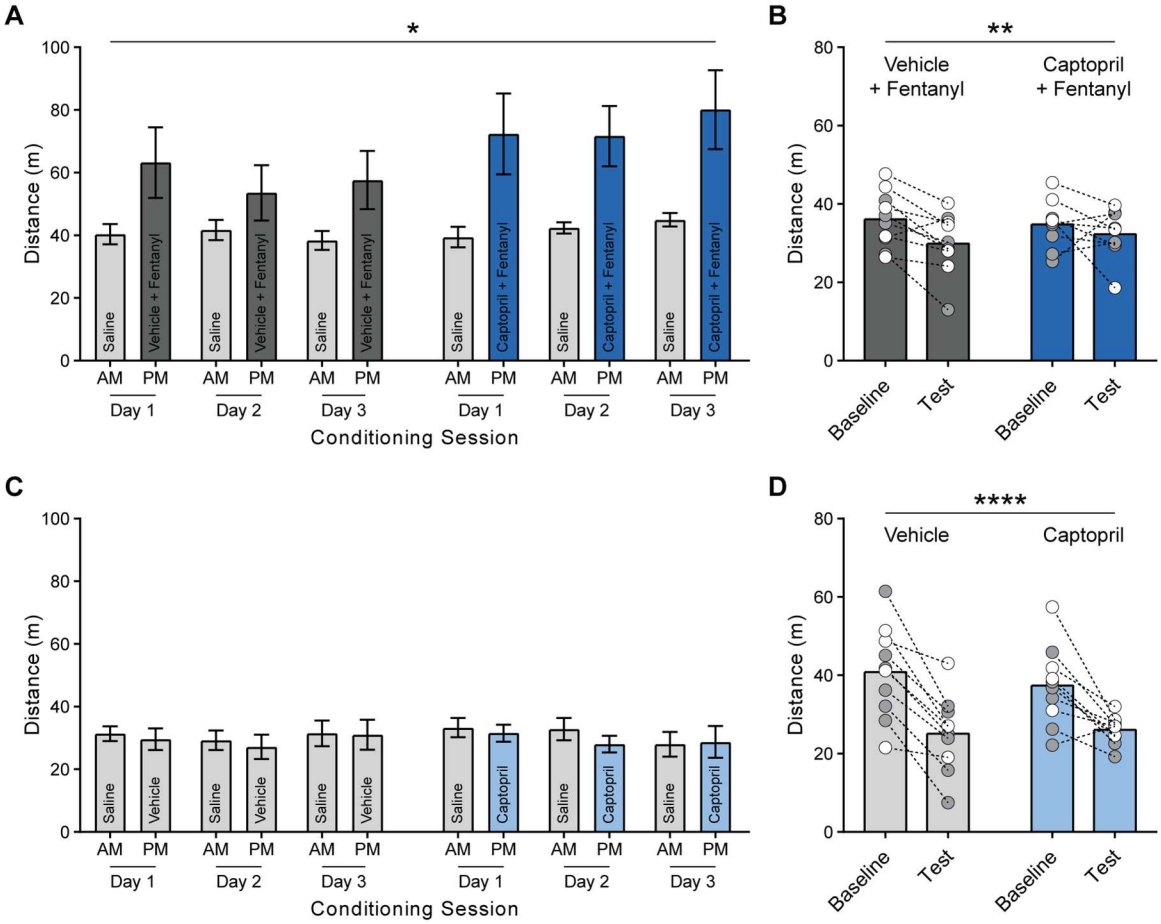

Figure 4-16. Captopril does not alter locomotion. (**A**, **B**) Total ambulatory distance of mice receiving vehicle plus fentanyl (0.04 mg/kg, s.c.; *n*=10) or captopril (30 mg/kg, i.p.) plus fentanyl (*n*=9) throughout unbiased place conditioning assay during conditioning sessions (A) and on baseline and test day (B). (**C**, **D**) Total ambulatory distance of mice receiving vehicle (*n*=10) or captopril (*n*=10) throughout unbiased place conditioning assay during conditioning sessions (C) and on baseline and test day (D). Data are mean ± s.e.m. for all panels; open and closed circles indicate female and male mice, respectively. **P*<0.05, ***P*<0.01, *****P*<0.0001, ANOVA time main effect (A, B, D); see Appendix A for complete statistics.

Figure 4-17

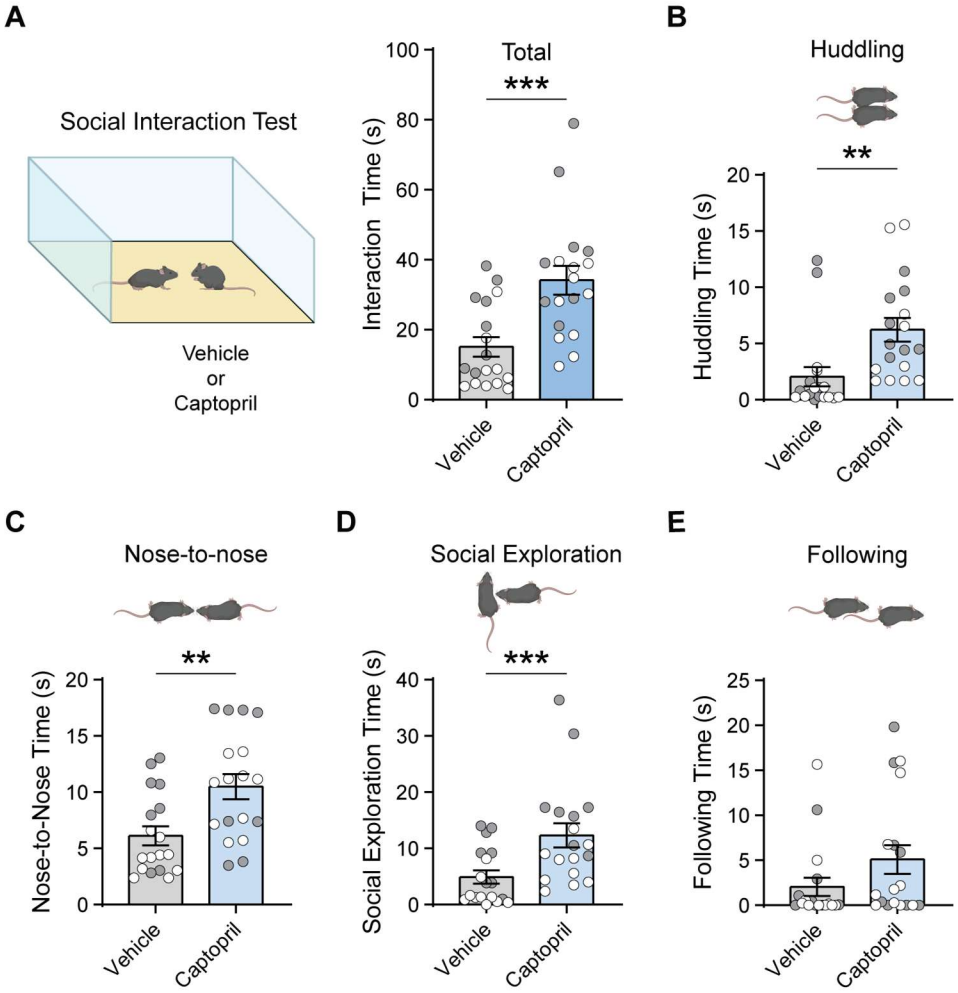

Figure 4-17. Captopril increases social interaction between mice. (**A**) Left, schematic of reciprocal social interaction test following injection of vehicle or captopril (30 mg/kg, i.p.). Right, total social interaction time after captopril (*n*=18, blue) or vehicle (*n*=18, grey). (**B-E**) Time spent huddling (B), interacting nose-to-nose (C), socially exploring (D), or following (E) the partner mouse throughout the assay. Data are mean ± s.e.m. for all panels; open and closed circles indicate female and male mice, respectively. ***P*<0.01, ****P*<0.001, ANOVA treatment main effect (B, C, D); see Appendix A for complete statistics.

Chapter 5: Discussion, Future Directions, and Impact

This chapter contains work that was adapted with permission from the following article: Trieu et al., Science, 2022 [205].

Discussion

The work presented in this dissertation can largely be divided into two types of experiments - those that measured changes in synaptic transmission after application of *exogenous* MERF onto acute brain slices (Chapter 3) and those that explored the impact of *endogenous* MERF as unveiled by ACE inhibitors (Chapter 4). Combined, they elucidated how inhibition of ACE promoted the synaptic longevity of MERF thereby enhancing MOR signaling to mediate presynaptic depression of excitatory synaptic transmission onto D1-MSNs in the nucleus accumbens (figure 5-1). This mechanism is in sharp contrast to the classical pathway in the periphery where ACE inhibitors prevent the formation of angiotensin II which results in AT1R hypoactivation (figure 5-2).

Overall, these findings refine our understanding of how peptidases may selectively regulate neuropeptide longevity and emphasize intricacies that, under physiological conditions, may impact microcircuit function through quite specific mechanisms. This specificity is divergent to the relatively non-specific enzymatic action that peptidases are known for which is conferred by their ability to recognize a multitude of functional peptides through similar molecular properties inherent in specific peptide bonds. Therefore, it is interesting that ACE expression is relatively high in the striatum [181-183,185,186] which may limit the number of potential substrates it can act upon, like angiotensin I or bradykinin which were present at negligible concentrations in our preparation. Furthermore, the enrichment of ACE expression in D1-MSNs is one nuance that may have promoted cell type-specific effects on synaptic plasticity even though MERF showed similar efficacy in both cell types when present at relatively high concentrations.

MERF potently binds to MOR, DOR, and KOR [151,158-160] making it a unique enkephalin. Despite this, only MOR activation was necessary to depress synaptic transmission following ACE inhibition. This is surprising given the high expression of MOR, DOR, and KOR throughout the striatum. Perhaps factors like subcellular receptor localization, relative receptor potency, or local ligand concentration may underlie the specific effects observed in our experiments. Considering that Met- and Leu-enkephalin are known to have affinity towards DOR, and slightly less so towards MOR [115,118,158,159,248,249], the possibility of a marginally altered enkephalin like MERF whose physiological role is instead oriented towards MOR activation is not so farfetched. Indeed, MERF

displayed higher potency (IC_{50} = 409 nM) relative to Met-enkephalin (IC_{50} = 1060 nM) when analyzing only D1-MSN responses (as compared to figures 3-2 and 3-3). However, specificity due to increased potency may be offset when considering that MERF is present at a hypothesized 1:4 ratio relative to Met-enkephalin, assuming all potential enkephalin congeners from proenkephalin are processed and released [232-235]; LC-MS/MS data in Chapter 4 support similar ratios of MERF to Met-enkephalin at baseline (figures 4-2 and 4-5, tables 4-1 and 4-2). Although increased receptor potency and decreased ligand concentration appear contradictory in their ability to drive a signaling pathway (i.e. reduced presynaptic glutamate release), it also accentuates the significant role of ACE in regulating the extracellular longevity of MERF. These intricacies in sum highlight the potential for ACE inhibitors to shift synaptic homeostasis towards MOR activation.

Our proposed mechanism highlights an intriguing interaction between D2- and D1-MSNs, namely the release of MERF by D2-MSNs and their effect on D1-MSN glutamatergic inputs which are constrained by ACE expression in D1-MSNs. In this schema, ACE inhibition unveils a form of *indirect* lateral inhibition mediated by presynaptic MOR activation via MERF. This is in contrast to direct lateral inhibition by fast neurotransmitters (i.e. GABA) that are formed by axon collaterals from D2-MSNs to D1-MSNs (and other D2-MSNs) [250-253]. Asymmetric connections between D1- and D2-MSNs [254-256], local inhibitory microcircuitry [124,229,257-261], and neuromodulators [262-266] are hypothesized to provide a layer of complex regulation that largely remains unexplored under physiological or disease states, especially in the context of neuropeptides.

Furthering the nuances of intra-accumbal circuitry, it is unknown if dynorphins released by D1-MSNs participate in a mechanism mirroring that of MERF and ACE. Such a mechanism is plausible given that multiple forms of dynorphin are biologically active, and although their canonical cognate receptor are KORs, some dynorphin subtypes do display relatively high affinity amongst all three classical opioid receptors [151,158,164,165]. Also worth considering is the role of substance P in mechanisms of local synaptic transmission, particularly because substance P has long been hypothesized as a major substrate of ACE, albeit with conflicting evidence [193-195]. D1-MSNs are more likely to synapse onto other D1-MSNs rather than D2-MSNs [254-256] and, surprisingly, high-frequency stimulation of D1-MSNs can *indirectly* induce increased responsiveness of D2-MSNs to excitatory input through substance P [267]. In our LC-MS/MS experiments, substance P was expectedly present at relatively high concentrations following KCl-stimulation, however it was also unaffected by ACE inhibition (figures 4-2 and 4-4). Combined inhibition of neprilysin and APN, but not ACE, boosted substance P levels and provide contrasting evidence to the long-held notion that substance P is degraded by ACE.

The subtleties described so far only begin to portray the complex role of neuropeptides in the NAc and much remains to be examined. Nonetheless, these subtleties underlie and allow the circuit specificity of our proposed mechanism which is dependent upon the presence of ACE in D1-MSNs and its negative regulation over the potent MOR agonist MERF, which can then be preserved upon ACE inhibitor exposure. Indeed, excitatory synapses onto D2-MSNs (figure 4-6) or layer V pyramidal cells in anterior cingulate cortex (figure 4-7) were insensitive to ACE inhibition but displayed robust synaptic depression following exogenous MERF application. By selectively and locally enhancing endogenous opioid signaling in the vicinity of D1-MSNs, centrally active ACE inhibitors may limit abuse liability by avoiding MOR activation in other brain circuits. In fact, systemic ACE inhibition demonstrated therapeutic potential by reducing the rewarding effects of fentanyl and increasing reciprocal social interaction. Conversely, rodents that exhibit reduced social interaction after chronic social stress have upregulated ACE expression in NAc tissue [268] and D1-MSNs [269].

Future Directions

The synaptic mechanism described throughout this dissertation is a major step in our understanding of neuropeptide function and their regulation in the brain. However, much remains to be investigated, particularly in how to use or improve ACE inhibitors to modulate synaptic plasticity more effectively. The *in vivo* effects (figures 4-12 through 4-17) are encouraging from a clinically translational proof-of-concept perspective and serve to inform future directions. Here, I discuss three immediately relevant avenues to be explored for ACE inhibitors: 1) regional specificity and efficacy, 2) generalizability, and 3) refinement.

5.1 Regional Specificity and Efficacy

This body of work focused on local NAc circuitry and the presynaptic glutamatergic inputs that innervate it. However, it is unclear if ACE inhibition induces LTD broadly or in specific afferents. Evidence of the latter has been shown in dorsal striatum where MOR-mediated LTD occurs differentially at specific terminals dependent on striatal subregion [119,120]. A similar possibility may be hinted given the diversity of glutamatergic inputs and differences in relative input strength across NAc subregions [15,24]. At the very least, our fiber photometry experiments demonstrated efficacy of captopril at mPFC terminals and extending optogenetically-guided investigation to other inputs either *in vitro* or *in vivo* is a possibility.

It also remains to be seen if ACE inhibition can modulate synaptic transmission at downstream projection sites of D1-MSNs like VTA or ventral pallidum [17-19] and if this would alter behavior. This could be possible if an ACE-specific substrate interacts with D1-MSN terminals in these brain regions. This possibility may underlie some evidence suggesting that ACE inhibitors can modulate dopamine circuits [270-273]. A screen for such a peptide could be accomplished with a variety of comparative LC-MS/MS approaches [187,274]. To extend behavioral investigations into the VTA or ventral pallidum, targeted intracranial infusions of ACE inhibitors could also be used instead of systemic administration to rigorously define region-specific alterations.

A major impetus for our examination of the NAc was due to the prominent expression of ACE in the striatum [181-186]. However, proteomic expression differs between rodents and humans. In fact, while ACE expression is highest in human basal ganglia like rodents (specifically putamen, caudate nucleus, and nucleus accumbens) it is also diffusely present in cortex [275] and poses a confounding variable for future translational studies. Unfortunately, the relative scarcity of ACE in rodent cortex makes it difficult to predict and examine cortex-dependent effects due to ACE inhibition. On the contrary, a recent paper demonstrated antidepressant effects in mice following captopril administration which was mediated by a bradykinin-dependent pathway localized to mPFC [276]. This highlights that while differences in ACE expression should be kept in mind, captopril could induce other effects not discussed in this dissertation.

One novel aspect of an ACE-regulated mechanism that gates synaptic plasticity lies in how we can leverage endogenous mechanisms to slightly shift circuit dynamics. The capacity for lateral inhibition between MSNs supports the overall hypothesis that different types of MSNs work in concert, perhaps through negative feedback, to drive basal ganglia-related behaviors. However, the efficacy of ACE inhibitors relies on the presence of MERF at the synapse. Consequently, ACE inhibitors may be less efficacious in states where D2-MSN activity is depressed physiologically or pathologically. Work by Meaghan Creed demonstrated that a combination of low-frequency deep brain stimulation and pharmacological administration abolished rodent locomotor sensitization to cocaine [277]. Similarly, a combination of ACE inhibition with optogenetic stimulation of D2-MSNs could enhance ACE inhibitor efficacy and provide extended behavioral benefits.

5.2 Generalizability

When considered collectively, the behavioral effects observed in tests of conditioned place preference and social interaction are striking given the dissimilarities between assays. As alluded to before, upregulated ACE expression has been detected under pathological states [268,269,278].

Intriguingly, genetic variants of ACE that alter protein expression or enzymatic activity in humans [279-281] have been associated with various brain conditions including affective disorders [282-291], schizophrenia [286,292,293], Alzheimer's disease [294-298], or even autism spectrum disorder [299]. It would be interesting to investigate if these correlative genetic and molecular changes could serve as a generalized biomarker for disease, if it is also present in rodent studies, or if ACE inhibitors confer benefits against other pathological behavioral phenotypes. The circuit-specific nature of ACE inhibition in the accumbens could be one strategy that allows us to selectively modulate a molecular target for therapeutic benefit across multiple disease states [61,300].

Of immediate interest is the prospect that ACE inhibitors could attenuate addiction-like behaviors caused by substances other than opiates, like cocaine. Although the pathophysiology underlying cocaine and opiates are different, a commonality arises wherein D1-MSNs are hyperactive relative to D2-MSNs [85,301]. The work presented here would suggest that ACE inhibitors can attenuate addiction-like behaviors, like CPP, after cocaine use in rodents by restoring the relative balance between D1- and D2-MSN activity (figure 5.3). Alternatively, ACE inhibition and subsequent MOR activation by MERF may actually occlude the direct effects of exogenous opiates on MORs, thus attenuating fentanyl CPP via an alternate or parallel mechanism. Also relevant is the role of ACE inhibitors in modifying the complexities underlying cellular adaptation across various modes of drug intake like self-administration behavior (e.g. acquisition versus maintenance) [72,228,302].

We replicated several effects with trandolapril/trandolaprilat, an ACE inhibitor that is more potent and lipophilic [177,303]. This invites the possibility of using more efficacious and longer lasting ACE inhibitors in future studies, namely those that are centrally active and widely used by people. Indeed, human studies measuring changes in cognition, dementia, and Alzheimer's disease found positive effects of ACE inhibitors that cross the blood-brain barrier versus those that are not permeable [304-309]. Additionally, CNS-dependent effects have been observed across a wide range of ACE inhibitors in rodents [310-324]. However, it is unclear if striatal synaptic depression from ACE inhibition underlies these reports; the controversial role of the renin-angiotensin system (i.e. angiotensin congeners and their receptors) in other brain regions should not be discounted [325-331]. CNS effects could also be dependent upon the form of these ACE inhibitors; captopril (and lisinopril) are unique in that they are ingested in their active form whereas newer inhibitors are ingested as a prodrug which then undergoes hepatic biotransformation into a more potent form.

It is also unclear on what timescale the observed synaptic effects are present, and if this can be modulated depending on the duration of ACE inhibition. Our electrophysiology findings

examined synaptic plasticity on the scale of minutes after brief exposure to captopril, while mice were given captopril 30 minutes prior to behavioral testing. Captopril itself has a half-life of 1.7 hours [332]. Perhaps only acute ACE inhibition that aligns with behaviorally relevant epochs are necessary to modulate synaptic circuits making durable ACE inhibitors either unnecessary, ineffective, or even counterproductive due to their slower onset. Conversely, it is possible that ACE inhibitors more durable than captopril may extend the window of synaptic modulation given the aforementioned positive effects in humans measured across several years and several different ACE inhibitors.

5.3 Refinement

For the purposes of targeting ACE in the brain, current ACE inhibitors are relatively inadequate. Refinement by way of redesigning current or synthesizing new ACE inhibitors can maximize efficacy and potency while theoretically reducing off-target effects.

One approach to refine the action of ACE inhibitors on accumbal circuitry involves enhancing blood-brain barrier penetrance. Since captopril was first marketed in 1981, several iterations of ACE inhibitors have been developed with varying lipophilic properties and central activity [333,334]. However, their immense role in modifying cardiovascular disease have made them a mainstay medication allowing for relatively large retrospective clinical studies that can analyze differences between brain penetrant and peripherally restricted ACE inhibitors.

Probably the most thought-provoking idea to be immediately explored is the fact that ACE contains two catalytic domains which enzymatically cleaves MERF at notably different rates. These domains are referred to as the N- and C-domain. Both are highly homologous and contain the same zinc-binding amino acid moiety responsible for coordinating catalytic cleavage of substrates [335-338]. Despite this, both domains exhibit distinct substrate specificity as actualized by differential catalysis rate which is largely due to different surrounding amino acids [339], glycosylation patterns [340,341], local chloride ion concentration [342-344], and structural conformations [345]. Although support for domain-specific cleavage of MERF is quite sparse, the evidence available suggest that MERF is primarily cleaved by the N-domain [168] while more substantial evidence demonstrate that angiotensin I is primarily cleaved by the C-domain [192]. Both domains do have the capacity to hydrolyze the same substrates, but they do so at inefficient rates.

Genetic and pharmacological tools in the form of domain-specific knockout mice [346-348] and domain-specific inhibitors [349-355] are available to test the hypothesis that MERF is cleaved by the N-domain in striatal circuits. As mentioned above, newer ACE inhibitors have varying

properties and it is interesting to note that the majority are significantly biased towards the C-domain while captopril is the only ACE inhibitor to have greater N-domain affinity [344,356]. A double dissociation between domains and substrates would be quite remarkable and may generate an incentive to develop new N-domain-specific pharmacotherapeutics.

Impact

The discovery of teprotide from the venom of the *Bothrops Jararaca* pit viper in the 1960's by Brazilian physician scientist Sergio Ferreira [357] and subsequent advent of ACE inhibitors represent a landmark in pharmacotherapy [358-362]. Their widespread use for several cardiovascular conditions underscores their impact on disease management and prevention. In fact, work by Ken Bernstein's group has possibly paved the way for broadening clinical indications for their work on ACE's novel roles in renal physiology independent of the classical angiotensin pathway [363] as well as immune responses to tumors and bacteria [364-366]. It is therefore surprising that relatively little is known about ACE's role in the brain. ACE inhibitors positively impact a variety of brain conditions like affective disorders [367-373], anxiety [374], neurodegeneration [305,306,308,375-378], and overall quality of life [309,379-387] since 1984 [388]. Moreover, considering the evidence associating altered genetic expression of ACE with brain conditions (see page 80), there is a conceivable pharmacogenomic role for ACE inhibitors in psychiatry [389,390]. Our work now adds addiction to this list as substance use disorder and overdose deaths continue to increase throughout the world. There is a clear need for new therapeutics [391,392] and the few that are available are also underutilized [393]. Perhaps the use of ACE inhibitors to modulate MOR signaling can restore aberrations within the endogenous opioid system which have been implicated in several disease states [53,268,278,394-406].

This dissertation has contributed new insights into ACE function in the brain and provided a mechanism that could explain how ACE inhibitors modulate a variety of brain conditions, specifically by amplifying endogenous MERF to reverse underlying striatal dysfunction. It should be noted that boosting endogenous neurochemical concentrations at the synapse is not a novel concept. Similar approaches have been employed for a variety of pharmacotherapeutics such as serotonin-norepinephrine reuptake inhibitors (SNRIs) and selective-serotonin reuptake inhibitors (SSRIs) for depression or anxiety disorders, or amphetamines for ADHD. But, while these medications have been substantially impactful in the treatment of psychiatric disease, their lack of spatial or cell type selectivity is reflected in the potential side effects of these therapeutics. Therefore, brain-targeting ACE inhibitors can leverage a highly regulated and potent mechanism of synaptic plasticity that is confined to a brain region and cell type. Our findings may thus herald

a new era of repositioning and redesigning ACE inhibitors with central activity as a brain circuit-specific pharmacotherapy.

Figure 5-1

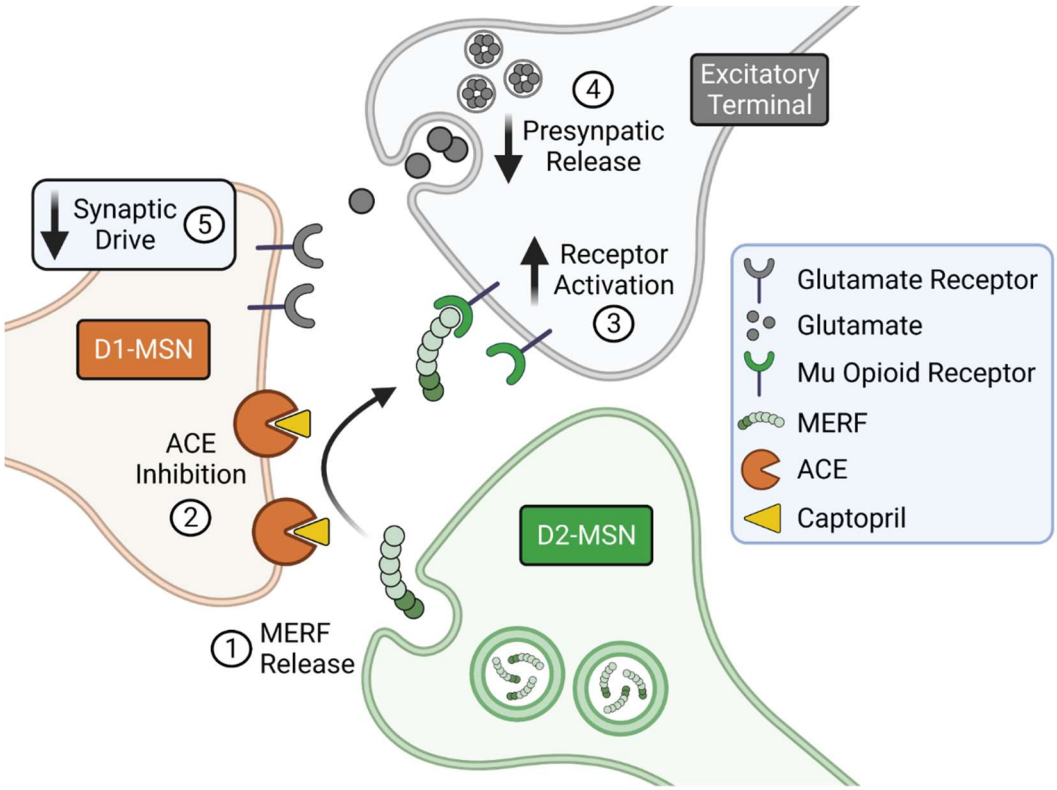

Figure 5-1. Mechanism by which captopril regulates synaptic drive of D1-MSNs via MERF. Pharmacological inhibition of ACE prevents degradation of MERF when released by D2-MSNs. Increased MERF longevity drives endogenous MOR signaling resulting in depressed presynaptic release of glutamate and ultimately reduced synaptic drive of D1-MSN.

Figure 5-2

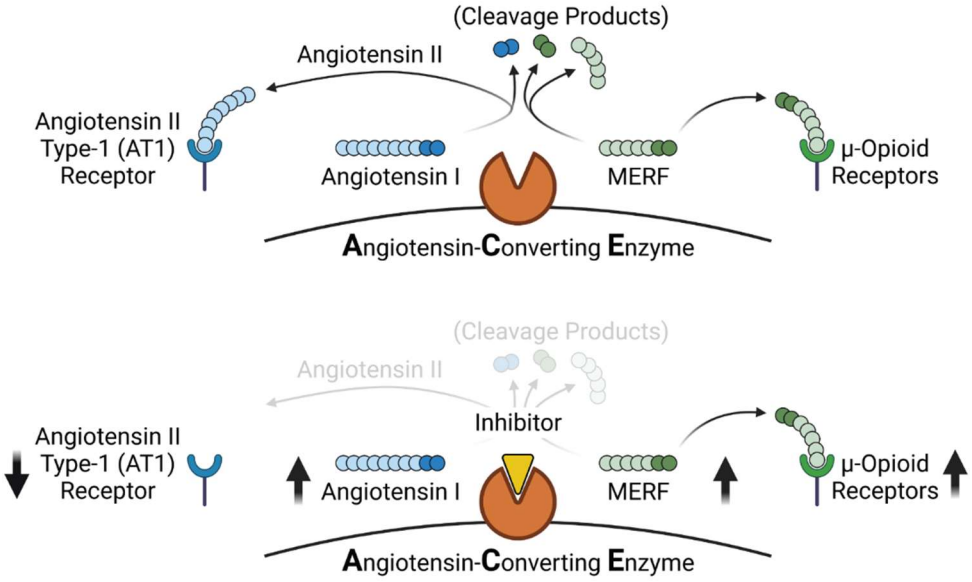

Figure 5-2. Schematic of peptide regulation by ACE within the classical Angiotensin I pathway and non-canonical MERF pathway. Under physiological conditions, ACE forms Angiotensin II peptide to drive AT1R activation, but degrades MERF to gate MOR activation. ACE inhibitors prevent AT1R signaling but stimulate MOR signaling by preserving extracellular MERF.

Figure 5-3

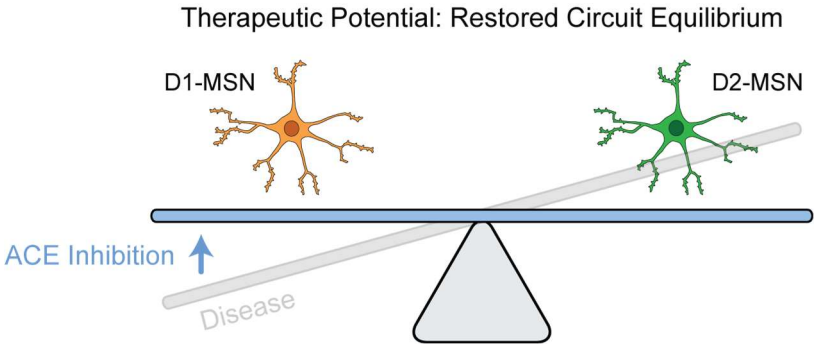

Figure 5-3. Role of ACE inhibition in restoring circuit equilibrium. Central ACE inhibition may provide therapeutic benefit and restore circuit equilibrium in brain conditions characterized by excessive D1-MSNs activity relative to D2-MSNs by reducing the synaptic drive onto D1-MSNs.

Bibliography

1 Nelson, A. B. & Kreitzer, A. C. in *Annual Review of Neuroscience, Vol 37* Vol. 37 *Annual Review of Neuroscience* (ed S. E. Hyman) 117-135 (2014).

2 Redgrave, P. *et al.* Goal-directed and habitual control in the basal ganglia: implications for Parkinson's disease. *Nat. Rev. Neurosci.* **11**, 760-772, doi:10.1038/nrn2915 (2010).

3 Graybiel, A. M. Habits, rituals, and the evaluative brain. *Annu. Rev. Neurosci.* **31**, 359-387, doi:10.1146/annurev.neuro.29.051605.112851 (2008).

4 Floresco, S. B. in *Annual Review of Psychology, Vol 66* Vol. 66 *Annual Review of Psychology* (ed S. T. Fiske) 25-52 (2015).

5 Haber, S. N., Fudge, J. L. & McFarland, N. R. Striatonigrostriatal pathways in primates form an ascending spiral from the shell to the dorsolateral striatum. *J. Neurosci.* **20**, 2369-2382 (2000).

6 Sivils, A., Wang, J. Q. & Chu, X. P. Striatonigrostriatal Spirals in Addiction. *Front Neural Circuits* **15**, 803501, doi:10.3389/fncir.2021.803501 (2021).

7 Belin, D. & Everitt, B. J. Cocaine seeking habits depend upon doparnine-dependent serial connectivity linking the ventral with the dorsal striatum. *Neuron* **57**, 432-441, doi:10.1016/j.neuron.2007.12.019 (2008).

8 Yin, H. H. & Knowlton, B. J. The role of the basal ganglia in habit formation. *Nature Reviews Neuroscience* **7**, 464-476, doi:10.1038/nrn1919 (2006).

9 Gertler, T. S., Chan, C. S. & Surmeier, D. J. Dichotomous Anatomical Properties of Adult Striatal Medium Spiny Neurons. *J. Neurosci.* **28**, 10814-10824, doi:10.1523/jneurosci.2660-08.2008 (2008).

10 Chen, R. *et al.* Decoding molecular and cellular heterogeneity of mouse nucleus accumbens. *Nat. Neurosci.* **24**, 1757-1771, doi:10.1038/s41593-021-00938-x (2021).

11 Gokce, O. *et al.* Cellular Taxonomy of the Mouse Striatum as Revealed by Single-Cell RNA-Seq. *Cell Rep.* **16**, 1126-1137, doi:10.1016/j.celrep.2016.06.059 (2016).

12 Stanley, G., Gokce, O., Malenka, R. C., Sudhof, T. C. & Quake, S. R. Continuous and Discrete Neuron Types of the Adult Murine Striatum. *Neuron* **105**, 688-699 e688, doi:10.1016/j.neuron.2019.11.004 (2020).

13 Saunders, A. *et al.* Molecular Diversity and Specializations among the Cells of the Adult Mouse Brain. *Cell* **174**, 1015-+, doi:10.1016/j.cell.2018.07.028 (2018).

14 Choi, K., Holly, E. N., Davatolhagh, M. F., Beier, K. T. & Fuccillo, M. V. Integrated anatomical and physiological mapping of striatal afferent projections. *Eur. J. Neurosci.* **49**, 623-636, doi:10.1111/ejn.13829 (2019).

15 Li, Z. *et al.* Cell-Type-Specific Afferent Innervation of the Nucleus Accumbens Core and Shell. *Front. Neuroanat.* **12**, 84, doi:10.3389/fnana.2018.00084 (2018).

16 Scofield, M. D. *et al.* The Nucleus Accumbens: Mechanisms of Addiction across Drug Classes Reflect the Importance of Glutamate Homeostasis. *Pharmacol. Rev.* **68**, 816-871, doi:10.1124/pr.116.012484 (2016).

17 Kupchik, Y. M. *et al.* Coding the direct/indirect pathways by D1 and D2 receptors is not valid for accumbens projections. *Nat. Neurosci.* **18**, 1230-1232, doi:10.1038/nn.4068 (2015).

18 Smith, R. J., Lobo, M. K., Spencer, S. & Kalivas, P. W. Cocaine-induced adaptations in D1 and D2 accumbens projection neurons (a dichotomy not necessarily synonymous with direct and indirect pathways). *Curr. Opin. Neurobiol.* **23**, 546-552, doi:10.1016/j.conb.2013.01.026 (2013).

19 Lu, X. Y., Ghasemzadeh, M. B. & Kalivas, P. W. Expression of D1 receptor, D2 receptor, substance P and enkephalin messenger RNAs in the neurons projecting from the nucleus accumbens. *Neuroscience* **82**, 767-780, doi:10.1016/s0306-4522(97)00327-8 (1998).

20 Martin, A. *et al.* A Spatiomolecular Map of the Striatum. *Cell Rep.* **29**, 4320-4333 e4325, doi:10.1016/j.celrep.2019.11.096 (2019).

21 Castro, D. C. & Bruchas, M. R. A Motivational and Neuropeptidergic Hub: Anatomical and Functional Diversity within the Nucleus Accumbens Shell. *Neuron* **102**, 529-552, doi:10.1016/j.neuron.2019.03.003 (2019).

22 Voorn, P., Gerfen, C. R. & Groenewegen, H. J. Compartmental organization of the ventral striatum of the rat: immunohistochemical distribution of enkephalin, substance P, dopamine, and calcium-binding protein. *J. Comp. Neurol.* **289**, 189-201, doi:10.1002/cne.902890202 (1989).

23 Gangarossa, G. *et al.* Distribution and compartmental organization of GABAergic medium-sized spiny neurons in the mouse nucleus accumbens. *Front Neural Circuits* **7**, 22, doi:10.3389/fncir.2013.00022 (2013).

24 Britt, J. P. *et al.* Synaptic and behavioral profile of multiple glutamatergic inputs to the nucleus accumbens. *Neuron* **76**, 790-803, doi:10.1016/j.neuron.2012.09.040 (2012).

25 Hearing, M. C. *et al.* Reversal of morphine-induced cell-type-specific synaptic plasticity in the nucleus accumbens shell blocks reinstatement. *Proc. Natl. Acad. Sci. U. S. A.* **113**, 757-762, doi:10.1073/pnas.1519248113 (2016).

26 Kourrich, S. & Thomas, M. J. Similar neurons, opposite adaptations: psychostimulant experience differentially alters firing properties in accumbens core versus shell. *J. Neurosci.* **29**, 12275-12283, doi:10.1523/JNEUROSCI.3028-09.2009 (2009).

27 Banghart, M. R., Neufeld, S. Q., Wong, N. C. & Sabatini, B. L. Enkephalin Disinhibits Mu Opioid Receptor-Rich Striatal Patches via Delta Opioid Receptors. *Neuron* **88**, 1227-1239, doi:10.1016/j.neuron.2015.11.010 (2015).

28 Shukla, A. *et al.* Calcium-permeable AMPA receptors and silent synapses in cocaine-conditioned place preference. *EMBO J.* **36**, 458-474, doi:10.15252/embj.201695465 (2017).

29 Volkow, N. D. & Morales, M. The Brain on Drugs: From Reward to Addiction. *Cell* **162**, 712-725, doi:10.1016/j.cell.2015.07.046 (2015).

30 Muntean, B. S., Dao, M. T. & Martemyanov, K. A. Allostatic Changes in the cAMP System Drive Opioid-Induced Adaptation in Striatal Dopamine Signaling. *Cell Rep.* **29**, 946-+, doi:10.1016/j.celrep.2019.09.034 (2019).

31 Campbell, R. R. *et al.* HDAC3 Activity within the Nucleus Accumbens Regulates Cocaine-induced Plasticity and Behavior in a Cell-Type Specific Manner. *J. Neurosci.* **41**, 2814-2827, doi:10.1523/JNEUROSCI.2829-20.2021 (2021).

32 Pascoli, V. *et al.* Contrasting forms of cocaine-evoked plasticity control components of relapse. *Nature* **509**, 459-+, doi:10.1038/nature13257 (2014).

33 Sun, H. *et al.* Morphine epigenomically regulates behavior through alterations in histone H3 lysine 9 dimethylation in the nucleus accumbens. *J. Neurosci.* **32**, 17454-17464, doi:10.1523/JNEUROSCI.1357-12.2012 (2012).

34 Koo, J. W. *et al.* BDNF is a negative modulator of morphine action. *Science* **338**, 124-128, doi:10.1126/science.1222265 (2012).

35 Lobo, M. K. *et al.* Cell Type-Specific Loss of BDNF Signaling Mimics Optogenetic Control of Cocaine Reward. *Science* **330**, 385-390, doi:10.1126/science.1188472 (2010).

36 Pascoli, V., Turiault, M. & Luscher, C. Reversal of cocaine-evoked synaptic potentiation resets drug-induced adaptive behaviour. *Nature* **481**, 71-U76, doi:10.1038/nature10709 (2012).

37 Lobo, M. K. & Nestler, E. J. The striatal balancing act in drug addiction: distinct roles of direct and indirect pathway medium spiny neurons. *Front. Neuroanat.* **5**, 41, doi:10.3389/fnana.2011.00041 (2011).

38 Williams, J. T., Christie, M. J. & Manzoni, O. Cellular and synaptic adaptations mediating opioid dependence. *Physiol. Rev.* **81**, 299-343, doi:10.1152/physrev.2001.81.1.299 (2001).

39 Kourrich, S., Rothwell, P. E., Klug, J. R. & Thomas, M. J. Cocaine experience controls bidirectional synaptic plasticity in the nucleus accumbens. *J. Neurosci.* **27**, 7921-7928, doi:10.1523/JNEUROSCI.1859-07.2007 (2007).

40 Luscher, C., Robbins, T. W. & Everitt, B. J. The transition to compulsion in addiction. *Nature Reviews Neuroscience* **21**, 247-263, doi:10.1038/s41583-020-0289-z (2020).

41 Koob, G. F. & Volkow, N. D. Neurobiology of addiction: a neurocircuitry analysis. *Lancet Psychiatry* **3**, 760-773, doi:10.1016/S2215-0366(16)00104-8 (2016).

42 Everitt, B. J. & Robbins, T. W. in *Annual Review of Psychology, Vol 67* Vol. 67 *Annual Review of Psychology* (ed S. T. Fiske) 23-50 (2016).

43 Kalivas, P. W. & O'Brien, C. Drug addiction as a pathology of staged neuroplasticity. *Neuropsychopharmacology* **33**, 166-180, doi:10.1038/sj.npp.1301564 (2008).

44 Lim, B. K., Huang, K. W., Grueter, B. A., Rothwell, P. E. & Malenka, R. C. Anhedonia requires MC4R-mediated synaptic adaptations in nucleus accumbens. *Nature* **487**, 183-189, doi:10.1038/nature11160 (2012).

45 Francis, T. C. *et al.* Nucleus Accumbens Medium Spiny Neuron Subtypes Mediate Depression-Related Outcomes to Social Defeat Stress. *Biol. Psychiatry* **77**, 212-222, doi:10.1016/j.biopsych.2014.07.021 (2015).

46 Bewernick, B. H. *et al.* Nucleus accumbens deep brain stimulation decreases ratings of depression and anxiety in treatment-resistant depression. *Biol. Psychiatry* **67**, 110-116, doi:10.1016/j.biopsych.2009.09.013 (2010).

47 Scarpa, J. R. *et al.* Shared Transcriptional Signatures in Major Depressive Disorder and Mouse Chronic Stress Models. *Biol. Psychiatry* **88**, 159-168, doi:10.1016/j.biopsych.2019.12.029 (2020).

48 Heshmati, M. *et al.* Depression and Social Defeat Stress Are Associated with Inhibitory Synaptic Changes in the Nucleus Accumbens. *J. Neurosci.* **40**, 6228-6233, doi:10.1523/JNEUROSCI.2568-19.2020 (2020).

49 Fox, M. E., Figueiredo, A., Menken, M. S. & Lobo, M. K. Dendritic spine density is increased on nucleus accumbens D2 neurons after chronic social defeat. *Sci. Rep.* **10**, 12393, doi:10.1038/s41598-020-69339-7 (2020).

50 Francis, T. C. *et al.* Molecular basis of dendritic atrophy and activity in stress susceptibility. *Mol. Psychiatry* **22**, 1512-1519, doi:10.1038/mp.2017.178 (2017).

51 Heshmati, M. & Russo, S. J. Anhedonia and the brain reward circuitry in depression. *Current behavioral neuroscience reports* **2**, 146-153, doi:10.1007/s40473-015-0044-3 (2015).

52 Russo, S. J. & Nestler, E. J. The brain reward circuitry in mood disorders. *Nature Reviews Neuroscience* **14**, 609-625, doi:10.1038/nrn3381 (2013).

53 Ballester, J. *et al.* Risk for opioid misuse in chronic pain patients is associated with endogenous opioid system dysregulation. *Transl Psychiatry* **12**, 20, doi:10.1038/s41398-021-01775-z (2022).

54 Liu, S. W. *et al.* Kappa Opioid Receptors Drive a Tonic Aversive Component of Chronic Pain. *J. Neurosci.* **39**, 4162-4178, doi:10.1523/jneurosci.0274-19.2019 (2019).

55 Schwartz, N. *et al.* Decreased motivation during chronic pain requires long-term depression in the nucleus accumbens. *Science* **345**, 535-542, doi:10.1126/science.1253994 (2014).

56 Ferrario, C. R. Why did I eat that? Contributions of individual differences in incentive motivation and nucleus accumbens plasticity to obesity. *Physiol Behav* **227**, 113114, doi:10.1016/j.physbeh.2020.113114 (2020).

57 Derman, R. C. & Ferrario, C. R. Enhanced incentive motivation in obesity-prone rats is mediated by NAc core CP-AMPARs. *Neuropharmacology* **131**, 326-336, doi:10.1016/j.neuropharm.2017.12.039 (2018).

58 Friend, D. M. *et al.* Basal Ganglia Dysfunction Contributes to Physical Inactivity in Obesity. *Cell Metab.* **25**, 312-321, doi:10.1016/j.cmet.2016.12.001 (2017).

59 Gendelis, S., Inbar, D. & Kupchik, Y. M. The role of the nucleus accumbens and ventral pallidum in feeding and obesity. *Prog. Neuropsychopharmacol. Biol. Psychiatry* **111**, 110394, doi:10.1016/j.pnpbp.2021.110394 (2021).

60 Volkow, N. D., Wang, G. J., Tomasi, D. & Baler, R. D. Obesity and addiction: neurobiological overlaps. *Obes. Rev.* **14**, 2-18, doi:10.1111/j.1467-789X.2012.01031.x (2013).

61 Rothwell, P. E. Autism Spectrum Disorders and Drug Addiction: Common Pathways, Common Molecules, Distinct Disorders? *Front. Neurosci.* **10**, 20, doi:10.3389/fnins.2016.00020 (2016).

62 Rothwell, P. E. *et al.* Autism-associated neuroligin-3 mutations commonly impair striatal circuits to boost repetitive behaviors. *Cell* **158**, 198-212, doi:10.1016/j.cell.2014.04.045 (2014).

63 Brandenburg, C. *et al.* Increased Dopamine Type 2 Gene Expression in the Dorsal Striatum in Individuals With Autism Spectrum Disorder Suggests Alterations in Indirect Pathway Signaling and Circuitry. *Front. Cell. Neurosci.* **14**, 577858, doi:10.3389/fncel.2020.577858 (2020).

64 Grissom, N. M. *et al.* Male-specific deficits in natural reward learning in a mouse model of neurodevelopmental disorders. *Mol. Psychiatry* **23**, 544-555, doi:10.1038/mp.2017.184 (2018).

65 Lee, Y. *et al.* Excessive D1 Dopamine Receptor Activation in the Dorsal Striatum Promotes Autistic-Like Behaviors. *Mol. Neurobiol.* **55**, 5658-5671, doi:10.1007/s12035-017-0770-5 (2017).

66 Fuccillo, M. V. Striatal Circuits as a Common Node for Autism Pathophysiology. *Front. Neurosci.* **10**, 27, doi:10.3389/fnins.2016.00027 (2016).

67 Damiano, C. R. *et al.* Neural mechanisms of negative reinforcement in children and adolescents with autism spectrum disorders. *J. Neurodev. Disord.* **7**, 12, doi:10.1186/s11689-015-9107-8 (2015).

68 Portmann, T. *et al.* Behavioral Abnormalities and Circuit Defects in the Basal Ganglia of a Mouse Model of 16p11.2 Deletion Syndrome. *Cell Rep.* **7**, 1077-1092, doi:10.1016/j.celrep.2014.03.036 (2014).

69 Lee, H. J. *et al.* Activation of Direct and Indirect Pathway Medium Spiny Neurons Drives Distinct Brain-wide Responses. *Neuron* **91**, 412-424, doi:10.1016/j.neuron.2016.06.010 (2016).

70 Freeze, B. S., Kravitz, A. V., Hammack, N., Berke, J. D. & Kreitzer, A. C. Control of basal ganglia output by direct and indirect pathway projection neurons. *J. Neurosci.* **33**, 18531-18539, doi:10.1523/JNEUROSCI.1278-13.2013 (2013).

71 Kravitz, A. V., Tye, L. D. & Kreitzer, A. C. Distinct roles for direct and indirect pathway striatal neurons in reinforcement. *Nat. Neurosci.* **15**, 816-U823, doi:10.1038/nn.3100 (2012).

72 O'Neal, T. J., Nooney, M. N., Thien, K. & Ferguson, S. M. Chemogenetic modulation of accumbens direct or indirect pathways bidirectionally alters reinstatement of heroin-seeking in high- but not low-risk rats. *Neuropsychopharmacology* **45**, 1251-1262, doi:10.1038/s41386-019-0571-9 (2020).

73 Cole, S. L., Robinson, M. J. F. & Berridge, K. C. Optogenetic self-stimulation in the nucleus accumbens: D1 reward versus D2 ambivalence. *PLoS One* **13**, e0207694, doi:10.1371/journal.pone.0207694 (2018).

74 Shan, Q., Ge, M., Christie, M. J. & Balleine, B. W. The Acquisition of Goal-Directed Actions Generates Opposing Plasticity in Direct and Indirect Pathways in Dorsomedial Striatum. *J. Neurosci.* **34**, 9196-9201, doi:10.1523/jneurosci.0313-14.2014 (2014).

75 Tritsch, N. X. & Sabatini, B. L. Dopaminergic Modulation of Synaptic Transmission in Cortex and Striatum. *Neuron* **76**, 33-50, doi:10.1016/j.neuron.2012.09.023 (2012).

76 Augustin, S. M., Loewinger, G. C., O'Neal, T. J., Kravitz, A. V. & Lovinger, D. M. Dopamine D2 receptor signaling on iMSNs is required for initiation and vigor of learned actions. *Neuropsychopharmacology* **45**, 2087-2097, doi:10.1038/s41386-020-00799-1 (2020).

77 Soares-Cunha, C. *et al.* Nucleus accumbens medium spiny neurons subtypes signal both reward and aversion. *Mol. Psychiatry* **25**, 3241-3255, doi:10.1038/s41380-019-0484-3 (2020).

78 Matamales, M. *et al.* Local D2- to D1-neuron transmodulation updates goal-directed learning in the striatum. *Science* **367**, 549-555, doi:10.1126/science.aaz5751 (2020).

79 Iino, Y. *et al.* Dopamine D2 receptors in discrimination learning and spine enlargement. *Nature* **579**, 555-+, doi:10.1038/s41586-020-2115-1 (2020).

80 Tecuapetla, F., Matias, S., Dugue, G. P., Mainen, Z. F. & Costa, R. M. Balanced activity in basal ganglia projection pathways is critical for contraversive movements. *Nature Communications* **5**, 4315, doi:10.1038/ncomms5315 (2014).

81 Calabresi, P., Picconi, B., Tozzi, A., Ghiglieri, V. & Di Filippo, M. Direct and indirect pathways of basal ganglia: a critical reappraisal. *Nat. Neurosci.* **17**, 1022-1030, doi:10.1038/nn.3743 (2014).

82 Cui, G. H. *et al.* Concurrent activation of striatal direct and indirect pathways during action initiation. *Nature* **494**, 238-242, doi:10.1038/nature11846 (2013).

83 Gong, S. C. *et al.* A gene expression atlas of the central nervous system based on bacterial artificial chromosomes. *Nature* **425**, 917-925, doi:10.1038/nature02033 (2003).

84 Shuen, J. A., Chen, M., Gloss, B. & Calakos, N. Drd1a-tdTomato BAC transgenic mice for simultaneous visualization of medium spiny neurons in the direct and indirect pathways of the basal ganglia. *J. Neurosci.* **28**, 2681-2685, doi:10.1523/jneurosci.5492-07.2008 (2008).

85 Allichon, M. C. *et al.* Cell-Type-Specific Adaptions in Striatal Medium-Sized Spiny Neurons and Their Roles in Behavioral Responses to Drugs of Abuse. *Front. Synaptic Neurosci.* **13**, 799274, doi:10.3389/fnsyn.2021.799274 (2021).

86 Salery, M., Trifilieff, P., Caboche, J. & Vanhoutte, P. From Signaling Molecules to Circuits and Behaviors: Cell-Type-Specific Adaptations to Psychostimulant Exposure in the Striatum. *Biol. Psychiatry* **87**, 944-953, doi:10.1016/j.biopsych.2019.11.001 (2020).

87 Creed, M., Ntamati, N. R., Chandra, R., Lobo, M. K. & Luscher, C. Convergence of Reinforcing and Anhedonic Cocaine Effects in the Ventral Pallidum. *Neuron* **92**, 214-226, doi:10.1016/j.neuron.2016.09.001 (2016).

88 Bock, R. *et al.* Strengthening the accumbal indirect pathway promotes resilience to compulsive cocaine use. *Nat. Neurosci.* **16**, 632-638, doi:10.1038/nn.3369 (2013).

89 Koo, J. W. *et al.* Loss of BDNF Signaling in DIR-Expressing NAc Neurons Enhances Morphine Reward by Reducing GABA Inhibition. *Neuropsychopharmacology* **39**, 2646-2653, doi:10.1038/npp.2014.118 (2014).

90 Hikida, T., Kimura, K., Wada, N., Funabiki, K. & Nakanishi, S. Distinct Roles of Synaptic Transmission in Direct and Indirect Striatal Pathways to Reward and Aversive Behavior. *Neuron* **66**, 896-907, doi:10.1016/j.neuron.2010.05.011 (2010).

91 Meunier, J. C. *et al.* Isolation and structure of the endogenous agonist of opioid receptor-like ORL1 receptor. *Nature* **377**, 532-535, doi:10.1038/377532a0 (1995).

92 Reinscheid, R. K. *et al.* Orphanin FQ: a neuropeptide that activates an opioidlike G protein-coupled receptor. *Science* **270**, 792-794, doi:10.1126/science.270.5237.792 (1995).

93 Le Merrer, J., Becker, J. A. J., Befort, K. & Kieffer, B. L. Reward Processing by the Opioid System in the Brain. *Physiol. Rev.* **89**, 1379-1412, doi:10.1152/physrev.00005.2009 (2009).

94 Valentino, R. J. & Volkow, N. D. Untangling the complexity of opioid receptor function. *Neuropsychopharmacology* **43**, 2514-2520, doi:10.1038/s41386-018-0225-3 (2018).

95 Darcq, E. & Kieffer, B. L. Opioid receptors: drivers to addiction? *Nat. Rev. Neurosci.* **19**, 499-514, doi:10.1038/s41583-018-0028-x (2018).

96 Lutz, P. E. & Kieffer, B. L. Opioid receptors: distinct roles in mood disorders. *Trends Neurosci.* **36**, 195-206, doi:10.1016/j.tins.2012.11.002 (2013).

97 Galaj, E. & Xi, Z. X. Progress in opioid reward research: From a canonical two-neuron hypothesis to two neural circuits. *Pharmacol Biochem Behav* **200**, 173072, doi:10.1016/j.pbb.2020.173072 (2021).

98 Trang, T. *et al.* Pain and Poppies: The Good, the Bad, and the Ugly of Opioid Analgesics. *J. Neurosci.* **35**, 13879-13888, doi:10.1523/JNEUROSCI.2711-15.2015 (2015).

99 Al-Hasani, R. & Bruchas, M. R. Molecular Mechanisms of Opioid Receptor-dependent Signaling and Behavior. *Anesthesiology* **115**, 1363-1381, doi:10.1097/ALN.0b013e318238bba6 (2011).

100 Rusin, K. I., Giovannucci, D. R., Stuenkel, E. L. & Moises, H. C. Kappa-opioid receptor activation modulates Ca2+ currents and secretion in isolated neuroendocrine nerve terminals. *J. Neurosci.* **17**, 6565-6574 (1997).

101 Torrecilla, M. *et al.* G-protein-gated potassium channels containing Kir3.2 and Kir3.3 subunits mediate the acute inhibitory effects of opioids on locus ceruleus neurons. *J. Neurosci.* **22**, 4328-4334, doi:20026414 (2002).

102 Betke, K. M., Wells, C. A. & Hamm, H. E. GPCR mediated regulation of synaptic transmission. *Prog. Neurobiol.* **96**, 304-321, doi:10.1016/j.pneurobio.2012.01.009 (2012).

103 North, R. A., Williams, J. T., Surprenant, A. & Christie, M. J. MU-RECEPTOR AND DELTA-RECEPTOR BELONG TO A FAMILY OF RECEPTORS THAT ARE COUPLED TO POTASSIUM CHANNELS. *Proc. Natl. Acad. Sci. U. S. A.* **84**, 5487-5491, doi:10.1073/pnas.84.15.5487 (1987).

104 Blackmer, T. *et al.* G protein betagamma subunit-mediated presynaptic inhibition: regulation of exocytotic fusion downstream of Ca2+ entry. *Science* **292**, 293-297, doi:10.1126/science.1058803 (2001).

105 Zurawski, Z., Yim, Y. Y., Alford, S. & Hamm, H. E. The expanding roles and mechanisms of G protein-mediated presynaptic inhibition. *J. Biol. Chem.* **294**, 1661-1670, doi:10.1074/jbc.TM118.004163 (2019).

106 He, X. J. *et al.* Convergent, functionally independent signaling by mu and delta opioid receptors in hippocampal parvalbumin interneurons. *Elife* **10**, doi:10.7554/eLife.69746 (2021).

107 Kabli, N., Fan, T., O'Dowd, B. F. & George, S. R. mu-delta opioid receptor heteromer-specific signaling in the striatum and hippocampus. *Biochem Biophys Res Commun* **450**, 906-911, doi:10.1016/j.bbrc.2014.06.099 (2014).

108 Gomes, I. *et al.* Heterodimerization of mu and delta opioid receptors: A role in opiate synergy. *J. Neurosci.* **20**, art. no.-RC110, doi:10.1523/JNEUROSCI.20-22-j0007.2000 (2000).

109 Arttamangkul, S., Platt, E. J., Carroll, J. & Farrens, D. Functional independence of endogenous mu- and delta-opioid receptors co-expressed in cholinergic interneurons. *Elife* **10**, doi:10.7554/eLife.69740 (2021).

110 Surmeier, D. J., Ding, J., Day, M., Wang, Z. F. & Shen, W. X. D1 and D2 dopamine-receptor modulation of striatal glutamatergic signaling in striatal medium spiny neurons. *Trends Neurosci.* **30**, 228-235, doi:10.1016/j.tins.2007.03.008 (2007).

111 Nugent, F. S., Penick, E. C. & Kauer, J. A. Opioids block long-term potentiation of inhibitory synapses. *Nature* **446**, 1086-1090, doi:10.1038/nature05726 (2007).

112 Lau, B. K., Ambrose, B. P., Thomas, C. S., Qiao, M. & Borgland, S. L. Mu-Opioids Suppress GABAergic Synaptic Transmission onto Orbitofrontal Cortex Pyramidal Neurons with Subregional Selectivity. *J. Neurosci.* **40**, 5894-5907, doi:10.1523/JNEUROSCI.2049-19.2020 (2020).

113 Wagner, J. J., Etemad, L. R. & Thompson, A. M. Opioid-mediated facilitation of long-term depression in rat hippocampus. *Journal of Pharmacology and Experimental Therapeutics* **296**, 776-781 (2001).

114 Jiang, Z. G. & North, R. A. Pre- and postsynaptic inhibition by opioids in rat striatum. *J. Neurosci.* **12**, 356-361 (1992).

115 Winters, B. L. *et al.* Endogenous opioids regulate moment-to-moment neuronal communication and excitability. *Nat Commun* **8**, 14611, doi:10.1038/ncomms14611 (2017).

116 Johnson, S. W. & North, R. A. Opioids excite dopamine neurons by hyperpolarization of local interneurons. *J. Neurosci.* **12**, 483-488 (1992).

117 Turner, B. D., Kashima, D. T., Manz, K. M., Grueter, C. A. & Grueter, B. A. Synaptic Plasticity in the Nucleus Accumbens: Lessons Learned from Experience. *ACS Chem. Neurosci.* **9**, 2114-2126, doi:10.1021/acschemneuro.7b00420 (2018).

118 Atwood, B. K., Kupferschmidt, D. A. & Lovinger, D. M. Opioids induce dissociable forms of long-term depression of excitatory inputs to the dorsal striatum. *Nat. Neurosci.* **17**, 540-548, doi:10.1038/nn.3652 (2014).

119 Muñoz, B., Haggerty, D. L. & Atwood, B. K. Synapse-specific expression of mu opioid receptor long-term depression in the dorsomedial striatum. *Sci. Rep.* **10**, 7234, doi:10.1038/s41598-020-64203-0 (2020).

120 Muñoz, B., Fritz, B. M., Yin, F. & Atwood, B. K. Alcohol exposure disrupts mu opioid receptor-mediated long-term depression at insular cortex inputs to dorsolateral striatum. *Nat Commun* **9**, 1318, doi:10.1038/s41467-018-03683-1 (2018).

121 Miura, M., Saino-Saito, S., Masuda, M., Kobayashi, K. & Aosaki, T. Compartment-specific modulation of GABAergic synaptic transmission by mu-opioid receptor in the mouse striatum with green fluorescent protein-expressing dopamine islands. *J. Neurosci.* **27**, 9721-9728, doi:10.1523/jneurosci.2993-07.2007 (2007).

122 Tejeda, H. A. *et al.* Pathway- and Cell-Specific Kappa-Opioid Receptor Modulation of Excitation-Inhibition Balance Differentially Gates D1 and D2 Accumbens Neuron Activity. *Neuron* **93**, 147-163, doi:10.1016/j.neuron.2016.12.005 (2017).

123 Manz, K. M., Baxley, A. G., Zurawski, Z., Hamm, H. E. & Grueter, B. A. Heterosynaptic GABAB Receptor Function within Feedforward Microcircuits Gates Glutamatergic Transmission in the Nucleus Accumbens Core. *J. Neurosci.* **39**, 9277-9293, doi:10.1523/JNEUROSCI.1395-19.2019 (2019).

124 Wright, W. J., Schluter, O. M. & Dong, Y. A Feedforward Inhibitory Circuit Mediated by CB1-Expressing Fast-Spiking Interneurons in the Nucleus Accumbens. *Neuropsychopharmacology* **42**, 1146-1156, doi:10.1038/npp.2016.275 (2017).

125 Mathur, B. N., Tanahira, C., Tamamaki, N. & Lovinger, D. M. Voltage drives diverse endocannabinoid signals to mediate striatal microcircuit-specific plasticity. *Nat. Neurosci.* **16**, 1275-U1157, doi:10.1038/nn.3478 (2013).

126 Grueter, B. A., Brasnjo, G. & Malenka, R. C. Postsynaptic TRPV1 triggers cell type-specific long-term depression in the nucleus accumbens. *Nat. Neurosci.* **13**, 1519-U1107, doi:10.1038/nn.2685 (2010).

127 Singla, S., Kreitzer, A. C. & Malenka, R. C. Mechanisms for synapse specificity during striatal long-term depression. *J. Neurosci.* **27**, 5260-5264, doi:10.1523/JNEUROSCI.0018-07.2007 (2007).

128 Kreitzer, A. C. & Malenka, R. C. Dopamine modulation of state-dependent endocannabinoid release and long-term depression in the striatum. *J. Neurosci.* **25**, 10537-10545, doi:10.1523/jneurosci.2959-05.2005 (2005).

129 Hoffman, A. F. & Lupica, C. R. Direct actions of cannabinoids on synaptic transmission in the nucleus accumbens: A comparison with opioids. *J. Neurophysiol.* **85**, 72-83, doi:10.1152/jn.2001.85.1.72 (2001).

130 Mathur, B. N., Capik, N. A., Alvarez, V. A. & Lovinger, D. M. Serotonin induces long-term depression at corticostriatal synapses. *J. Neurosci.* **31**, 7402-7411, doi:10.1523/JNEUROSCI.6250-10.2011 (2011).

131 Dolen, G., Darvishzadeh, A., Huang, K. W. & Malenka, R. C. Social reward requires coordinated activity of nucleus accumbens oxytocin and serotonin. *Nature* **501**, 179-184, doi:10.1038/nature12518 (2013).

132 Huang, C. C. *et al.* Cocaine Withdrawal Impairs Metabotropic Glutamate Receptor-Dependent Long-Term Depression in the Nucleus Accumbens. *J. Neurosci.* **31**, 4194-4203, doi:10.1523/jneurosci.5239-10.2011 (2011).

133 Luscher, C. & Huber, K. M. Group 1 mGIuR-Dependent Synaptic Long-Term Depression: Mechanisms and Implications for Circuitry and Disease. *Neuron* **65**, 445-459, doi:10.1016/j.neuron.2010.01.016 (2010).

134 Martin, T. F. Tuning exocytosis for speed: fast and slow modes. *Biochim Biophys Acta* **1641**, 157-165, doi:10.1016/s0167-4889(03)00093-4 (2003).

135 Tallent, M. K. Presynaptic inhibition of glutamate release by neuropeptides: use-dependent synaptic modification. *Results Probl. Cell Differ.* **44**, 177-200, doi:10.1007/400_2007_037 (2008).

136 van den Pol, A. N. Neuropeptide Transmission in Brain Circuits. *Neuron* **76**, 98-115, doi:10.1016/j.neuron.2012.09.014 (2012).

137 Bruns, D. & Jahn, R. Real-time measurement of transmitter release from single synaptic vesicles. *Nature* **377**, 62-65, doi:10.1038/377062a0 (1995).

138 De Camilli, P. & Jahn, R. Pathways to regulated exocytosis in neurons. *Annu. Rev. Physiol.* **52**, 625-645, doi:10.1146/annurev.ph.52.030190.003205 (1990).

139 Gregoriou, G. C., Patel, S. D., Winters, B. L. & Bagley, E. E. Neprilysin Controls the Synaptic Activity of Neuropeptides in the Intercalated Cells of the Amygdala. *Mol. Pharmacol.* **98**, 454-461, doi:10.1124/mol.119.119370 (2020).

140 Blomeley, C. P. & Bracci, E. Opioidergic Interactions between Striatal Projection Neurons. *J. Neurosci.* **31**, 13346-13356, doi:10.1523/jneurosci.1775-11.2011 (2011).

141 Muschol, M. & Salzberg, B. M. Dependence of transient and residual calcium dynamics on action-potential patterning during neuropeptide secretion. *J. Neurosci.* **20**, 6773-6780 (2000).

142 Weisskopf, M. G., Zalutsky, R. A. & Nicoll, R. A. The opioid peptide dynorphin mediates heterosynaptic depression of hippocampal mossy fibre synapses and modulates long-term potentiation. *Nature* **362**, 423-427, doi:10.1038/362423a0 (1993).

143 Iremonger, K. J. & Bains, J. S. Retrograde Opioid Signaling Regulates Glutamatergic Transmission in the Hypothalamus. *J. Neurosci.* **29**, 7349-7358, doi:10.1523/jneurosci.0381-09.2009 (2009).

144 Al-Hasani, R. *et al.* Distinct Subpopulations of Nucleus Accumbens Dynorphin Neurons Drive Aversion and Reward. *Neuron* **87**, 1063-1077, doi:10.1016/j.neuron.2015.08.019 (2015).

145 Adamantidis, A. R., Zhang, F., Aravanis, A. M., Deisseroth, K. & de Lecea, L. Neural substrates of awakening probed with optogenetic control of hypocretin neurons. *Nature* **450**, 420-424, doi:10.1038/nature06310 (2007).

146 Schone, C., Apergis-Schoute, J., Sakurai, T., Adamantidis, A. & Burdakov, D. Coreleased Orexin and Glutamate Evoke Nonredundant Spike Outputs and Computations in Histamine Neurons. *Cell Rep.* **7**, 697-704, doi:10.1016/j.celrep.2014.03.055 (2014).

147 Arrigoni, E. & Saper, C. B. What optogenetic stimulation is telling us (and failing to tell us) about fast neurotransmitters and neuromodulators in brain circuits for wake-sleep regulation. *Curr. Opin. Neurobiol.* **29**, 165-171, doi:10.1016/j.conb.2014.07.016 (2014).

148 Qiu, J. *et al.* High-frequency stimulation-induced peptide release synchronizes arcuate kisspeptin neurons and excites GnRH neurons. *Elife* **5**, doi:10.7554/eLife.16246 (2016).

149 Bartfai, T., Iverfeldt, K., Fisone, G. & Serfozo, P. Regulation of the release of coexisting neurotransmitters. *Annu Rev Pharmacol Toxicol* **28**, 285-310, doi:10.1146/annurev.pa.28.040188.001441 (1988).

150 Muschamp, J. W. *et al.* Hypocretin (orexin) facilitates reward by attenuating the antireward effects of its cotransmitter dynorphin in ventral tegmental area. *Proc. Natl. Acad. Sci. U. S. A.* **111**, E1648-1655, doi:10.1073/pnas.1315542111 (2014).

151 Mansour, A., Hoversten, M. T., Taylor, L. P., Watson, S. J. & Akil, H. THE CLONED MU-RECEPTORS, DELTA-RECEPTORS AND KAPPA-RECEPTORS AND THEIR ENDOGENOUS LIGANDS - EVIDENCE FOR 2 OPIOID PEPTIDE RECOGNITION CORES. *Brain Res.* **700**, 89-98, doi:10.1016/0006-8993(95)00928-j (1995).

152 Schmid, C. L. *et al.* Bias Factor and Therapeutic Window Correlate to Predict Safer Opioid Analgesics. *Cell* **171**, 1165-+, doi:10.1016/j.cell.2017.10.035 (2017).

153 Conibear, A. E. & Kelly, E. A Biased View of mu-Opioid Receptors? *Mol. Pharmacol.* **96**, 542-549, doi:10.1124/mol.119.115956 (2019).

154 Pradhan, A. A., Smith, M. L., Kieffer, B. L. & Evans, C. J. Ligand-directed signalling within the opioid receptor family. *Br. J. Pharmacol.* **167**, 960-969, doi:10.1111/j.1476-5381.2012.02075.x (2012).

155 Gomes, I. *et al.* Biased signaling by endogenous opioid peptides. *Proc. Natl. Acad. Sci. U. S. A.* **117**, 11820-11828, doi:10.1073/pnas.2000712117 (2020).

156 Thompson, G. L. *et al.* Biased Agonism of Endogenous Opioid Peptides at the mu-Opioid Receptor. *Mol. Pharmacol.* **88**, 335-346, doi:10.1124/mol.115.098848 (2015).

157 Kunselman, J. M., Gupta, A., Gomes, I., Devi, L. A. & Puthenveedu, M. A. Compartment-specific opioid receptor signaling is selectively modulated by different dynorphin peptides. *Elife* **10**, doi:10.7554/eLife.60270 (2021).

158 Garzon, J., Sanchez-Blazquez, P., Hollt, V., Lee, N. M. & Loh, H. H. Endogenous opioid peptides: comparative evaluation of their receptor affinities in the mouse brain. *Life Sci.* **33 Suppl 1**, 291-294, doi:10.1016/0024-3205(83)90500-3 (1983).

159 Magnan, J., Paterson, S. J. & Kosterlitz, H. W. The interaction of [MET5]enkephalin and [LEU5]enkephalin sequences, extended at the C-terminus, with the mu-, delta- and

kappa-binding sites in the guinea-pig brain. *Life Sci.* **31**, 1359-1361, doi:10.1016/0024-3205(82)90381-2 (1982).

160 Wuster, M., Rubini, P. & Schulz, R. The preference of putative pro-enkephalins for different types of opiate receptors. *Life Sci.* **29**, 1219-1227, doi:10.1016/0024-3205(81)90226-5 (1981).

161 Vats, I. D. *et al.* Endogenous peptide: Met-enkephalin-Arg-Phe, differently regulate expression of opioid receptors on chronic treatment. *Neuropeptides* **43**, 355-362, doi:10.1016/j.npep.2009.07.003 (2009).

162 Mellstrom, B., Iadarola, M. J. & Costa, E. Effect of peptidase inhibitors on [Met5]enkephalin-Arg6-Phe7 and [Met5]enkephalin-Arg6-Gly7-Leu8-induced antinociception. *Eur. J. Pharmacol.* **133**, 185-190, doi:10.1016/0014-2999(87)90149-x (1987).

163 Inturrisi, C. E. *et al.* ANALGESIC ACTIVITY OF THE NATURALLY-OCCURRING HEPTAPEPTIDE MET ENKEPHALIN-ARG6-PHE7. *Proceedings of the National Academy of Sciences of the United States of America-Biological Sciences* **77**, 5512-5514, doi:10.1073/pnas.77.9.5512 (1980).

164 Corbett, A. D., Paterson, S. J., McKnight, A. T., Magnan, J. & Kosterlitz, H. W. Dynorphin and dynorphin are ligands for the kappa-subtype of opiate receptor. *Nature* **299**, 79-81, doi:10.1038/299079a0 (1982).

165 Goldstein, A., Tachibana, S., Lowney, L. I., Hunkapiller, M. & Hood, L. Dynorphin-(1-13), an extraordinarily potent opioid peptide. *Proc. Natl. Acad. Sci. U. S. A.* **76**, 6666-6670, doi:10.1073/pnas.76.12.6666 (1979).

166 Song, B. & Marvizón, J. C. Peptidases prevent mu-opioid receptor internalization in dorsal horn neurons by endogenously released opioids. *J. Neurosci.* **23**, 1847-1858 (2003).

167 Khaket, T. P., Singh, J., Attri, P. & Dhanda, S. Enkephalin Degrading Enzymes: Metalloproteases with High Potential for Drug Development. *Curr. Pharm. Des.* **18**, 220-230, doi:10.2174/138161212799040547 (2012).

168 Deddish, P. A., Jackman, H. L., Skidgel, R. A. & Erdos, E. G. Differences in the hydrolysis of enkephalin congeners by the two domains of angiotensin converting enzyme. *Biochem. Pharmacol.* **53**, 1459-1463, doi:10.1016/s0006-2952(97)00087-7 (1997).

169 Mosnaim, A. D. *et al.* In vitro Methionine(5)-enkephalin degradation kinetics by human brain preparations. *Neurochem. Res.* **33**, 81-86, doi:10.1007/s11064-007-9418-6 (2008).

170 Mellstrom, B., Iadarola, M. J., Yang, H. Y. & Costa, E. Inhibition of Met5-enkephalin-Arg6-Phe7 degradation by inhibitors of dipeptidyl carboxypeptidase. *J Pharmacol Exp Ther* **239**, 174-178 (1986).

171 Patey, G., Cupo, A., Mazarguil, H., Morgat, J. L. & Rossier, J. RELEASE OF PROENKEPHALIN-DERIVED OPIOID-PEPTIDES FROM RAT STRIATUM INVITRO AND THEIR RAPID DEGRADATION. *Neuroscience* **15**, 1035-1044, doi:10.1016/0306-4522(85)90252-0 (1985).

172 Patey, G. *et al.* SELECTIVE PROTECTION OF METHIONINE ENKEPHALIN RELEASED FROM BRAIN-SLICES BY ENKEPHALINASE INHIBITION. *Science* **212**, 113-1155, doi:10.1126/science.7015510 (1981).

173 Norman, J. A., Autry, W. L. & Barbaz, B. S. Angiotensin-converting enzyme inhibitors potentiate the analgesic activity of [Met]-enkephalin-Arg6-Phe7 by inhibiting its degradation in mouse brain. *Mol. Pharmacol.* **28**, 521-526 (1985).

174 Benuck, M., Berg, M. J. & Marks, N. SEPARATE METABOLIC PATHWAYS FOR LEU-ENKEPHALIN AND MET-ENKEPHALIN-ARG6-PHE7 DEGRADATION BY RAT STRIATAL SYNAPTOSOMAL MEMBRANES. *Neurochem. Int.* **4**, 389-396, doi:10.1016/0197-0186(82)90081-x (1982).

175 Yang, H. Y. T., Majane, E. & Costa, E. CONVERSION OF MET5 -ENKEPHALIN-ARG6-PHE7 TO MET5 -ENKEPHALIN BY DIPEPTIDYL CARBOXYPEPTIDASE. *Neuropharmacology* **20**, 891-894, doi:10.1016/0028-3908(81)90084-8 (1981).

176 Brown, N. J. & Vaughan, D. E. Angiotensin-converting enzyme inhibitors. *Circulation* **97**, 1411-1420, doi:10.1161/01.Cir.97.14.1411 (1998).

177 Song, J. C. & White, C. M. Clinical pharmacokinetics and selective pharmacodynamics of new angiotensin converting enzyme inhibitors: an update. *Clin. Pharmacokinet.* **41**, 207-224, doi:10.2165/00003088-200241030-00005 (2002).

178 Hanif, K., Bid, H. K. & Konwar, R. Reinventing the ACE inhibitors: some old and new implications of ACE inhibition. *Hypertens. Res.* **33**, 11-21, doi:10.1038/hr.2009.184 (2010).

179 Bader, M. & Ganten, D. Update on tissue renin-angiotensin systems. *Journal of Molecular Medicine-Jmm* **86**, 615-621, doi:10.1007/s00109-008-0336-0 (2008).

180 Paul, M., Mehr, A. P. & Kreutz, R. Physiology of local renin-angiotensin systems. *Physiol. Rev.* **86**, 747-803, doi:10.1152/physrev.00036.2005 (2006).

181 Strittmatter, S. M., Lo, M. M., Javitch, J. A. & Snyder, S. H. Autoradiographic visualization of angiotensin-converting enzyme in rat brain with [3H]captopril: localization to a striatonigral pathway. *Proc. Natl. Acad. Sci. U. S. A.* **81**, 1599-1603, doi:10.1073/pnas.81.5.1599 (1984).

182 Chai, S. Y., Mendelsohn, F. A. & Paxinos, G. Angiotensin converting enzyme in rat brain visualized by quantitative in vitro autoradiography. *Neuroscience* **20**, 615-627, doi:10.1016/0306-4522(87)90114-x (1987).

183 Whiting, P., Nava, S., Mozley, L., Eastham, H. & Poat, J. Expression of angiotensin converting enzyme mRNA in rat brain. *Brain Res. Mol. Brain Res.* **11**, 93-96, doi:10.1016/0169-328x(91)90026-t (1991).

184 Strittmatter, S. M. & Snyder, S. H. ANGIOTENSIN CONVERTING ENZYME IMMUNOHISTOCHEMISTRY IN RAT-BRAIN AND PITUITARY-GLAND - CORRELATION OF ISOZYME TYPE WITH CELLULAR-LOCALIZATION. *Neuroscience* **21**, 407-420, doi:10.1016/0306-4522(87)90131-x (1987).

185 Poth, M. M., Heath, R. G. & Ward, M. Angiotensin-converting enzyme in human brain. *J. Neurochem.* **25**, 83-85, doi:10.1111/j.1471-4159.1975.tb07698.x (1975).

186 Yang, H. Y. T. & Neff, N. H. DISTRIBUTION AND PROPERTIES OF ANGIOTENSIN CONVERTING ENZYME OF RAT-BRAIN. *J. Neurochem.* **19**, 2443-&, doi:10.1111/j.1471-4159.1972.tb01298.x (1972).

187 Semis, M., Gugiu, G. B., Bernstein, E. A., Bernstein, K. E. & Kalkum, M. The Plethora of Angiotensin-Converting Enzyme-Processed Peptides in Mouse Plasma. *Anal. Chem.* **91**, 6440-6453, doi:10.1021/acs.analchem.8b03828 (2019).

188 Skidgel, R. A. & Erdos, E. G. THE BROAD SUBSTRATE-SPECIFICITY OF HUMAN ANGIOTENSIN-I CONVERTING ENZYME. *Clinical and Experimental Hypertension Part a-Theory and Practice* **9**, 243-259, doi:10.3109/10641968709164184 (1987).

189 Skidgel, R. A., Engelbrecht, S., Johnson, A. R. & Erdos, E. G. Hydrolysis of substance p and neurotensin by converting enzyme and neutral endopeptidase. *Peptides* **5**, 769-776, doi:10.1016/0196-9781(84)90020-2 (1984).

190 Hallberg, M. Neuropeptides: metabolism to bioactive fragments and the pharmacology of their receptors. *Med. Res. Rev.* **35**, 464-519, doi:10.1002/med.21323 (2015).

191 Marvizon, J. C. G., Wang, X. R., Lao, L. J. & Song, B. B. Effect of peptidases on the ability of exogenous and endogenous neurokinins to produce neurokinin 1 receptor internalization in the rat spinal cord. *Br. J. Pharmacol.* **140**, 1389-1398, doi:10.1038/sj.bjp.0705578 (2003).

192 Bernstein, K. E. *et al.* A Modern Understanding of the Traditional and Nontraditional Biological Functions of Angiotensin-Converting Enzyme. *Pharmacol. Rev.* **65**, 1-46, doi:10.1124/pr.112.006809 (2013).

193 Oblin, A., Danse, M. J. & Zivkovic, B. Degradation of substance P by membrane peptidases in the rat substantia nigra: effect of selective inhibitors. *Neurosci. Lett.* **84**, 91-96, doi:10.1016/0304-3940(88)90343-6 (1988).

194 Mitchell, A. J., Lone, A. M., Tinoco, A. D. & Saghatelian, A. Proteolysis controls endogenous substance P levels. *PLoS One* **8**, e68638, doi:10.1371/journal.pone.0068638 (2013).

195 Skidgel, R. A. & Erdos, E. G. Angiotensin converting enzyme (ACE) and neprilysin hydrolyze neuropeptides: a brief history, the beginning and follow-ups to early studies. *Peptides* **25**, 521-525, doi:10.1016/j.peptides.2003.12.010 (2004).

196 Hartman, K., Mielczarek, P., Smoluch, M. & Silberring, J. Inhibitors of neuropeptide peptidases engaged in pain and drug dependence. *Neuropharmacology* **175**, 108137, doi:10.1016/j.neuropharm.2020.108137 (2020).

197 Poras, H., Bonnard, E., Dange, E., Fournie-Zaluski, M. C. & Roques, B. P. New orally active dual enkephalinase inhibitors (DENKIs) for central and peripheral pain treatment. *J. Med. Chem.* **57**, 5748-5763, doi:10.1021/jm500602h (2014).

198 Southerland, W. A. *et al.* Dual Enkephalinase Inhibitors and Their Role in Chronic Pain Management. *Curr Pain Headache Rep* **25**, 29, doi:10.1007/s11916-021-00949-0 (2021).

199 Roques, B. P., Fournie-Zaluski, M. C. & Wurm, M. Inhibiting the breakdown of endogenous opioids and cannabinoids to alleviate pain. *Nature Reviews Drug Discovery* **11**, 292-310, doi:10.1038/nrd3673 (2012).

200 Thanawala, V., Kadam, V. J. & Ghosh, R. Enkephalinase Inhibitors: Potential Agents for the Management of Pain. *Curr. Drug Targets* **9**, 887-894, doi:10.2174/138945008785909356 (2008).

201 Jutkiewicz, E. M. RB101-mediated protection of endogenous opioids: potential therapeutic utility? *CNS Drug Rev* **13**, 192-205, doi:10.1111/j.1527-3458.2007.00011.x (2007).

202 Gaspari, S. *et al.* Suppression of RGSz1 function optimizes the actions of opioid analgesics by mechanisms that involve the Wnt/beta-catenin pathway. *Proc. Natl. Acad. Sci. U. S. A.* **115**, E2085-E2094, doi:10.1073/pnas.1707887115 (2018).

203 Matsui, A., Jarvie, B. C., Robinson, B. G., Hentges, S. T. & Williams, J. T. Separate GABA afferents to dopamine neurons mediate acute action of opioids, development of tolerance, and expression of withdrawal. *Neuron* **82**, 1346-1356, doi:10.1016/j.neuron.2014.04.030 (2014).

204 Cordonnier, L., Sanchez, M., Roques, B. P. & Noble, F. Blockade of morphine-induced behavioral sensitization by a combination of amisulpride and RB101, comparison with classical opioid maintenance treatments. *Br. J. Pharmacol.* **151**, 94-102, doi:10.1038/sj.bjp.0707195 (2007).

205 Trieu, B. H. *et al.* Angiotensin-converting enzyme gates brain circuit-specific plasticity via an endogenous opioid. *Science* **375**, 1177-1182, doi:10.1126/science.abl5130 (2022).

206 Shansky, R. M. Are hormones a "female problem" for animal research? *Science* **364**, 825-826, doi:10.1126/science.aaw7570 (2019).

207 Konig, M. *et al.* Pain responses, anxiety and aggression in mice deficient in pre-proenkephalin. *Nature* **383**, 535-538, doi:10.1038/383535a0 (1996).

208 Madisen, L. *et al.* A toolbox of Cre-dependent optogenetic transgenic mice for light-induced activation and silencing. *Nat. Neurosci.* **15**, 793-802, doi:10.1038/nn.3078 (2012).

209 Gerfen, C. R., Paletzki, R. & Heintz, N. GENSAT BAC cre-recombinase driver lines to study the functional organization of cerebral cortical and basal ganglia circuits. *Neuron* **80**, 1368-1383, doi:10.1016/j.neuron.2013.10.016 (2013).

210 Chen, X. F. *et al.* Angiotensin-Converting Enzyme in Smooth Muscle Cells Promotes Atherosclerosis-Brief Report. *Arteriosclerosis Thrombosis and Vascular Biology* **36**, 1085-+, doi:10.1161/atvbaha.115.307038 (2016).

211 Gong, S. *et al.* Targeting Cre recombinase to specific neuron populations with bacterial artificial chromosome constructs. *J. Neurosci.* **27**, 9817-9823, doi:10.1523/JNEUROSCI.2707-07.2007 (2007).

212 Matthes, H. W. D. *et al.* Loss of morphine-induced analgesia, reward effect and withdrawal symptoms in mice lacking the mu-opioid-receptor gene. *Nature* **383**, 819-823, doi:10.1038/383819a0 (1996).

213 Matsuda, H., Kurata, Y., Imanishi, S., Sato, R. & Shibamoto, T. Effects of angiotensin II on sustained outward currents in rat ventricular myocytes. *Pflugers Arch.* **448**, 54-62, doi:10.1007/s00424-003-1217-6 (2004).

214 Shetty, S. S. & DelGrande, D. Differential inhibition of the prejunctional actions of angiotensin II in rat atria by valsartan, irbesartan, eprosartan, and losartan. *J Pharmacol Exp Ther* **294**, 179-186 (2000).

215 Wang, J. *et al.* Valsartan lowers brain beta-amyloid protein levels and improves spatial learning in a mouse model of Alzheimer disease. *J. Clin. Invest.* **117**, 3393-3402, doi:10.1172/JCI31547 (2007).

216 Sohn, Y. I. *et al.* Antihypertensive drug Valsartan promotes dendritic spine density by altering AMPA receptor trafficking. *Biochem Biophys Res Commun* **439**, 464-470, doi:10.1016/j.bbrc.2013.08.091 (2013).

217 Ong, E. W., Xue, L., Olmstead, M. C. & Cahill, C. M. Prolonged morphine treatment alters delta opioid receptor post-internalization trafficking. *Br. J. Pharmacol.* **172**, 615-629, doi:10.1111/bph.12761 (2015).

218 Hjelmstad, G. O. & Fields, H. L. Kappa opioid receptor inhibition of glutamatergic transmission in the nucleus accumbens shell. *J. Neurophysiol.* **85**, 1153-1158, doi:10.1152/jn.2001.85.3.1153 (2001).

219 Chieng, B., Connor, M. & Christie, M. J. The mu-opioid receptor antagonist D-Phe-Cys-Tyr-D-Trp-Orn-Thr-Pen-Thr-NH2 (CTOP) [but not D-Phe-Cys-Tyr-D-Trp-Arg-Thr-Pen-Thr-NH2 (CTAP)] produces a nonopioid receptor-mediated increase in K+ conductance of rat locus ceruleus neurons. *Mol. Pharmacol.* **50**, 650-655 (1996).

220 Bagley, E. E., Gerke, M. B., Vaughan, C. W., Hack, S. P. & Christie, M. J. GABA transporter currents activated by protein kinase A excite midbrain neurons during opioid withdrawal. *Neuron* **45**, 433-445, doi:10.1016/j.neuron.2004.12.049 (2005).

221 Harrison, J. M., Allen, R. G., Pellegrino, M. J., Williams, J. T. & Manzoni, O. J. Chronic morphine treatment alters endogenous opioid control of hippocampal mossy fiber synaptic transmission. *J. Neurophysiol.* **87**, 2464-2470, doi:10.1152/jn.2002.87.5.2464 (2002).

222 Pennock, R. L. & Hentges, S. T. Direct inhibition of hypothalamic proopiomelanocortin neurons by dynorphin A is mediated by the mu-opioid receptor. *J. Physiol.* **592**, 4247-4256, doi:10.1113/jphysiol.2014.275339 (2014).

223 Levitt, E. S., Abdala, A. P., Paton, J. F., Bissonnette, J. M. & Williams, J. T. mu opioid receptor activation hyperpolarizes respiratory-controlling Kolliker-Fuse neurons and suppresses post-inspiratory drive. *J. Physiol.* **593**, 4453-4469, doi:10.1113/JP270822 (2015).

224 Rappsilber, J., Ishihama, Y. & Mann, M. Stop and go extraction tips for matrix-assisted laser desorption/ionization, nanoelectrospray, and LC/MS sample pretreatment in proteomics. *Anal. Chem.* **75**, 663-670, doi:10.1021/ac026117i (2003).

225 Li, D. *et al.* Plasma lipoproteome in Alzheimer's disease: a proof-of-concept study. *Clin. Proteomics* **15**, 31, doi:10.1186/s12014-018-9207-z (2018).

226 Toddes, C., Lefevre, E. M., Brandner, D. D., Zugschwert, L. & Rothwell, P. E. mu-Opioid Receptor (Oprm1) Copy Number Influences Nucleus Accumbens Microcircuitry and

Reciprocal Social Behaviors. *J. Neurosci.* **41**, 7965-7977, doi:10.1523/JNEUROSCI.2440-20.2021 (2021).

227 Terranova, M. L. & Laviola, G. Scoring of social interactions and play in mice during adolescence. *Curr. Protoc. Toxicol.* **Chapter 13**, Unit13 10, doi:10.1002/0471140856.tx1310s26 (2005).

228 Lefevre, E. M. *et al.* Interruption of continuous opioid exposure exacerbates drug-evoked adaptations in the mesolimbic dopamine system. *Neuropsychopharmacology* **45**, 1781-1792, doi:10.1038/s41386-020-0643-x (2020).

229 Pisansky, M. T. *et al.* Nucleus Accumbens Fast-Spiking Interneurons Constrain Impulsive Action. *Biol. Psychiatry* **86**, 836-847, doi:10.1016/j.biopsych.2019.07.002 (2019).

230 Savell, K. E. *et al.* A dopamine-induced gene expression signature regulates neuronal function and cocaine response. *Sci Adv* **6**, eaba4221, doi:10.1126/sciadv.aba4221 (2020).

231 Nieuwenhuis, S., Forstmann, B. U. & Wagenmakers, E. J. Erroneous analyses of interactions in neuroscience: a problem of significance. *Nat. Neurosci.* **14**, 1105-1107, doi:10.1038/nn.2886 (2011).

232 Yoshikawa, K., Williams, C. & Sabol, S. L. Rat brain preproenkephalin mRNA. cDNA cloning, primary structure, and distribution in the central nervous system. *J. Biol. Chem.* **259**, 14301-14308 (1984).

233 Rosen, H., Douglass, J. & Herbert, E. Isolation and characterization of the rat proenkephalin gene. *J. Biol. Chem.* **259**, 14309-14313 (1984).

234 Comb, M., Rosen, H., Seeburg, P., Adelman, J. & Herbert, E. Primary structure of the human proenkephalin gene. *DNA* **2**, 213-229, doi:10.1089/dna.1983.2.213 (1983).

235 Gubler, U., Seeburg, P., Hoffman, B. J., Gage, L. P. & Udenfriend, S. Molecular cloning establishes proenkephalin as precursor of enkephalin-containing peptides. *Nature* **295**, 206-208, doi:10.1038/295206a0 (1982).

236 Brock, J. A., Thomazeau, A., Watanabe, A., Li, S. S. Y. & Sjostrom, P. J. A Practical Guide to Using CV Analysis for Determining the Locus of Synaptic Plasticity. *Front. Synaptic Neurosci.* **12**, 11, doi:10.3389/fnsyn.2020.00011 (2020).

237 Choi, S. & Lovinger, D. M. Decreased probability of neurotransmitter release underlies striatal long-term depression and postnatal development of corticostriatal synapses. *Proc. Natl. Acad. Sci. U. S. A.* **94**, 2665-2670, doi:10.1073/pnas.94.6.2665 (1997).

238 Orning, L. *et al.* INHIBITION OF LEUKOTRIENE-A4 HYDROLASE AMINOPEPTIDASE BY CAPTOPRIL. *J. Biol. Chem.* **266**, 16507-16511 (1991).

239 Charbogne, P. *et al.* Mu Opioid Receptors in Gamma-Aminobutyric Acidergic Forebrain Neurons Moderate Motivation for Heroin and Palatable Food. *Biol. Psychiatry* **81**, 778-788, doi:10.1016/j.biopsych.2016.12.022 (2017).

240 Zhou, Y., Mabrouk, O. S. & Kennedy, R. T. Rapid Preconcentration for Liquid Chromatography-Mass Spectrometry Assay of Trace Level Neuropeptides. *J. Am. Soc. Mass Spectrom.* **24**, 1700-1709, doi:10.1007/s13361-013-0605-1 (2013).

241 Aebersold, R. & Mann, M. Mass spectrometry-based proteomics. *Nature* **422**, 198-207, doi:10.1038/nature01511 (2003).

242 Aebersold, R. & Mann, M. Mass-spectrometric exploration of proteome structure and function. *Nature* **537**, 347-355, doi:10.1038/nature19949 (2016).

243 Al-Hasani, R. *et al.* In vivo detection of optically-evoked opioid peptide release. *Elife* **7**, doi:10.7554/eLife.36520 (2018).

244 Augustine, F., Rajendran, S. & Singer, H. S. Cortical endogenous opioids and their role in facilitating repetitive behaviors in deer mice. *Behav. Brain Res.* **379**, 112317, doi:10.1016/j.bbr.2019.112317 (2020).

245 Richter, J. A., Wesche, D. L. & Frederickson, R. C. A. K-STIMULATED RELEASE OF LEU-ENKEPHALIN AND MET-ENKEPHALIN FROM RAT STRIATAL SLICES - LACK OF EFFECT OF MORPHINE AND NALOXONE. *Eur. J. Pharmacol.* **56**, 105-113, doi:10.1016/0014-2999(79)90439-4 (1979).

246 Calipari, E. S. *et al.* In vivo imaging identifies temporal signature of D1 and D2 medium spiny neurons in cocaine reward. *Proc. Natl. Acad. Sci. U. S. A.* **113**, 2726-2731, doi:10.1073/pnas.1521238113 (2016).

247 Trezza, V., Damsteegt, R., Achterberg, E. J. & Vanderschuren, L. J. Nucleus accumbens mu-opioid receptors mediate social reward. *J. Neurosci.* **31**, 6362-6370, doi:10.1523/JNEUROSCI.5492-10.2011 (2011).

248 Raynor, K. *et al.* Pharmacological characterization of the cloned kappa-, delta-, and mu-opioid receptors. *Mol. Pharmacol.* **45**, 330-334 (1994).

249 Nieto, M. M., Guen, S. L. E., Kieffer, B. L., Roques, B. P. & Noble, F. Physiological control of emotion-related behaviors by endogenous enkephalins involves essentially the delta opioid receptors. *Neuroscience* **135**, 305-313, doi:10.1016/j.neuroscience.2005.06.025 (2005).

250 Burke, D. A., Rotstein, H. G. & Alvarez, V. A. Striatal Local Circuitry: A New Framework for Lateral Inhibition. *Neuron* **96**, 267-284, doi:10.1016/j.neuron.2017.09.019 (2017).

251 Tunstall, M. J., Oorschot, D. E., Kean, A. & Wickens, J. R. Inhibitory interactions between spiny projection neurons in the rat striatum. *J. Neurophysiol.* **88**, 1263-1269, doi:10.1152/jn.2002.88.3.1263 (2002).

252 Taverna, S., van Dongen, Y. C., Groenewegen, H. J. & Pennartz, C. M. Direct physiological evidence for synaptic connectivity between medium-sized spiny neurons in rat nucleus accumbens in situ. *J. Neurophysiol.* **91**, 1111-1121, doi:10.1152/jn.00892.2003 (2004).

253 Czubayko, U. & Plenz, D. Fast synaptic transmission between striatal spiny projection neurons. *Proc. Natl. Acad. Sci. U. S. A.* **99**, 15764-15769, doi:10.1073/pnas.242428599 (2002).

254 Taverna, S., Ilijic, E. & Surmeier, D. J. Recurrent collateral connections of striatal medium spiny neurons are disrupted in models of Parkinson's disease. *J. Neurosci.* **28**, 5504-5512, doi:10.1523/JNEUROSCI.5493-07.2008 (2008).

255 Wei, W., Ding, S. & Zhou, F. M. Dopaminergic treatment weakens medium spiny neuron collateral inhibition in the parkinsonian striatum. *J. Neurophysiol.* **117**, 987-999, doi:10.1152/jn.00683.2016 (2017).

256 Planert, H., Szydlowski, S. N., Hjorth, J. J., Grillner, S. & Silberberg, G. Dynamics of synaptic transmission between fast-spiking interneurons and striatal projection neurons of the direct and indirect pathways. *J. Neurosci.* **30**, 3499-3507, doi:10.1523/JNEUROSCI.5139-09.2010 (2010).

257 Gazan, A., Rial, D. & Schiffmann, S. N. Ablation of striatal somatostatin interneurons affects MSN morphology and electrophysiological properties, and increases cocaine-induced hyperlocomotion in mice. *Eur. J. Neurosci.* **51**, 1388-1402, doi:10.1111/ejn.14581 (2020).

258 Holly, E. N. *et al.* Striatal Low-Threshold Spiking Interneurons Regulate Goal-Directed Learning. *Neuron* **103**, 92-+, doi:10.1016/j.neuron.2019.04.016 (2019).

259 Owen, S. F., Berke, J. D. & Kreitzer, A. C. Fast-Spiking Interneurons Supply Feedforward Control of Bursting, Calcium, and Plasticity for Efficient Learning. *Cell* **172**, 683-695 e615, doi:10.1016/j.cell.2018.01.005 (2018).

260 Gittis, A. H., Nelson, A. B., Thwin, M. T., Palop, J. J. & Kreitzer, A. C. Distinct Roles of GABAergic Interneurons in the Regulation of Striatal Output Pathways. *J. Neurosci.* **30**, 2223-2234, doi:10.1523/jneurosci.4870-09.2010 (2010).

261 Ibanez-Sandoval, O. *et al.* A Novel Functionally Distinct Subtype of Striatal Neuropeptide Y Interneuron. *J. Neurosci.* **31**, 16757-16769, doi:10.1523/jneurosci.2628-11.2011 (2011).

262 Burke, D. A. & Alvarez, V. A. Serotonin receptors contribute to dopamine depression of lateral inhibition in the nucleus accumbens. *Cell Rep.* **39**, 110795, doi:10.1016/j.celrep.2022.110795 (2022).

263 Dobbs, L. K. *et al.* Dopamine Regulation of Lateral Inhibition between Striatal Neurons Gates the Stimulant Actions of Cocaine. *Neuron* **90**, 1100-1113, doi:10.1016/j.neuron.2016.04.031 (2016).

264 Wang, Z. F. *et al.* Dopaminergic control of corticostriatal long-term synaptic depression in medium spiny neurons is mediated by cholinergic interneurons. *Neuron* **50**, 443-452, doi:10.1016/j.neuron.2006.04.010 (2006).

265 English, D. F. *et al.* GABAergic circuits mediate the reinforcement-related signals of striatal cholinergic interneurons. *Nat. Neurosci.* **15**, 123-U155, doi:10.1038/nn.2984 (2012).

266 Oldenburg, I. A. & Ding, J. B. Cholinergic modulation of synaptic integration and dendritic excitability in the striatum. *Curr. Opin. Neurobiol.* **21**, 425-432, doi:10.1016/j.conb.2011.04.004 (2011).

267 Francis, T. C., Yano, H., Demarest, T. G., Shen, H. & Bonci, A. High-Frequency Activation of Nucleus Accumbens D1-MSNs Drives Excitatory Potentiation on D2-MSNs. *Neuron* **103**, 432-+, doi:10.1016/j.neuron.2019.05.031 (2019).

268 Nam, H. *et al.* Reduced nucleus accumbens enkephalins underlie vulnerability to social defeat stress. *Neuropsychopharmacology* **44**, 1876-1885, doi:10.1038/s41386-019-0422-8 (2019).

269 Kim, H. D. *et al.* Shisa6 mediates cell-type specific regulation of depression in the nucleus accumbens. *Mol. Psychiatry* **26**, 7316-7327, doi:10.1038/s41380-021-01217-8 (2021).

270 van den Buuse, M., Zheng, T. W., Lesley, L. W. & Denton, D. A. Angiotensin-converting enzyme (ACE) interacts with dopaminergic mechanisms in the brain to modulate prepulse inhibition in mice. *Neurosci. Lett.* **380**, 6-11, doi:10.1016/j.neulet.2005.01.009 (2005).

271 Jenkins, T. A., Mendelsohn, F. A. O. & Chai, S. Y. Angiotensin-converting enzyme modulates dopamine turnover in the striatum. *J. Neurochem.* **68**, 1304-1311, doi:10.1046/j.1471-4159.1997.68031304.x (1997).

272 Neasta, J. *et al.* The novel nonapeptide acein targets angiotensin converting enzyme in the brain and induces dopamine release. *Br. J. Pharmacol.* **173**, 1314-1328, doi:10.1111/bph.13424 (2016).

273 Jenkins, T. A. Effect of angiotensin-related antihypertensives on brain neurotransmitter levels in rats. *Neurosci. Lett.* **444**, 186-189, doi:10.1016/j.neulet.2008.08.021 (2008).

274 Zhang, Y., Fonslow, B. R., Shan, B., Baek, M. C. & Yates, J. R., 3rd. Protein analysis by shotgun/bottom-up proteomics. *Chem. Rev.* **113**, 2343-2394, doi:10.1021/cr3003533 (2013).

275 Uhlen, M. *et al.* Proteomics. Tissue-based map of the human proteome. *Science* **347**, 1260419, doi:10.1126/science.1260419 (2015).

276 Luo, H. *et al.* Angiotensin-Converting Enzyme Inhibitor Rapidly Ameliorates Depressive-Type Behaviors via Bradykinin-Dependent Activation of Mammalian Target of Rapamycin Complex 1. *Biol. Psychiatry* **88**, 415-425, doi:10.1016/j.biopsych.2020.02.005 (2020).

277 Creed, M., Pascoli, V. J. & Luscher, C. Refining deep brain stimulation to emulate optogenetic treatment of synaptic pathology. *Science* **347**, 659-664, doi:10.1126/science.1260776 (2015).

278 Winkler, A., Buzas, B., Siems, W. E., Heder, G. & Cox, B. M. Effect of ethanol drinking on the gene expression of opioid receptors, enkephalinase, and angiotensin-converting enzyme in two inbred mice strains. *Alcoholism-Clinical and Experimental Research* **22**, 1262-1271, doi:10.1111/j.1530-0277.1998.tb03907.x (1998).

279 Sayed-Tabatabaei, F. A., Oostra, B. A., Isaacs, A., Van Duijn, C. M. & Witteman, J. C. M. ACE polymorphisms. *Circulation Research* **98**, 1123-1133, doi:10.1161/01.RES.0000223145.74217.e7 (2006).

280 Suehiro, T. *et al.* Increased amount of the angiotensin-converting enzyme (ACE) mRNA originating from the ACE allele with deletion. *Hum. Genet.* **115**, 91-96, doi:10.1007/s00439-004-1136-4 (2004).

281 Hamdi, H. K. & Castellon, R. A genetic variant of ACE increases cell survival: a new paradigm for biology and disease. *Biochem Biophys Res Commun* **318**, 187-191, doi:10.1016/j.bbrc.2004.04.004 (2004).

282 Arinami, T. *et al.* An insertion/deletion polymorphism in the angiotensin converting enzyme gene is associated with both brain substance P contents and affective disorders. *Biol. Psychiatry* **40**, 1122-1127, doi:10.1016/s0006-3223(95)00597-8 (1996).

283 Zill, P. *et al.* DNA Methylation Analysis of the Angiotensin Converting Enzyme (ACE) Gene in Major Depression. *PLoS One* **7**, e40479, doi:10.1371/journal.pone.0040479 (2012).

284 Baghai, T. C. *et al.* Polymorphisms in the angiotensin-converting enzyme gene are associated with unipolar depression, ACE activity and hypercortisolism. *Mol. Psychiatry* **11**, 1003-1015, doi:10.1038/sj.mp.4001884 (2006).

285 Bondy, B. *et al.* Genetic variants in the angiotensin I-converting-enzyme (ACE) and angiotensin II receptor (AT1) gene and clinical outcome in depression. *Prog. Neuropsychopharmacol. Biol. Psychiatry* **29**, 1094-1099, doi:10.1016/j.pnpbp.2005.03.015 (2005).

286 Chauquet, S. *et al.* Association of Antihypertensive Drug Target Genes With Psychiatric Disorders: A Mendelian Randomization Study. *JAMA Psychiatry* **78**, 623-631, doi:10.1001/jamapsychiatry.2021.0005 (2021).

287 Sanches, M. *et al.* Decreased Plasma Levels of Angiotensin-Converting Enzyme Among Patients With Bipolar Disorder. *Front. Neurosci.* **15**, 617888, doi:10.3389/fnins.2021.617888 (2021).

288 Mohite, S., Sanches, M. & Teixeira, A. L. Exploring the Evidence Implicating the Renin-Angiotensin System (RAS) in the Physiopathology of Mood Disorders. *Protein Pept Lett* **27**, 449-455, doi:10.2174/0929866527666191223144000 (2020).

289 Meyer, T. *et al.* Length Polymorphisms in the Angiotensin I-Converting Enzyme Gene and the Serotonin-Transporter-Linked Polymorphic Region Constitute a Risk Haplotype for Depression in Patients with Coronary Artery Disease. *Biochem. Genet.* **58**, 631-648, doi:10.1007/s10528-020-09967-w (2020).

290 Kucukali, C. I. *et al.* Angiotensin-converting enzyme polymorphism in schizophrenia, bipolar disorders, and their first-degree relatives. *Psychiatr. Genet.* **20**, 14-19, doi:10.1097/YPG.0b013e3283351194 (2010).

291 Ancelin, M. L. *et al.* Angiotensin-converting enzyme gene variants are associated with both cortisol secretion and late-life depression. *Translational Psychiatry* **3**, e322, doi:10.1038/tp.2013.95 (2013).

292 Trubetskoy, V. *et al.* Mapping genomic loci implicates genes and synaptic biology in schizophrenia. *Nature* **604**, 502-508, doi:10.1038/s41586-022-04434-5 (2022).

293 Gadelha, A. *et al.* Convergent evidences from human and animal studies implicate angiotensin I-converting enzyme activity in cognitive performance in schizophrenia. *Translational Psychiatry* **5**, e691, doi:10.1038/tp.2015.181 (2015).

294 Koronyo-Hamaoui, M. *et al.* Peripherally derived angiotensin converting enzyme-enhanced macrophages alleviate Alzheimer-related disease. *Brain* **143**, 336-358, doi:10.1093/brain/awz364 (2020).

295 Koronyo-Hamaoui, M. *et al.* ACE overexpression in myelomonocytic cells: effect on a mouse model of Alzheimer's disease. *Curr. Hypertens. Rep.* **16**, 444, doi:10.1007/s11906-014-0444-x (2014).

296 Kehoe, P. G. *et al.* Common variants of ACE contribute to variable age-at-onset of Alzheimer's disease. *Hum. Genet.* **114**, 478-483, doi:10.1007/s00439-004-1093-y (2004).

297 Cuddy, L. K. *et al.* Abeta-accelerated neurodegeneration caused by Alzheimer's-associated ACE variant R1279Q is rescued by angiotensin system inhibition in mice. *Sci. Transl. Med.* **12**, doi:10.1126/scitranslmed.aaz2541 (2020).

298 Sun, Y. *et al.* A transcriptome-wide association study of Alzheimer's disease using prediction models of relevant tissues identifies novel candidate susceptibility genes. *Genome Med.* **13**, 141, doi:10.1186/s13073-021-00959-y (2021).

299 Firouzabadi, N. *et al.* Genetic Variants of Angiotensin-Converting Enzyme Are Linked to Autism: A Case-Control Study. *PLoS One* **11**, e0153667, doi:10.1371/journal.pone.0153667 (2016).

300 Gordon, J. A. On being a circuit psychiatrist. *Nat. Neurosci.* **19**, 1385-1386, doi:10.1038/nn.4419 (2016).

301 Hearing, M., Graziane, N., Dong, Y. & Thomas, M. J. Opioid and Psychostimulant Plasticity: Targeting Overlap in Nucleus Accumbens Glutamate Signaling. *Trends Pharmacol. Sci.* **39**, 276-294, doi:10.1016/j.tips.2017.12.004 (2018).

302 James, A. S. *et al.* Opioid self-administration results in cell-type specific adaptations of striatal medium spiny neurons. *Behav. Brain Res.* **256**, 279-283, doi:10.1016/j.bbr.2013.08.009 (2013).

303 Regulski, M. *et al.* Chemistry and Pharmacology of Angiotensin-Converting Enzyme Inhibitors. *Curr. Pharm. Des.* **21**, 1764-1775, doi:10.2174/1381612820666141112160013 (2015).

304 Sink, K. M. *et al.* Angiotensin-Converting Enzyme Inhibitors and Cognitive Decline in Older Adults With Hypertension Results From the Cardiovascular Health Study. *Arch. Intern. Med.* **169**, 1195-1202, doi:10.1001/archinternmed.2009.175 (2009).

305 Gao, Y. *et al.* Effects of centrally acting ACE inhibitors on the rate of cognitive decline in dementia. *Bmj Open* **3**, doi:10.1136/bmjopen-2013-002881 (2013).

306 O'Caoimh, R. *et al.* Effects of Centrally Acting Angiotensin Converting Enzyme Inhibitors on Functional Decline in Patients with Alzheimer's Disease. *Journal of Alzheimers Disease* **40**, 595-603, doi:10.3233/jad-131694 (2014).

307 Zhuang, S. *et al.* Renin-angiotensin system blockade use and risks of cognitive decline and dementia: A meta-analysis. *Neurosci. Lett.* **624**, 53-61, doi:10.1016/j.neulet.2016.05.003 (2016).

308 Fazal, K., Perera, G., Khondoker, M., Howard, R. & Stewart, R. Associations of centrally acting ACE inhibitors with cognitive decline and survival in Alzheimer's disease. *Bjpsych Open* **3**, 158-164, doi:10.1192/bjpo.bp.116.004184 (2017).

309 Ho, J. K. *et al.* Blood-Brain Barrier Crossing Renin-Angiotensin Drugs and Cognition in the Elderly: A Meta-Analysis. *Hypertension* **78**, 629-643, doi:10.1161/HYPERTENSIONAHA.121.17049 (2021).

310 Porter, A. J., Pillidge, K., Grabowska, E. M. & Stanford, S. C. The angiotensin converting enzyme inhibitor, captopril, prevents the hyperactivity and impulsivity of neurokinin-1 receptor gene 'knockout' mice: sex differences and implications for the treatment of attention deficit hyperactivity disorder. *Eur. Neuropsychopharmacol.* **25**, 512-521, doi:10.1016/j.euroneuro.2015.01.013 (2015).

311 Raghavendra, V., Chopra, K. & Kulkarni, S. K. Comparative studies on the memory-enhancing actions of captopril and losartan in mice using inhibitory shock avoidance paradigm. *Neuropeptides* **35**, 65-69, doi:10.1054/npep.2000.0845 (2001).

312 Hosseini, M., Alaei, H. A., Headari, R. & Eslamizadeh, M. J. Effects of microinjection of angiotensin II and captopril into nucleus accumbens on morphine self-administration in rats. *Indian J. Exp. Biol.* **47**, 361-367 (2009).

313 Hosseini, M., Sharifi, M. R., Alaei, H., Shafei, M. N. & Karimooy, H. A. N. Effects of angiotensin II and captopril on rewarding propreties of morphine. *Indian J. Exp. Biol.* **45**, 770-777 (2007).

314 Tan, J. H., Wang, J. M. & Leenen, F. H. H. Inhibition of brain angiotensin-converting enzyme by peripheral administration of trandolapril versus lisinopril in Wistar rats. *Am. J. Hypertens.* **18**, 158-164, doi:10.1016/j.amjhyper.2004.09.004 (2005).

315 Gard, P. R., Mandy, A. & Sutcliffe, M. A. Evidence of a possible role of altered angiotensin function in the treatment, but not etiology, of depression. *Biol. Psychiatry* **45**, 1030-1034, doi:10.1016/s0006-3223(98)00101-2 (1999).

316 Takai, S., Song, K., Tanaka, O., Okunishi, H. & Miyazaki, M. Antinociceptive effects of angiotensin-converting enzyme inhibitors and an angiotensin II receptor antagonist in mice. *Life Sci.* **59**, PL331-PL336, doi:10.1016/0024-3205(96)00527-9 (1996).

317 Jouquey, S., Mathieu, M. N., Hamon, G. & Chevillard, C. Effect of chronic treatment with trandolapril or enalapril on brain ACE activity in spontaneously hypertensive rats. *Neuropharmacology* **34**, 1689-1692, doi:10.1016/0028-3908(95)00146-8 (1995).

318 Martin, P., Massol, J. & Puech, A. J. Captopril as an antidepressant? Effects on the learned helplessness paradigm in rats. *Biol. Psychiatry* **27**, 968-974, doi:10.1016/0006-3223(90)90034-y (1990).

319 Costall, B. *et al.* EFFECTS OF CAPTOPRIL AND SQ29,852 ON ANXIETY-RELATED BEHAVIORS IN RODENT AND MARMOSET. *Pharmacol. Biochem. Behav.* **36**, 13-20, doi:10.1016/0091-3057(90)90118-2 (1990).

320 Gohlke, P., Urbach, H., Scholkens, B. & Unger, T. Inhibition of converting enzyme in the cerebrospinal fluid of rats after oral treatment with converting enzyme inhibitors. *J Pharmacol Exp Ther* **249**, 609-616 (1989).

321 Gohlke, P., Scholkens, B., Henning, R., Urbach, H. & Unger, T. Inhibition of converting enzyme in brain tissue and cerebrospinal fluid of rats following chronic oral treatment with the converting enzyme inhibitors ramipril and Hoe 288. *J. Cardiovasc. Pharmacol.* **14 Suppl 4**, S32-36 (1989).

322 Giardina, W. J. & Ebert, D. M. Positive effects of captopril in the behavioral despair swim test. *Biol. Psychiatry* **25**, 697-702, doi:10.1016/0006-3223(89)90240-0 (1989).

323 Sakaguchi, K., Chai, S. Y., Jackson, B., Johnston, C. I. & Mendelsohn, F. A. Differential angiotensin-converting enzyme inhibition in brain after oral administration of perindopril demonstrated by quantitative in vitro autoradiography. *Neuroendocrinology* **48**, 223-228, doi:10.1159/000125015 (1988).

324 Stine, S. M., Yang, H. Y. & Costa, E. Inhibition of in situ metabolism of [3H](met5)-enkephalin and potentiation of (met5)-enkephalin analgesia by captopril. *Brain Res.* **188**, 295-299, doi:10.1016/0006-8993(80)90581-8 (1980).

325 McKinley, M. J. *et al.* The brain renin-angiotensin system: location and physiological roles. *Int. J. Biochem. Cell Biol.* **35**, 901-918, doi:10.1016/s1357-2725(02)00306-0 (2003).

326 Cosardereliogiu, C. *et al.* Brain Renin-Angiotensin System at the Intersect of Physical and Cognitive Frailty. *Front. Neurosci.* **14**, 586314, doi:10.3389/fnins.2020.586314 (2020).

327 Uijl, E., Ren, L. & Danser, A. H. J. Angiotensin generation in the brain: a re-evaluation. *Clin. Sci. (Lond.)* **132**, 839-850, doi:10.1042/CS20180236 (2018).

328 Gironacci, M. M., Vicario, A., Cerezo, G. & Silva, M. G. The depressor axis of the renin-angiotensin system and brain disorders: a translational approach. *Clin. Sci.* **132**, 1021-1038, doi:10.1042/cs20180189 (2018).

329 van Thiel, B. S. *et al.* Brain Renin-Angiotensin System: Does It Exist? *Hypertension* **69**, 1136-1144, doi:10.1161/HYPERTENSIONAHA.116.08922 (2017).

330 Bali, A., Randhawa, P. K. & Jaggi, A. S. Interplay between RAS and opioids: Opening the Pandora of complexities. *Neuropeptides* **48**, 249-256, doi:10.1016/j.npep.2014.05.002 (2014).

331 Wright, J. W. & Harding, J. W. Brain renin-angiotensin-A new look at an old system. *Prog. Neurobiol.* **95**, 49-67, doi:10.1016/j.pneurobio.2011.07.001 (2011).

332 Duchin, K. L., Singhvi, S. M., Willard, D. A., Migdalof, B. H. & McKinstry, D. N. Captopril kinetics. *Clin. Pharmacol. Ther.* **31**, 452-458, doi:10.1038/clpt.1982.59 (1982).

333 Ranadive, S. A., Chen, A. X. & Serajuddin, A. T. Relative lipophilicities and structural-pharmacological considerations of various angiotensin-converting enzyme (ACE) inhibitors. *Pharm. Res.* **9**, 1480-1486, doi:10.1023/a:1015823315983 (1992).

334 Cushman, D. W., Wang, F. L., Fung, W. C., Harvey, C. M. & Deforrest, J. M. DIFFERENTIATION OF ANGIOTENSIN-CONVERTING ENZYME (ACE) INHIBITORS BY THEIR SELECTIVE-INHIBITION OF ACE IN PHYSIOLOGICALLY IMPORTANT TARGET ORGANS. *Am. J. Hypertens.* **2**, 294-306, doi:10.1093/ajh/2.4.294 (1989).

335 Corradi, H. R., Schwager, S. L. U., Nchinda, A. T., Sturrock, E. D. & Acharya, K. R. Crystal structure of the N domain of human somatic angiotensin I-converting enzyme provides

a structural basis for domain-specific inhibitor design. *J. Mol. Biol.* **357**, 964-974, doi:10.1016/j.jmb.2006.01.048 (2006).

336 Acharya, K. R., Sturrock, E. D., Riordan, J. F. & Ehlers, M. R. W. ACE revisited: A new target for structure-based drug design. *Nature Reviews Drug Discovery* **2**, 891-902, doi:10.1038/nrd1227 (2003).

337 Wei, L., Alhencgelas, F., Corvol, P. & Clauser, E. THE 2 HOMOLOGOUS DOMAINS OF HUMAN ANGIOTENSIN-I-CONVERTING ENZYME ARE BOTH CATALYTICALLY ACTIVE. *J. Biol. Chem.* **266**, 9002-9008 (1991).

338 Hubert, C., Houot, A. M., Corvol, P. & Soubrier, F. Structure of the angiotensin I-converting enzyme gene. Two alternate promoters correspond to evolutionary steps of a duplicated gene. *J. Biol. Chem.* **266**, 15377-15383 (1991).

339 Polakovicova, M. & Jampilek, J. Advances in Structural Biology of ACE and Development of Domain Selective ACE-inhibitors. *Med. Chem.* **15**, 574-587, doi:10.2174/1573406415666190514081132 (2019).

340 Anthony, C. S. *et al.* The N Domain of Human Angiotensin-I-converting Enzyme THE ROLE OF N-GLYCOSYLATION AND THE CRYSTAL STRUCTURE IN COMPLEX WITH AN N DOMAIN-SPECIFIC PHOSPHINIC INHIBITOR, RXP407. *J. Biol. Chem.* **285**, 35685-35693, doi:10.1074/jbc.M110.167866 (2010).

341 O'Neill, H. G., Redelinghuys, P., Schwager, S. L. & Sturrock, E. D. The role of glycosylation and domain interactions in the thermal stability of human angiotensin-converting enzyme. *Biol. Chem.* **389**, 1153-1161, doi:10.1515/BC.2008.131 (2008).

342 Yates, C. J. *et al.* Molecular and thermodynamic mechanisms of the chloride-dependent human angiotensin-I-converting enzyme (ACE). *J. Biol. Chem.* **289**, 1798-1814, doi:10.1074/jbc.M113.512335 (2014).

343 Tzakos, A. G. *et al.* Structure-function discrimination of the N- and C- catalytic domains of human angiotensin-converting enzyme: implications for Cl- activation and peptide hydrolysis mechanisms. *Protein Eng.* **16**, 993-1003, doi:10.1093/protein/gzg122 (2003).

344 Wei, L., Clauser, E., Alhencgelas, F. & Corvol, P. THE 2 HOMOLOGOUS DOMAINS OF HUMAN ANGIOTENSIN-I-CONVERTING ENZYME INTERACT DIFFERENTLY WITH COMPETITIVE INHIBITORS. *J. Biol. Chem.* **267**, 13398-13405 (1992).

345 Cozier, G. E., Lubbe, L., Sturrock, E. D. & Acharya, K. R. Angiotensin-converting enzyme open for business: structural insights into the subdomain dynamics. *FEBS J.* **288**, 2238-2256, doi:10.1111/febs.15601 (2021).

346 Fuchs, S. *et al.* Angiotensin-converting enzyme C-terminal catalytic domain is the main site of angiotensin I cleavage in vivo. *Hypertension* **51**, 267-274, doi:10.1161/hypertensionaha.107.097865 (2008).

347 Shen, X. Z. *et al.* New insights into the role of angiotensin-converting enzyme obtained from the analysis of genetically modified mice. *J. Mol. Med. (Berl.)* **86**, 679-684, doi:10.1007/s00109-008-0325-3 (2008).

348 Fuchs, S. *et al.* Role of the N-terminal catalytic domain of angiotensin-converting enzyme investigated by targeted inactivation in mice. *J. Biol. Chem.* **279**, 15946-15953, doi:10.1074/jbc.M400149200 (2004).

349 Kroger, W. L., Douglas, R. G., O'Neill, H. G., Dive, V. & Sturrock, E. D. Investigating the Domain Specificity of Phosphinic Inhibitors RXPA380 and RXP407 in Angiotensin-Converting Enzyme. *Biochemistry* **48**, 8405-8412, doi:10.1021/bi9011226 (2009).

350 Georgiadis, D., Cuniasse, P., Cotton, J., Yiotakis, A. & Dive, V. Structural determinants of RXPA380, a potent and highly selective inhibitor of the angiotensin-converting enzyme C-domain. *Biochemistry* **43**, 8048-8054, doi:10.1021/bi049504q (2004).

351 Georgiadis, D. *et al.* Roles of the two active sites of somatic angiotensin-converting enzyme in the cleavage of angiotensin I and bradykinin - Insights from selective inhibitors. *Circulation Research* **93**, 148-154, doi:10.1161/01.Res.0000081593.33848.Fc (2003).

352 Junot, C. *et al.* RXP 407, a selective inhibitor of the N-domain of angiotensin I-converting enzyme, blocks in vivo the degradation of hemoregulatory peptide acetyl-Ser-Asp-Lys-Pro with no effect on angiotensin I hydrolysis. *Journal of Pharmacology and Experimental Therapeutics* **297**, 606-611 (2001).

353 Vazeux, G., Cotton, J., Cuniasse, P. & Dive, V. Potency and selectivity of RXP407 on human, rat, and mouse angiotensin-converting enzyme. *Biochem. Pharmacol.* **61**, 835-841, doi:10.1016/s0006-2952(01)00550-0 (2001).

354 Dive, V. *et al.* RXP 407, a phosphinic peptide, is a potent inhibitor of angiotensin I converting enzyme able to differentiate between its two active sites. *Proc. Natl. Acad. Sci. U. S. A.* **96**, 4330-4335, doi:10.1073/pnas.96.8.4330 (1999).

355 van Esch, J. H. M. *et al.* Different contributions of the angiotensin-converting enzyme C-domain and N-domain in subjects with the angiotensin-converting enzyme II and DD genotype. *J. Hypertens.* **26**, 706-713, doi:10.1097/HJH.0b013e3282f465d2 (2008).

356 Perich, R. B., Jackson, B. & Johnston, C. I. Structural constraints of inhibitors for binding at two active sites on somatic angiotensin converting enzyme. *Eur. J. Pharmacol.* **266**, 201-211, doi:10.1016/0922-4106(94)90128-7 (1994).

357 Ferreira, S. H. A Bradykinin-Potentiating Factor (Bpf) Present in the Venom of Bothrops Jararca. *Br. J. Pharmacol. Chemother.* **24**, 163-169, doi:10.1111/j.1476-5381.1965.tb02091.x (1965).

358 Patchett, A. A. *et al.* A new class of angiotensin-converting enzyme inhibitors. *Nature* **288**, 280-283, doi:10.1038/288280a0 (1980).

359 Ondetti, M. A., Rubin, B. & Cushman, D. W. Design of specific inhibitors of angiotensin-converting enzyme: new class of orally active antihypertensive agents. *Science* **196**, 441-444, doi:10.1126/science.191908 (1977).

360 Ondetti, M. A. *et al.* Angiotensin-converting enzyme inhibitors from the venom of Bothrops jararaca. Isolation, elucidation of structure, and synthesis. *Biochemistry* **10**, 4033-4039, doi:10.1021/bi00798a004 (1971).

361 Yang, H. Y., Erdos, E. G. & Levin, Y. A dipeptidyl carboxypeptidase that converts angiotensin I and inactivates bradykinin. *Biochim Biophys Acta* **214**, 374-376, doi:10.1016/0005-2795(70)90017-6 (1970).

362 Ferreira, S. H., Bartelt, D. C. & Greene, L. J. Isolation of bradykinin-potentiating peptides from Bothrops jararaca venom. *Biochemistry* **9**, 2583-2593, doi:10.1021/bi00815a005 (1970).

363 Giani, J. F. *et al.* Novel roles of the renal angiotensin-converting enzyme. *Mol Cell Endocrinol* **529**, 111257, doi:10.1016/j.mce.2021.111257 (2021).

364 Cao, D. *et al.* The non-cardiovascular actions of ACE. *Peptides* **152**, 170769, doi:10.1016/j.peptides.2022.170769 (2022).

365 Khan, Z. *et al.* Overexpression of the C-domain of angiotensin-converting enzyme reduces melanoma growth by stimulating M1 macrophage polarization. *J. Biol. Chem.* **294**, 4368-4380, doi:10.1074/jbc.RA118.006275 (2019).

366 Bernstein, K. E. *et al.* Angiotensin-converting enzyme in innate and adaptive immunity. *Nat Rev Nephrol* **14**, 325-336, doi:10.1038/nrneph.2018.15 (2018).

367 Deicken, R. F. Captopril treatment of depression. *Biol. Psychiatry* **21**, 1425-1428, doi:10.1016/0006-3223(86)90334-3 (1986).

368 Cohen, B. M. & Zubenko, G. S. Captopril in the treatment of recurrent major depression. *J. Clin. Psychopharmacol.* **8**, 143-144, doi:10.1097/00004714-198804000-00018 (1988).

369 Germain, L. & Chouinard, G. Treatment of recurrent unipolar major depression with captopril. *Biol. Psychiatry* **23**, 637-641, doi:10.1016/0006-3223(88)90010-8 (1988).

370 Vuckovic, A., Cohen, B. M. & Zubenko, G. S. The use of captopril in treatment-resistant depression: an open trial. *J. Clin. Psychopharmacol.* **11**, 395-396, doi:10.1097/00004714-199112000-00025 (1991).

371 Rathmann, W., Haastert, B., Roseman, J. M. & Giani, G. Cardiovascular drug prescriptions and risk of depression in diabetic patients. *J. Clin. Epidemiol.* **52**, 1103-1109, doi:10.1016/s0895-4356(99)00082-7 (1999).

372 Braszko, J. J., Karwowska-Polecka, W., Halicka, D. & Gard, P. R. Captopril and enalapril improve cognition and depressed mood in hypertensive patients. *J. Basic Clin. Physiol. Pharmacol.* **14**, 323-343, doi:10.1515/jbcpp.2003.14.4.323 (2003).

373 Boal, A. H. *et al.* Monotherapy With Major Antihypertensive Drug Classes and Risk of Hospital Admissions for Mood Disorders. *Hypertension* **68**, 1132-1138, doi:10.1161/hypertensionaha.116.08188 (2016).

374 Repova, K., Aziriova, S., Krajcirovicova, K. & Simko, F. Cardiovascular therapeutics: A new potential for anxiety treatment? *Med. Res. Rev.* **42**, 1202-1245, doi:10.1002/med.21875 (2022).

375 Quitterer, U. & AbdAlla, S. Improvements of symptoms of Alzheimer`s disease by inhibition of the angiotensin system. *Pharmacol. Res.* **154**, 104230, doi:10.1016/j.phrs.2019.04.014 (2020).

376 Messiha, B. A. S., Ali, M. R. A., Khattab, M. M. & Abo-Youssef, A. M. Perindopril ameliorates experimental Alzheimer's disease progression: role of amyloid beta degradation, central estrogen receptor and hyperlipidemic-lipid raft signaling. *Inflammopharmacology* **28**, 1343-1364, doi:10.1007/s10787-020-00724-4 (2020).

377 Torika, N., Asraf, K., Roasso, E., Danon, A. & Fleisher-Berkovich, S. Angiotensin Converting Enzyme Inhibitors Ameliorate Brain Inflammation Associated with Microglial Activation: Possible Implications for Alzheimer's Disease. *J. Neuroimmune Pharmacol.* **11**, 774-785, doi:10.1007/s11481-016-9703-8 (2016).

378 Kaur, P., Muthuraman, A. & Kaur, M. The implications of angiotensin-converting enzymes and their modulators in neurodegenerative disorders: current and future perspectives. *ACS Chem. Neurosci.* **6**, 508-521, doi:10.1021/cn500363g (2015).

379 Croog, S. H. *et al.* EFFECTS OF ANTIHYPERTENSIVE MEDICATIONS ON QUALITY-OF-LIFE IN ELDERLY HYPERTENSIVE WOMEN. *Am. J. Hypertens.* **7**, 329-339, doi:10.1093/ajh/7.4.329 (1994).

380 Croog, S. H. *et al.* The effects of antihypertensive therapy on the quality of life. *N. Engl. J. Med.* **314**, 1657-1664, doi:10.1056/NEJM198606263142602 (1986).

381 Fletcher, A. E. *et al.* Quality of life on antihypertensive therapy: a randomized double-blind controlled trial of captopril and atenolol. *J. Hypertens.* **8**, 463-466, doi:10.1097/00004872-199005000-00011 (1990).

382 Frimodt-Moeller, J., Poulsen, D. L., Kornerup, H. J. & Bech, P. Quality of life, side effects and efficacy of lisinopril compared with metoprolol in patients with mild to moderate essential hypertension. *J. Hum. Hypertens.* **5**, 215-221 (1991).

383 Steiner, S. S., Friedhoff, A. J., Wilson, B. L., Wecker, J. R. & Santo, J. P. Antihypertensive therapy and quality of life: a comparison of atenolol, captopril, enalapril and propranolol. *J. Hum. Hypertens.* **4**, 217-225 (1990).

384 Testa, M. A., Anderson, R. B., Nackley, J. F. & Hollenberg, N. K. QUALITY-OF-LIFE AND ANTIHYPERTENSIVE THERAPY IN MEN - A COMPARISON OF CAPTOPRIL WITH ENALAPRIL. *New England Journal of Medicine* **328**, 907-913, doi:10.1056/nejm199304013281302 (1993).

385 Brownstein, D. J. *et al.* Blockade of the angiotensin system improves mental health domain of quality of life: A meta-analysis of randomized clinical trials. *Australian and New Zealand Journal of Psychiatry* **52**, 24-38, doi:10.1177/0004867417721654 (2018).

386 Laudisio, A. *et al.* Use of ACE-inhibitors and Quality of Life in an Older Population. *Journal of Nutrition Health & Aging* **22**, 1162-1166, doi:10.1007/s12603-018-1135-0 (2018).

387 Handa, K. *et al.* EFFECTS OF CAPTOPRIL ON OPIOID-PEPTIDES DURING EXERCISE AND QUALITY-OF-LIFE IN NORMAL SUBJECTS. *Am. Heart J.* **122**, 1389-1394, doi:10.1016/0002-8703(91)90582-3 (1991).

388 Zubenko, G. S. & Nixon, R. A. Mood-elevating effect of captopril in depressed patients. *Am. J. Psychiatry* **141**, 110-111, doi:10.1176/ajp.141.1.110 (1984).

389 Pardinas, A. F., Owen, M. J. & Walters, J. T. R. Pharmacogenomics: A road ahead for precision medicine in psychiatry. *Neuron* **109**, 3914-3929, doi:10.1016/j.neuron.2021.09.011 (2021).

390 Insel, T. R. & Cuthbert, B. N. Brain disorders? Precisely. *Science* **348**, 499-500, doi:10.1126/science.aab2358 (2015).

391 Chalhoub, R. M. & Kalivas, P. W. Non-Opioid Treatments for Opioid Use Disorder: Rationales and Data to Date. *Drugs* **80**, 1509-1524, doi:10.1007/s40265-020-01373-1 (2020).

392 Volkow, N. D., Koob, G. F. & McLellan, A. T. Neurobiologic Advances from the Brain Disease Model of Addiction. *N. Engl. J. Med.* **374**, 363-371, doi:10.1056/NEJMra1511480 (2016).

393 Mauro, P. M., Gutkind, S., Annunziato, E. M. & Samples, H. Use of Medication for Opioid Use Disorder Among US Adolescents and Adults With Need for Opioid Treatment, 2019. *JAMA Netw Open* **5**, e223821, doi:10.1001/jamanetworkopen.2022.3821 (2022).

394 Sun, H., Luessen, D. J., Kind, K. O., Zhang, K. & Chen, R. Cocaine Self-administration Regulates Transcription of Opioid Peptide Precursors and Opioid Receptors in Rat Caudate Putamen and Prefrontal Cortex. *Neuroscience* **443**, 131-139, doi:10.1016/j.neuroscience.2020.07.035 (2020).

395 Nummenmaa, L. *et al.* Lowered endogenous mu-opioid receptor availability in subclinical depression and anxiety. *Neuropsychopharmacology* **45**, 1953-1959, doi:10.1038/s41386-020-0725-9 (2020).

396 Emery, M. A. & Akil, H. in *Annual Review of Neuroscience, Vol 43* Vol. 43 *Annual Review of Neuroscience* (eds B. Roska & H. Y. Zoghbi) 355-374 (2020).

397 Pecina, M. *et al.* Endogenous opioid system dysregulation in depression: implications for new therapeutic approaches. *Mol. Psychiatry* **24**, 576-587, doi:10.1038/s41380-018-0117-2 (2019).

398 Granholm, L., Segerstrom, L. & Nylander, I. Episodic Ethanol Exposure in Adolescent Rats Causes Residual Alterations in Endogenous Opioid Peptides. *Frontiers in Psychiatry* **9**, 425, doi:10.3389/fpsyt.2018.00425 (2018).

399 Moeller, S. J. *et al.* Effects of an opioid (proenkephalin) polymorphism on neural response to errors in health and cocaine use disorder. *Behav. Brain Res.* **293**, 18-26, doi:10.1016/j.bbr.2015.07.004 (2015).

400 Mendez, I. A., Ostlund, S. B., Maidment, N. T. & Murphy, N. P. Involvement of Endogenous Enkephalins and beta-Endorphin in Feeding and Diet-Induced Obesity. *Neuropsychopharmacology* **40**, 2103-2112, doi:10.1038/npp.2015.67 (2015).

401 Poulin, J. F., Laforest, S. & Drolet, G. Enkephalin downregulation in the nucleus accumbens underlies chronic stress-induced anhedonia. *Stress-the International Journal on the Biology of Stress* **17**, 88-96, doi:10.3109/10253890.2013.850669 (2014).

402 Berube, P., Poulin, J. F., Laforest, S. & Drolet, G. Enkephalin Knockdown in the Basolateral Amygdala Reproduces Vulnerable Anxiety-Like Responses to Chronic

Unpredictable Stress. *Neuropsychopharmacology* **39**, 1159-1168, doi:10.1038/npp.2013.316 (2014).

403 Bissonnette, S., Vaillancourt, M., Hebert, S. S., Drolet, G. & Samadi, P. Striatal Pre-Enkephalin Overexpression Improves Huntington's Disease Symptoms in the R6/2 Mouse Model of Huntington's Disease. *PLoS One* **8**, e75099, doi:10.1371/journal.pone.0075099 (2013).

404 Berube, P., Laforest, S., Bhatnagar, S. & Drolet, G. Enkephalin and dynorphin mRNA expression are associated with resilience or vulnerability to chronic social defeat stress. *Physiol. Behav.* **122**, 237-245, doi:10.1016/j.physbeh.2013.04.009 (2013).

405 Kennedy, S. E., Koeppe, R. A., Young, E. A. & Zubieta, J. K. Dysregulation of endogenous opioid emotion regulation circuitry in major depression in women. *Arch. Gen. Psychiatry* **63**, 1199-1208, doi:10.1001/archpsyc.63.11.1199 (2006).

406 Crespo, J. A. *et al.* Extinction of cocaine self-administration produces a differential time-related regulation of proenkephalin gene expression in rat brain. *Neuropsychopharmacology* **25**, 185-194, doi:10.1016/s0893-133x(01)00221-4 (2001).

Appendix A: Statistical Analyses

Figure		Test	Sample Size	Statistic	P value	Follow-up Test	Post-hoc comparison, statistic, and P value
3-2	C	Three-way ANOVA	D1-MSN: 8 (5F / 3M) D2-MSN: 9 (4F / 5F)	F (4,52) = 47.47 F (1,13) = 1.973 F (1,13) = 0.1868 F (4,52) = 0.3447 F (4,52) = 1.911 F (1,13) = 0.2550 F (4,52) = 0.2293	Concentration: P < 0.0001 Cell-type: P = 0.1838 Sex: P = 0.6727 Concentration x Cell-type: P = 0.8465 Concentration x Sex: P = 0.1224 Cell-type x Sex: P = 0.6220 Concentration x Cell-type x Sex: P = 0.9207	Main effect of Concentration: two-sample t-test versus baseline (two-tailed)	Combined cell-types: vs 0.01 uM: t(52) = 0.06204, P = 0.9508 vs 0.1 uM: t(52) = 2.982, P = 0.0044 vs 1 uM: t(52) = 7.893, P < 0.0001 vs 10 uM: t(52) = 10.88, P < 0.0001
	D	Three-way ANOVA	D1-MSN: 8 (5F / 3M) D2-MSN: 9 (4F / 5F)	F (3,39) = 111.1 F (1,13) = 2.093 F (1,13) = 3.441 F (3,39) = 0.9549 F (3,39) = 0.8139 F (1,13) = 0.00462 F (3,39) = 0.5165	Concentration: P < 0.0001 Cell-type: P = 0.1716 Sex: P = 0.0864 Concentration x Cell-type: P = 0.4236 Concentration x Sex: P = 0.4940 Cell-type x Sex: P = 0.9468 Concentration x Cell-type x Sex: P = 0.6734	Main effect of Concentration: one-sample t-test (two-tailed)	Combined cell-types: 0.01 uM: t(16) = 0.3522, P = 0.7293 0.1 uM: t(16) = 2.914, P = 0.0101 1 uM: t(16) = 11.91, P < 0.0001 10 uM: t(16) = 14.15, P < 0.0001
	E	Three-way ANOVA	D1-MSN: 8 (5F / 3M) D2-MSN: 9 (4F / 5F)	F (4,52) = 4.785 F (1,13) = 6.601 F (1,13) = 6.557 F (4,52) = 1.901 F (4,52) = 1.865 F (1,13) = 1.495 F (4,52) = 1.289	Concentration: P = 0.0023 Cell-type: P = 0.0233 Sex: P = 0.0237 Concentration x Cell-type: P = 0.1242 Concentration x Sex: P = 0.1306 Cell-type x Sex: P = 0.2432 Concentration x Cell-type x Sex: P = 0.2865	Main effect of Concentration: two-sample t-test versus baseline (two-tailed)	Combined cell-types: vs 0.01 uM: t(52) = 1.237, P = 0.2216 vs 0.1 uM: t(52) = 0.2434, P = 0.8086 vs 1 uM: t(52) = 0.9164, P = 0.3637 vs 10 uM: t(52) = 2.863, P = 0.0060
	F	Three-way ANOVA	D1-MSN: 8 (5F / 3M) D2-MSN: 9 (4F / 5F)	F (3,39) = 9.611 F (1,13) = 1.260 F (1,13) = 2.753 F (3,39) = 2.525 F (3,39) = 1.099 F (1,13) = 2.114 F (3,39) = 0.1856	Concentration: P < 0.0001 Cell-type: P = 0.2819 Sex: P = 0.1210 Concentration x Cell-type: P = 0.0716 Concentration x Sex: P = 0.3611 Cell-type x Sex: P = 0.1697 Concentration x Cell-type x Sex: P = 0.9055	Main effect of Concentration: one-sample t-test (two-tailed)	Combined cell-types: 0.01 uM: t(16) = 0.9933, P = 0.3354 0.1 uM: t(16) = 0.2839, P = 0.7801 1 uM: t(16) = 1.055, P = 0.3069 10 uM: t(16) = 3.081, P = 0.0072
3-3	C	Three-way ANOVA	D1-MSN: 8 (6M / 2F) D2-MSN: 8 (6M / 2F)	F(4,48) = 45.09 F(1,12) = 5.846 F(1,12) = 3.047 F(4,48) = 1.901 F(4,48) = 2.184 F(1,12) = 2.935 F(4,48) = 0.5346	Concentration: P < 0.0001 Cell-type: P = 0.0324 Sex: P = 0.1064 Concentration x Cell-type: P = 0.1256 Concentration x Sex: P = 0.0849 Cell-type x Sex: P = 0.1124 Concentration x Cell-type x Sex: P = 0.7109	Main effect of Concentration: two-sample t-test versus baseline (two-tailed)	Combined cell-types: vs 0.01 uM: t(48) = 0.05784, P = 0.9541 vs 0.1 uM: t(48) = 1.670, P = 0.1015 vs 1 uM: t(48) = 6.522, P < 0.001 vs 10 uM: t(48) = 10.86, P < 0.0001

Figure		Test	Sample Size	Statistic	P value	Follow-up Test	Post-hoc comparison, statistic, and P value
	D	Three-way ANOVA	D1-MSN: 8 (6M / 2F) D2-MSN: 8 (6M / 2F)	F(3,36) = 105.3 F(1,12) = 0.1133 F(1,12) = 0.3807 F(3,36) = 0.3166 F(3,36) = 0.6403 F(1,12) = 0.0676 F(3,36) = 1.189	Concentration: P < 0.0001 Cell-type: P = 0.7423 Sex: P = 0.5488 Concentration x Cell-type: P = 0.8133 Concentration x Sex: P = 0.5941 Cell-type x Sex: P = 0.7992 Concentration x Cell-type x Sex: P = 0.3277	Main effect of Concentration: one-sample t-test (two-tailed)	Combined cell-types: 0.01 uM: t(15) = 0.1182, P = 0.8532 0.1 uM: t(15) = 1.604, P = 0.1296 1 uM: t(15) = 9.254, P < 0.0001 10 uM: t(15) = 18.57, P < 0.0001
	E	Three-way ANOVA	D1-MSN: 8 (6M / 2F) D2-MSN: 8 (6M / 2F)	F(4,48) = 1.763 F(1,12) = 0.0001 F(1,12) = 0.3946 F(4,48) = 0.4945 F(4,48) = 0.5153 F(1,12) = 0.002 F(4,48) = 0.6707	Concentration: P = 0.1518 Cell-type: P = 0.9920 Sex: P = 0.5416 Concentration x Cell-type: P = 0.7398 Concentration x Sex: P = 0.7248 Cell-type x Sex: P = 0.9591 Concentration x Cell-type x Sex: P = 0.6155	n/a	n/a
	F	Three-way ANOVA	D1-MSN: 8 (6M / 2F) D2-MSN: 8 (6M / 2F)	F(3,36) = 1.309 F(1,12) = 0.8840 F(1,12) = 0.6685 F(3,36) = 0.4159 F(3,36) = 0.4779 F(1,12) = 0.3010 F(3,36) = 0.6949	Concentration: P = 0.2863 Cell-type: P = 0.3656 Sex: P = 0.4295 Concentration x Cell-type: P = 0.7426 Concentration x Sex: P = 0.6996 Cell-type x Sex: P = 0.5933 Concentration x Cell-type x Sex: P = 0.5612	n/a	n/a
3-4	B	Unpaired t-test (two-tailed)	D1-MSN: 6 (3M / 3F) D2-MSN: 7 (2M / 5F)	t(11) = 1.547	P = 0.1502	one-sample t-test (two-tailed)	D1-MSN: t(5) = 5.495, P = 0.0027 D2-MSN: t(6) = 19.74, P <0.0001
	D	Unpaired t-test (two-tailed)	MERF: 4 (2M / 2F) +Naloxone: 7 (3M / 4F)	t(9) = 3.626	P = 0.0055	one-sample t-test (two-tailed)	MERF: t(3) = 7.237, P = 0.0054 +Naloxone: t(6) = 2.386, P = 0.0543
	F	Unpaired t-test (two-tailed)	OPRM1+/+: 8 (6M / 2F) OPRM1-/-: 8 (6M / 2F)	t(14) = 2.064	P = 0.0580	one-sample t-test (two-tailed)	OPRM1+/+: t(7) = 4.525, P = 0.0027 OPRM1-/-: t(7) = 2.527, P = 0.0394
	H	Unpaired t-test (two-tailed)	OPRM1+/+: 7 (5M / 2F) OPRM1-/-: 9 (5M / 4F)	t(14) = 0.2173	P = 0.8311	one-sample t-test (two-tailed)	OPRM1+/+: t(6) = 5.658, P = 0.0013 OPRM1-/-: t(8) = 4.999, P = 0.0011
3-5	A	One-sample t-test (two-tailed)	D1-MSN: 6 (3M / 3F) D2-MSN: 7 (2M / 5F) MERF: 4 (2M / 2F) +Naloxone: 7 (3M / 4F) OPRM1+/+: 8 (6M / 2F) OPRM1-/-: 8 (6M / 2F) OPRM1+/+: 7 (5M / 2F) OPRM1-/-: 9 (5M / 4F) 1 uM: 19 (13M / 6F) 10 uM: 13 (5M / 8F)	t(5) = 1.935 t(6) = 3.970 t(3) = 1.665 t(6) = 0.5092 t(7) = 2.035 t(7) = 1.373 t(6) = 1.900 t(8) = 2.210 t(18) = 3.425 t(12) = 3.443	P = 0.1108 P = 0.0074 P = 0.1945 P = 0.6288 P = 0.0813 P = 0.2122 P = 0.1061 P = 0.0581 P = 0.0030 P = 0.0049	n/a	n/a
	B	Kolmogorov-Smirnov	8 cells (4M / 4F)	KS D = 0.2400	P < 0.0001	n/a	n/a

Figure		Test	Sample Size	Statistic	P value	Follow-up Test	Post-hoc comparison, statistic, and P value
	C	Kolmogorov-Smirnov	8 cells (4M / 4F)	KS D = 0.0900	P = 0.3927	n/a	n/a
	D	Paired t-test (two-tailed)	8 cells (4M / 4F)	t(7) = 5.748	P = 0.0007	n/a	n/a
	E	Paired t-test (two-tailed)	8 cells (4M / 4F)	t(7) = 3.287	P = 0.0134	n/a	n/a
3-7	A	Three-way ANOVA	D1-MSN Captopril: 8 (3F / 5M) MERF: 12 (10F / 2M) Captopril+MERF: 14 (7F / 7M) D2-MSN Captopril: 5 (1F / 4M) MERF: 10 (2F / 8M) Captopril+MERF: 12 (2F / 10M)	F(2,49) = 5.371 F(1,49) = 2.105 F(1,49) = 0.1183 F(2,49) = 7.750 F(2,49) = 0.4160 F(1,49) = 2.295 F(2,49) = 0.3498	Treatment: P = 0.0078 Cell-type: P = 0.1532 Sex: P = 0.7324 Treatment x Cell-type: P = 0.0012 Treatment x Sex: P = 0.6620 Cell-type x Sex: P = 0.1362 Treatment x Cell-type x Sex: P = 0.7066	Simple effect of Treatment for each Cell-type (see below)	n/a
		One-way ANOVA	D1-MSN Captopril: 8 MERF: 12 Captopril+MERF: 14	F(2,31) = 22.27	Treatment: P < 0.0001	Fisher's LSD post-hoc test	Captopril vs MERF: t(31) = 0.04375, P = 0.9654 Captopril vs Captopril+MERF: t(31) = 5.274, P < 0.0001 MERF vs Captopril+MERF: t(31) = 5.891, P < 0.0001
		One-way ANOVA	D2-MSN Captopril: 5 MERF: 10 Captopril+MERF: 12	F(2,24) = 1.597	Treatment: P = 0.2233	n/a	n/a
	B	Three-way ANOVA	D1-MSN Captopril: 8 (3F / 5M) MERF: 12 (10F / 2M) Captopril+MERF: 14 (7F / 7M) D2-MSN Captopril: 5 (1F / 4M) MERF: 10 (2F / 8M) Captopril+MERF: 12 (2F / 10M)	F(2,49) = 0.3745 F(1,49) = 2.993 F(1,49) = 0.2038 F(2,49) = 0.7955 F(2,49) = 2.707 F(1,49) = 5.187 F(2,49) = 0.9660	Treatment: P = 0.6896 Cell-type: P = 0.0899 Sex: P = 0.65364 Treatment x Cell-type: P = 0.4571 Treatment x Sex: P = 0.0767 Cell-type x Sex: P = 0.0272 Treatment x Cell-type x Sex: P = 0.3877	n/a	n/a

Figure		Test	Sample Size	Statistic	P value	Follow-up Test	Post-hoc comparison, statistic, and P value
	C	Four-way ANOVA	D1-MSN Captopril: 8 (3F / 5M) MERF: 12 (10F / 2M) Captopril + MERF: 14 (7F / 7M) D2-MSN: Captopril: 5 (1F / 4M) MERF: 10 (2F / 8M) Captopril + MERF: 12 (2F / 10M)	F(1,49) = 2.899 F(1,49) = 1.001 F(2,49) = 0.186 F(1,49) = 2.578 F(2,49) = 0.639 F(2,49) = 0.839 F(2,49) = 1.452 F(1,49) = 8.520 F(1,49) = 2.706 F(1,49) = 0.110 F(2,49) = 4.040 F(1,49) = 0.428 F(2,49) = 7.231 F(2,49) = 0.215 F(2,49) = 0.605	Cell-type: P = 0.095 Sex: P = 0.322 Treatment: P = 0.831 Cell-type x Sex: P = 0.115 Cell-type x Treatment: P = 0.532 Sex x Treatment: P = 0.438 Cell-type x Sex x Treatment: P = 0.244 Time: P = 0.005 Time x Cell-type: P = 0.106 Time x Sex: P = 0.741 Time x Treatment: P = 0.024 Time x Cell-type x Sex: P = 0.516 Time x Cell-type x Treatment: P = 0.002 Time x Sex x Treatment: P = 0.807 Time x Cell-type x Sex x Treatment: P = 0.550	Time x Cell-type x Treatment interaction: simple effect of Time for each Treatment in each Cell-type	D1-MSN Baseline vs Captopril: t(55) = 0.2302, P = 0.8188 Baseline vs MERF: t(55) = 0.0506, P = 0.9598 Baseline vs Captopril+MERF: t(55) = 8.282, P < 0.0001 D2-MSN Baseline vs Captopril: t(55) = 0.224, P = 0.8236 Baseline vs MERF: t(55) = 1.081, P = 0.2845 Baseline vs Captopril+MERF: t(55) = 0.3651, P = 0.7165
	D	Four-way ANOVA	D1-MSN Captopril: 8 (3F / 5M) MERF: 12 (10F / 2M) Captopril + MERF: 14 (7F / 7M) D2-MSN: Captopril: 5 (1F / 4M) MERF: 10 (2F / 8M) Captopril + MERF: 12 (2F / 10M)	F(1,49) = 4.149 F(1,49) = 0.007 F(2,49) = 0.613 F(1,49) = 0.049 F(2,49) = 1.061 F(2,49) = 0.510 F(2,49) = 0.819 F(1,49) = 21.947 F(1,49) = 3.624 F(1,49) = 0.216 F(2,49) = 0.257 F(1,49) = 4.656 F(2,49) = 1.004 F(2,49) = 2.586 F(2,49) = 1.265	Cell-type: P = 0.047 Sex: P = 0.934 Treatment: P = 0.546 Cell-type x Sex: P = 0.826 Cell-type x Treatment: P = 0.354 Sex x Treatment: P = 0.604 Cell-type x Sex x Treatment: P = 0.447 Time: P < 0.0001 Time x Cell-type: P = 0.063 Time x Sex: P = 0.644 Time x Treatment: P = 0.774 Time x Cell-type x Sex: P = 0.036 Time x Cell-type x Treatment: P = 0.374 Time x Sex x Treatment: P = 0.086 Time x Cell-type x Sex x Treatment: P = 0.291	n/a	n/a
3-8	D	Three-way ANOVA	D1-MSN: 9 (5F / 4M) D2-MSN: 9 (5F / 4M)	F(2,28) = 54.79 F(1,14) = 0.1489 F(1,14) = 0.02838 F(2,28) = 1.943 F(2,28) = 0.8846 F(1,14) = 1.890 F(2,28) = 0.8650	Treatment: P < 0.0001 Cell-type: P = 0.7054 Sex: P = 0.8686 Treatment x Cell-type: P = 0.1621 Treatment x Sex: P = 0.4241 Cell-type x Sex: P = 0.1908 Treatment x Cell-type x Sex: P = 0.4320	Main effect of Treatment: one-sample t-test (two-tailed)	Combined cell-types: Bestatin+Thiorphan: t(17) = 1.560, P = 0.1371 +MERF: t(17) = 1.310, P = 0.2075 +Met-Enk: t(17) = 7.642, P < 0.0001
	E	Three-way ANOVA	D1-MSN: 9 (5F / 4M) D2-MSN: 9 (5F / 4M)	F(2,28) = 5.120 F(1,14) = 1.555 F(1,14) = 0.08171 F(2,28) = 1.088 F(2,28) = 5.614 F(1,14) = 0.1572 F(2,28) = 1.511	Treatment: P = 0.0127 Cell-type: P = 0.2329 Sex: P = 0.7792 Treatment x Cell-type: P = 0.3508 Treatment x Sex: P = 0.0089 Cell-type x Sex: P = 0.6977 Treatment x Cell-type x Sex: P = 0.2382	Main effect of Treatment: one-sample t-test (two-tailed)	Combined cell-types: Bestatin+Thiorphan: t(17) = 1.504, P = 0.1508 +MERF: t(17) = 0.2947, P = 0.7718 +Met-Enk: t(17) = 2.825, P < 0.0117
3-9	B	Two-way ANOVA	Ace-wt/wt: 6 (3F / 3M) Ace-fl/fl: 6 (2F / 4M)	F(1,8) = 4.904 F(1,8) = 0.1624 F(1,8) = 24.42	Interaction: P = 0.0577 Sex: P = 0.6975 Genotype: P = 0.0011	n/a	n/a

Figure		Test	Sample Size	Statistic	P value	Follow-up Test	Post-hoc comparison, statistic, and P value
	C	Two-way ANOVA	Ace-wt/wt: 14 (5F / 9M) Ace-fl/fl: 14 (6F / 8M)	F(1,24) = 1.360 F(1,24) = 2.930 F(1,24) = 21.43	Interaction: P = 0.2550 Sex: P = 0.0999 Genotype: P < 0.0001	n/a	n/a
	D	Two-way ANOVA	Ace-wt/wt: 14 (5F / 9M) Ace-fl/fl: 14 (6F / 8M)	F(1,24) = 2.451 F(1,24) = 0.6176 F(1,24) = 0.6039	Interaction: P = 0.1305 Sex: P = 0.4396 Genotype: P = 0.4447	n/a	n/a
	G	Three-way ANOVA	Ace-wt/wt: 14 (5F / 9M) Ace-fl/fl: 14 (6F / 8M)	F(1,24) = 0.1549 F(1,24) = 0.1374 F(1,24) = 98.31 F(1,24) = 1.943 F(1,24) = 1.394 F(1,24) = 24.77 F(1,24) = 0.9606	Sex: P = 0.6974 Genotype: P = 0.7141 Time: P < 0.0001 Sex x Genotype: P = 0.1761 Sex x Time: P = 0.2493 Genotype x Time: P < 0.0001 Sex x Genotype x Time: P = 0.3368	Genotype x Time interaction: simple effect of Time for each Genotype	ACE-wt/wt - baseline vs captopril+MERF: t(26) = 11.20, P < 0.0001 ACE-fl/fl - baseline vs captopril+MERF: t(26) = 3.588, P = 0.0014
	H	Three-way ANOVA	Ace-wt/wt: 14 (5F / 9M) Ace-fl/fl: 14 (6F / 8M)	F(1,24) = 10.04 F(1,24) = 5.274 F(1,24) = 0.9604 F(1,24) = 2.843 F(1,24) = 0.7891 F(1,24) = 0.6739 F(1,24) = 1.351	Sex: P = 0.0041 Genotype: P = 0.0307 Time: P = 0.3369 Sex x Genotype: P = 0.1047 Sex x Time: P = 0.3832 Genotype x Time: P = 0.4198 Sex x Genotype x Time: P = 0.2565	n/a	n/a
3-10	A	Two-way ANOVA	Captopril+MERF: 8 (3F / 5M) +SDM25N: 9 (5F / 4M) +NOR-BNI: 11 (5F / 6M) +CTAP: 12 (6F / 6M)	F(3,32) = 0.8257 F(1,32) = 0.01262 F(3,32) = 11.66	Interaction: P = 0.4895 Sex: P = 0.9113 Treatment: P < 0.0001	Main effect of Treatment: Fisher's LSD post-hoc test	Captopril + MERF vs. +SDM25N: t(32) = 1.244, P = 0.2227 Captopril + MERF vs. +NOR-BNI: t(32) = 0.3275, P = 0.7454 Captopril + MERF vs. +CTAP: t(32) = 3.725, P = 0.0008 +SDM25N vs. +NOR-BNI: t(32) = 1.021, P = 0.3150 +SDM25N vs. +CTAP: t(32) = 5.311, P = <0.0001 +NOR-BNI vs. +CTAP: t(32) = 4.516, P = <0.0001
	B	Two-way ANOVA	Captopril+MERF: 8 (3F / 5M) +SDM25N: 9 (5F / 4M) +NOR-BNI: 11 (5F / 6M) +CTAP: 12 (6F / 6M)	F(3,32) = 0.9270 F(1,32) = 0.02104 F(3,32) = 0.6327	Interaction: P = 0.4389 Sex: P = 0.8856 Treatment: P = 0.5993	n/a	n/a
	C	Three-way ANOVA	Captopril+MERF: 8 (3F / 5M) +SDM24N: 9 (5F / 4M) +NOR-BNI: 11 (5F / 6M) +CTAP: 12 (6F / 6M)	F(3,32) = 1.532 F(1,32) = 0.06203 F(1,32) = 52.42 F(3,32) = 0.9574 F(3,32) = 10.59 F(1,32) = 0.7796 F(3,32) = 1.284	Treatment: P = 0.2252 Sex: P = 0.8049 Time: P < 0.0001 Treatment x Sex: P = 0.4247 Treatment x Time: P < 0.0001 Sex x Time: P = 0.3839 Treatment x Sex x Time: P = 0.2966	Treatment x Time interaction: simple effect of Time for each Treatment	Captopril+MERF – before vs after: t(36) = 3.619, P = 0.0009 +SDM25N – before vs after: t(36) = 5.358, P < 0.0001 +NOR-BNI – before vs after: t(36) = 5.508, P < 0.0001 +CTAP – before vs after: t(36) = 0.8786, P = 0.3855
	D	Three-way ANOVA	Captopril+MERF: 8 (3F / 5M) +SDM24N: 9 (5F / 4M) +NOR-BNI: 11 (5F / 6M) +CTAP: 12 (6F / 6M)	F(3,32) = 3.505 F(1,32) = 1.522 F(1,32) = 8.733 F(3,32) = 0.1576 F(3,32) = 0.7910 F(1,32) = 0.1255 F(3,32) = 0.7963	Treatment: P = 0.0264 Sex: P = 0.2263 Time: P = 0.0058 Treatment x Sex: P = 0.9240 Treatment x Time: P = 0.5079 Sex x Time: P = 0.7255 Treatment x Sex x Time: P = 0.5050	n/a	n/a

Figure		Test	Sample Size	Statistic	P value	Follow-up Test	Post-hoc comparison, statistic, and P value
3-11	A	Unpaired t-test (two-tailed)	DPDPE: 9 (4F / 5M) DPDPE + SDM25N: 7 (3F / 4M)	t(14) = 4.484	P = 0.0005	n/a	n/a
	B	Unpaired t-test (two-tailed)	U-69593: 6 (5F / 1M) U-69593 + NOR-BNI: 7 (4F / 3M)	t(11) = 4.956	P = 0.0004	n/a	n/a
3-12	B	Unpaired t-test (two-tailed)	Oprm1-wt: 8 (1F / 7M) Oprm1-ko: 8 (3F / 5M)	t(14) = 3.008	P = 0.0094	n/a	n/a
	C	Unpaired t-test (two-tailed)	Oprm1-wt: 8 (1F / 7M) Oprm1-ko: 8 (3F / 5M)	t(14) = 0.7557	P = 0.4624	n/a	n/a
	D	Two-way ANOVA	Oprm1-wt: 8 (1F / 7M) Oprm1-ko: 8 (3F / 5M)	F(1,14) = 9.083 F(1,14) = 6.047 F(1,14) = 1.939	Interaction: P = 0.0093 Time: P = 0.0276 Genotype: P = 0.1855	Treatment x Time interaction: simple effect of Time for each Genotype	Oprm1-wt - before vs after: t(14) = 3.870, P = 0.0017 Oprm1-ko - before vs after: t(14) = 0.3923, P = 0.7008
	E	Three-way ANOVA	Oprm1-wt: 8 (1F / 7M) Oprm1-ko: 8 (3F / 5M)	F(1,12) = 4.903 F(1,12) = 0.2703 F(1,12) = 2.409 F(1,12) = 0.04563 F(1,12) = 2.500 F(1,12) = 0.1261 F(1,12) = 0.9094	Time: P = 0.0469 Genotype: P = 0.6126 Sex: P = 0.1466 Time x Genotype: P = 0.8344 Time x Sex: P = 0.1398 Genotype x Sex: P = 0.7286 Time x Genotype x Sex: P = 0.3591	n/a	n/a
3-13	B	Two-way RM ANOVA (RM: current step)	Current steps: 40, 80, 120, 160 pA aCSF: 12 100 nM MERF: 7 1 uM MERF: 5	F(6,63) = 1.443 F(3,63) = 49.70 F(2,21) = 4.145 F(21,63) = 2.823	Interaction: P = 0.2125 Current step: P < 0.0001 Treatment: P = 0.0304	Main effect of Treatment: Fisher's LSD post-hoc test	aCSF vs 100 nM MERF: t(21) = 1.428, P = 0.1681 aCSF vs 1 uM MERF: t(21) = 2.831, P = 0.0100 100 nM vs 1 uM MERF: t(21) = 1.002, P = 0.3279
	D	One-way ANOVA	Captopril : 3 (2F / 1M) MERF: 5 (2F / 3M) Captopril + MERF: 7 (4F / 3M)	F(2,12) = 4.542	Treatment: P = 0.0340	Fisher's LSD post-hoc test	Captopril vs MERF: t(12) = 0.4366, P = 0.6702 Captopril vs Captopril+MERF: t(12) = 2.525, P = 0.0266 MERF vs Captopril+MERF: t(12) = 2.432, P = 0.0316
	E	Two-way RM ANOVA (RM: current step)	Current steps: 40, 80, 120, 160 pA aCSF: 8 100 nM MERF: 3 1 uM MERF: 5	F (6,39) = 0.2400 F (3,39) = 11.12 F (2,13) = 0.2981 F (13,39) = 2.241	Interaction: P = 0.9605 Current step: P < 0.0001 Treatment: P = 0.7472	n/a	n/a
	F	One-way ANOVA	Captopril : 5 (4F / 1M) MERF: 3 (2F / 1M) Captopril + MERF: 7 (5F / 2M)	F(2,12) = 0.9946	Treatment: P = 0.3984	n/a	n/a

Figure		Test	Sample Size	Statistic	P value	Follow-up Test	Post-hoc comparison, statistic, and P value
4-2		Three-way ANOVA	ACSF and KCl MERF: 7 (4F / 3M) Met-Enk: 7 (4F / 3M) Leu-Enk: 7 (4F / 3M) Sub P: 7 (4F / 3M) Dyn A (1-8): 7 (4F / 3M) Dyn B: 7 (4F / 3M) Ang II: 7 (4F / 3M)	F(6,35) = 9.487 F(1,35) = 24.71 F(1,35) = 0.000573 F(6,35) = 8.161 F(6,35) = 0.02084 F(1,35) = 0.01985 F(6,35) = 0.001955	Peptide: P < 0.0001 Treatment: P < 0.0001 Sex: P = 0.9810 Peptide x Treatment: P <0.0001 Peptide x Sex: P > 0.9999 Treatment x Sex: P = 0.8888 Peptide x Treatment x Sex: P > 0.9999	Peptide x Treatment interaction: simple effect of treatment (aCSF vs KCl) for each peptide	MERF: t(6) = 2.720, P = 0.0346 Met-Enk: t(6) = 3.445, P = 0.0137 Leu-Enk: t(6) = 4.272, P = 0.0053 Sub P: t(6) = 6.419, P = 0.0007 Dyn A (1-8): t(6) = 4.709, P = 0.0033 Dyn B: t(6) = 3.210, P = 0.0184 Ang II: t(6) = 0.1423, P = 0.8915
4-3	A	Two-way RM ANOVA (RM: treatment/region)	6 (4F / 2M)	F(1,5) = 0.02750 F(1,5) = 2.366 F(1,5) = 2.586	Treatment: P = 0.8748 Region: P = 0.1846 Treatment x Region: P = 0.1687	n/a	n/a
	B-E	Three-way RM ANOVA (RM: region)	10 (5F / 5M)	F(3,32) = 7.732 F(1,32) = 19.79 F(1,32) = 0.5026 F(3,32) = 5.375 F(3,32) = 0.4094 F(1,32) = 0.1760 F(3,32) = 0.1603	Peptide: P = 0.0005 Region: P < 0.0001 Sex: P = 0.4835 Peptide x Region: P = 0.0041 Peptide x Sex: P = 0.7473 Region x Sex: P = 0.6776 Peptide x Region x Sex: P = 0.9223	Peptide x Region interaction: simple effect of Region (Dorsal vs Ventral) for each Peptide	MERF: t(9) = 4.087, P = 0.0027 Met-Enk: t(9) = 3.052, P = 0.0138 Leu-Enk: t(9) = 3.520, P = 0.0065 Dyn A (1-8): t(9) = 3.802, P = 0.0042
	F-K	Three-way ANOVA	Penk-WT: 16 (8F, 8M) Penk-KO: 16 (4F, 12M)	F(5,168) = 37.21 F(1,168) = 82.78 F(1,168) = 0.7865 F(5,168) = 36.17 F(5,168) = 0.1902 F(1,168) = 0.00824 F(5,168) = 0.08023	Peptide: P <0.0001 Genotype: P < 0.0001 Sex: P = 0.3764 Peptide x Genotype: P < 0.0001 Peptide x Sex: P = 0.9660 Genotype x Sex: P = 0.9278 Peptide x Genotype x Sex: P = 0.9952	Peptide x Genotype interaction: simple effect of Genotype (WT vs KO) for each Peptide	MERF: t(30) = 9.980, P < 0.0001 Met-Enk: t(30) = 7.349, P < 0.0001 Leu-Enk: t(30) = 7.275, P < 0.0001 Dyn A (1-8): t(30) = 2.276, P = 0.0301 Dyn B: t(30) = 2.962, P = 0.0059 Sub P: t(30) = 1.796, P = 0.0826
4-4	A	Two-way ANOVA	MERF: 14 (8F / 6M) Met-Enk: 14 (8F / 6M) Leu-Enk: 14 (8F / 6M) Sub P: 14 (8F / 6M) Dyn A (1-8): 14 (8F / 6M) Dyn B: 14 (8F / 6M) Ang II: 14 (8F / 6M)	F(6,84) = 0.4018 F(1,84) = 2.150 F(6,84) = 12.59	Interaction: P = 0.8759 Sex: P = 0.1463 Peptide: P < 0.0001	Main effect of Peptide: Fisher's LSD post-hoc test	MERF vs Met-Enk: t(84) = 7.249, P < 0.0001 MERF vs Leu-Enk: t(84) = 7.004, P < 0.0001 MERF vs Sub P: t(84) = 6.725, P < 0.0001 MERF vs Dyn A (1-8): t(84) = 6.109, P < 0.0001 MERF vs Dyn B: t(84) = 5.858, P < 0.0001 MERF vs Ang II: t(84) = 5.963, P < 0.0001
	B	Two-way ANOVA	MERF: 8 (4F / 4M) Met-Enk: 8 (4F / 4M) Leu-Enk: 8 (4F / 4M) Sub P: 8 (4F / 4M) Dyn A (1-8): 8 (4F / 4M) Dyn B: 8 (4F / 4M) Ang II: 8 (4F / 4M)	F(6,42) = 0.1072 F(1,42) = 0.00376 F(6,42) = 4.369	Interaction: P = 0.9952 Sex: P = 0.9514 Peptide: P = 0.0016	Main effect of Peptide: Fisher's LSD post-hoc test	MERF vs Met-Enk: t(42) = 3.941, P = 0.0003 MERF vs Leu-Enk: t(42) = 3.497, P = 0.0011 MERF vs Sub P: t(42) = 3.612, P = 0.0008 MERF vs Dyn A (1-8): t(42) = 3.914, P = 0.0003 MERF vs Dyn B: t(42) = 3.657, P = 0.0007 MERF vs Ang II: t(42) = 4.380, P < 0.0001

Figure		Test	Sample Size	Statistic	P value	Follow-up Test	Post-hoc comparison, statistic, and P value
	C	Two-way ANOVA	MERF: 8 (4F / 4M) Met-Enk: 8 (4F / 4M) Leu-Enk: 8 (4F / 4M) Sub P: 8 (4F / 4M) Dyn A (1-8): 8 (4F / 4M) Dyn B: 8 (4F / 4M) Ang II: 8 (4F / 4M)	F(6,42) = 0.3344 F(6,42) = 3.912 F(1,42) = 0.01546	Interaction: P = 0.9149 Peptide: P = 0.0034 Sex: P = 0.9016	Main effect of Peptide: one-sample t-test (two-tailed)	MERF: t(7) = 1.458, P = 0.1882 Met-Enk: t(7) = 1.127, P = 0.2969 Leu-Enk: t(7) = 4.416, P = 0.0031 Sub P: t(7) = 3.517, P = 0.0098 Dyn A (1-8): t(7) = 2.627, P = 0.0341 Dyn B: t(7) = 2.985, P = 0.0204 Ang II: t(7) = 0.6343, P = 0.5461
	D	Two-way ANOVA	MERF: 8 (4F / 4M) Met-Enk: 8 (4F / 4M) Leu-Enk: 8 (4F / 4M) Sub P: 8 (4F / 4M) Dyn A (1-8): 8 (4F / 4M) Dyn B: 8 (4F / 4M) Ang II: 8 (4F / 4M)	F(6,42) = 0.3529 F(6,42) = 2.704 F(1,42) = 0.1505	Interaction: P = 0.9042 Peptide: P = 0.0260 Sex: P = 0.7000	Main effect of Peptide: one-sample t-test (two-tailed)	MERF: t(7) = 2.422, P = 0.0459 Met-Enk: t(7) = 1.714, P = 0.1302 Leu-Enk: t(7) = 3.018, P = 0.0194 Sub P: t(7) = 3.261, P = 0.0139 Dyn A (1-8): t(7) = 3.573, P = 0.0091 Dyn B: t(7) = 4.411, P = 0.0031 Ang II: t(7) = 1.314, P = 0.2301
4-5	D	Three-way ANOVA	Cre-: 4 (2F / 2M) ChR2: 7 (3F / 4M)	F(3,28) = 6.060 F(1,28) = 16.87 F(1,28) = 0.2238 F(3,28) = 6.378 F(3,28) = 0.03398 F(1,28) = 0.00893 F(3,28) = 0.00358	Peptide: P = 0.0026 Genotype: P = 0.0003 Sex: P = 0.6398 Peptide x Genotype: P = 0.002 Peptide x Sex: P = 0.9914 Genotype x Sex: P = 0.9254 Peptide x Genotype x Sex: P = 0.9997	Peptide x Genotype interaction: simple effect of genotype (Cre- vs ChR2) for each peptide	MERF: t(9) = 1.549, P = 0.1559 Met-Enk: t(9) = 3.251, P = 0.01 Leu-Enk: t(9) = 4.025, P = 0.003 Dyn A (1-8): t(9) = 0.8956, P = 0.3938
	E	Three-way ANOVA	Cre-: 4 (2F / 2M) ChR2: 7 (3F / 4M)	F(3,28) = 3.745 F(1,28) = 13.62 F(1,28) = 9.258 F(3,28) = 2.386 F(3,28) = 1.357 F(1,28) = 4.324 F(3,28) = 0.7704	Peptide: P = 0.0222 Genotype: P = 0.0010 Sex: P = 0.0051 Peptide x Genotype: P = 0.0903 Peptide x Sex: P = 0.2762 Genotype x Sex: P = 0.0469 Peptide x Genotype x Sex: P = 0.5203	Peptide x Genotype interaction: simple effect of genotype (Cre- vs ChR2) for each peptide	MERF: t(9) = 4.307, P = 0.0020 Met-Enk: t(9) = 0.6186, P = 0.5515 Leu-Enk: t(9) = 1.235, P = 0.2481 Dyn A (1-8): t(9) = 0.4531, P = 0.6612
4-6	D	Two-way ANOVA	Captopril (D2-MSN): 8 (5F / 3M) Captopril (D1-MSN): 11 (5F / 6M) Angiotensin I: 11 (7F / 4M) Valsartan: 17 (8F / 9M) Naloxone Chase: 9 (3F / 6M) Naloxone Block: 8 (6M / 2F)	F(5,52) = 1.229 F(1,52) = 0.00005 F(5,52) = 17.61	Interaction: P = 0.3091 Sex: P = 0.9942 Treatment: P < 0.0001	Main effect of Treatment: Fisher's LSD post-hoc test	Captopril (D1) vs Captopril (D2): t(52) = 5.288, P < 0.0001 Captopril (D1) vs Angiotensin I: t(52) = 5.974, P < 0.0001 Captopril (D1) vs Valsartan: t(52) = 7.464, P < 0.0001 Nal Chase vs Nal Block: t(52) = 4.151, P = 0.0001
		One-sample t-test (two-tailed)	Captopril (D2-MSN): 8 Captopril (D1-MSN): 11 Angiotensin I: 11 Valsartan: 17 (8F / 9M) Naloxone Chase: 9 Naloxone Block: 8	t(7) = 1.338 t(10) = 12.93 t(10) = 0.9453 t(16) = 0.5424 t(8) = 5.570 t(7) = 2.027	P = 0.2228 P < 0.0001 P = 0.3668 P = 0.5950 P = 0.0005 P = 0.0822	n/a	n/a

Figure		Test	Sample Size	Statistic	P value	Follow-up Test	Post-hoc comparison, statistic, and P value
	E	Two-way ANOVA	Captopril (D2-MSN): 8 (5F / 3M) Captopril (D1-MSN): 11 (5F / 6M) Angiotensin I: 11 (7F / 4M) Valsartan: 17 (8F / 9M) Naloxone Chase: 9 (3F / 6M) Naloxone Block: 8 (6M / 2F)	F(5,52) = 0.5190 F(1,52) = 0.0044 F(5,52) = 2.458	Interaction: P = 0.7607 Sex: P = 0.9475 Treatment: P = 0.0450	Main effect of Treatment: Fisher's LSD post-hoc test	Captopril (D1) vs Captopril (D2): t(52) = 2.577, P = 0.0128 Captopril (D1) vs Angiotensin I: t(52) = 1.043, P = 0.3019 Captopril (D1) vs Valsartan: t(52) = 2.425, P = 0.0188 Nal Chase vs Nal Block: t(52) = 1.180, P = 0.2432
		One-sample t-test (two-tailed)	Captopril (D2-MSN): 8 Captopril (D1-MSN): 11 Angiotensin I: 11 Valsartan: 17 Naloxone Chase: 9 Naloxone Block: 8	t(7) = 1.926 t(10) = 2.829 t(10) = 1.052 t(16) = 1.343 t(8) = 1.598 t(7) = 0.8039	P = 0.0955 P = 0.0179 P = 0.3174 P = 0.1979 P = 0.1487 P = 0.4479	n/a	n/a
	F	Two-way ANOVA	Captopril (D2-MSN): 8 (5F /3M) Captopril (D1-MSN): 11 (5F / 6M) Angiotensin I: 11 (7F / 4M) Valsartan: 17 (8F / 9M) Naloxone Chase: 9 (3F / 6M) Naloxone Block: 8 (6M / 2F)	F(5,52) = 0.3387 F(1,52) = 0.3229 F(5,52) = 3.231	Interaction: P = 0.8871 Sex: P = 0.5723 Treatment: P = 0.0129	Main effect of Treatment: Fisher's LSD post-hoc test	Captopril (D1) vs Captopril (D2): t(52) = 1.518, P = 0.1350 Captopril (D1) vs Angiotensin I: t(52) = 2.130, P = 0.0379 Captopril (D1) vs Valsartan: t(52) = 3.694, P = 0.0005 Nal Chase vs Nal Block: t(52) = 0.9483, P = 0.3474
		One-sample t-test (two-tailed)	Captopril (D2-MSN): 8 (5F / 3M) Captopril (D1-MSN): 11 (5F / 6M) Angiotensin I: 11 (7F / 4M) Valsartan: 17 (8F / 9M) Naloxone Chase: 9 (3F / 6M) Naloxone Block: 8 (6M / 2F)	t(7) = 0.6328 t(10) = 8.669 t(10) = 0.09110 t(16) = 1.439 t(8) = 3.364 t(7) = 0.7622	P = 0.5470 P < 0.0001 P = 0.9292 P = 0.1693 P = 0.0099 P = 0.4708	n/a	n/a
4-7	C	Two-way ANOVA	12 (4F, 8M) (each cell received captopril followed by MERF)	F(1,20) = 0.0435 F(1,20) = 6.636 F(1,20) = 0.1107	Interaction: P = 0.8367 Treatment: P = 0.018 Sex: P = 0.7428	n/a	n/a
4-9	B	Two-way ANOVA	No LTD: 45 (22F / 23M) Captopril-LTD: 28 (13F / 15M)	F(1,69) = 2.143 F(1,69) = 0.6171 F(1,69) = 96.49	Interaction: P = 0.1477 Sex: P = 0.4348 LTD: P < 0.0001	n/a	n/a
	C	Two-way ANOVA	No LTD: 45 (22F / 23M) Captopril-LTD: 28 (13F / 15M)	F(1,69) = 0.00887 F(1,69) = 0.01365 F(1,69) = 9.070	Interaction: P = 0.9252 Sex: P = 0.9073 LTD: P = 0.0036	n/a	n/a
	D	Two-way ANOVA	No LTD: 45 (22F / 23M) Captopril-LTD: 28 (13F / 15M)	F(1,69) = 0.01065 F(1,69) = 0.02541 F(1,69) = 14.84	Interaction: P = 0.9181 Sex: P = 0.8738 LTD: P = 0.0003	n/a	n/a
4-10	B	One-sample t-test (two-tailed)	12 (6F / 6M)	t(11) = 26.97	P < 0.0001	n/a	n/a
	C	One-sample t-test (two-tailed)	12 (6F / 6M)	t(11) = 5.593	P = 0.0002	n/a	n/a

Figure		Test	Sample Size	Statistic	P value	Follow-up Test	Post-hoc comparison, statistic, and P value
	D	One-sample t-test (two-tailed)	12 (6F / 6M)	t(11) = 0.6882	P = 0.5056	n/a	n/a
4-11	B	Two-way ANOVA	Oprm1-wt: 8 (5F / 3M) Oprm1-ko: 9 (5F / 4M)	F(1,13) = 0.8818 F(1,13) = 4.814 F(1,13) = 30.21	Interaction: P = 0.3648 Sex: P = 0.0470 Genotype: P = 0.0001	n/a	n/a
4-12	I	One-sample t-test	mice: 6 (4F / 1M)	t(5) = 4.368	P = 0.0072	n/a	n/a
4-13	B	Three-way ANOVA	Vehicle+Fentanyl: 11 (6F / 5M) Captopril+Fentanyl: 11 (5F / 6M)	F(1,18) = 1.694 F(1,18) = 0.7843 F(1,18) = 50.23 F(1,18) = 1.601 F(1,18) = 0.2879 F(1,18) = 7.374 F(1,18) = 0.00138	Sex: P=0.2094 Treatment: P=0.3875 Time: P<0.0001 Sex x Treatment: P=0.2219 Sex x Time: P=0.5982 Treatment x Time: P=0.0142 Sex x Treatment x Time: P=0.9707	Treatment x Time interaction: simple effect tests	Vehicle+Fentanyl - baseline vs test: t(20) = 7.240, P < 0.0001 Captopril+Fentanyl - baseline vs test: t(20) = 3.280, P = 0.0037 Baseline - Vehicle+Fentanyl vs Captopril+Fentanyl: t(40) = 0.4091, P = 0.6846 Test - Vehicle+Fentanyl vs Captopril+Fentanyl: t(40) = 2.148, P = 0.0379
	C	Two-way ANOVA	Vehicle+Fentanyl: 11 (6F / 5M) Captopril+Fentanyl: 11 (5F / 6M)	F(1,18) = 0.2182 F(1,18) = 0.3772 F(1,18) = 4.823	Interaction: P = 0.6460 Sex: P = 0.5468 Treatment: P = 0.0414	n/a	n/a
4-15	B	Three-way ANOVA	Vehicle: 11 (5F / 6M) Captopril: 11 (5F / 6M)	F(1,18) = 0.000397 F(1,18) = 0.1788 F(1,18) = 2.717 F(1,18) = 0.1977 F(1,18) = 4.403 F(1,18) = 0.1525 F(1 18) = 0.05996	Time: P = 0.9843 Treatment: P = 0.6774 Sex: P = 0.1167 Time x Treatment: P = 0.6619 Time x Sex: P=0.0502 Treatment x Sex: P = 0.7008 Time x Treatment x Sex: P = 0.8093	n/a	n/a
	C	Two-way ANOVA	Vehicle: 11 (5F / 6M) Captopril: 11 (5F / 6M)	F(1,18) = 0.0060 F(1,18) = 4.008 F(1,18) = 0.4069	Interaction: P = 0.9388 Sex: P = 0.0606 Treatment: P = 0.5316	n/a	n/a
4-16	A	Four-way ANOVA	Vehicle + Fentanyl: 10 (5F / 5M) Captopril + Fentanyl: 9 (3F / 6M)	F(1,12) = 1.820 F(1,12) = 0.471 F(1,12) = 0.096 F(1,12) = 8.874 F(1,12) = 7.438 F(1,12) = 0.214 F(1,12) = 0.394 F(2,24) = 0.045 F(2,24) = 1.708 F(2,24) = 0.113 F(2,24) = 0.390 F(2,24) = 0.230 F(2,24) = 1.704 F(2,24) = 0.134 F(2,24) = 0.054	Sex: P = 0.202 Treatment: P = 0.506 Sex x Treatment: P = 0.762 Time: P = 0.012 Time x Sex: P = 0.018 Time x Treatment: P = 0.652 Time x Sex x Treatment: P = 0.542 Day: P = 0.956 Day x Sex: P = 0.203 Day x Treatment: P = 0.894 Day x Sex x Treatment: P = 0.681 Time x Day: P = 0.796 Time x Day x Sex: P = 0.203 Time x Day x Treatment: P = 0.875 Time x Day x Sex x Treatment: P = 0.948	n/a	n/a

Figure		Test	Sample Size	Statistic	P value	Follow-up Test	Post-hoc comparison, statistic, and P value
	B	Three-way ANOVA	Vehicle + Fentanyl: 10 (5F / 5M) Captopril + Fentanyl: 9 (3F / 6M)	F(1,15) = 13.61 F(1,15) = 0.1462 F(1,15) = 1.790 F(1,15) = 0.3829 F(1,15) = 2.936 F(1,15) = 0.0386 F(1,15) = 5.136	Time: P = 0.0022 Treatment: P = 0.7075 Sex: P = 0.2008 Time x Treatment: P = 0.5453 Time x Sex: P = 0.1072 Treatment x Sex: P = 0.8468 Time x Treatment x Sex: P = 0.0387	n/a	n/a
	C	Four-way ANOVA	Vehicle: 10 (4F / 6M) Captopril: 10 (4F / 6M	F(1,16) = 0.754 F(1,16) = 0.023 F(1,16) = 0.076 F(1,16) = 0.615 F(1,16) = 0.346 F(1,16) = 0.021 F(1,16) = 0.062 F(2,32) = 0.763 F(2,32) = 0.402 F(2,32) = 1.807 F(2,32) = 0.313 F(2,32) = 0.832 F(2,32) = 1.029 F(2,32) = 0.349 F(2,32) = 0.847	Sex: P = 0.398 Treatment: P = 0.881 Sex x Treatment: P = 0.787 Time: P = 0.444 Time x Sex: P = 0.564 Time x Treatment: P = 0.887 Time x Sex x Treatment: P = 0.807 Day: P = 0.475 Day x Sex: P = 0.672 Day x Treatment: P = 0.181 Day x Sex x Treatment: P = 0.733 Time x Day: P = 0.445 Time x Day x Sex: P = 0.369 Time x Day x Treatment: P = 0.708 Time x Day x Sex x Treatment: P = 0.438	n/a	n/a
	D	Three-way ANOVA	Vehicle: 10 (4F / 6M) Captopril: 10 (4F / 6M	F(1,16) = 47.49 F(1,16) = 0.0687 F(1,16) = 1.410 F(1,16) = 0.7024 F(1,16) = 0.0419 F(1,16) = 0.1233 F(1,16) = 2.314	Time: P < 0.0001 Treatment: P = 0.7965 Sex: P = 0.2524 Time x Treatment: P = 0.4143 Time x Sex: P = 0.8404 Treatment x Sex: P = 0.7300 Time x Treatment x Sex: P=0.1477	n/a	n/a
4-17	A	Two-way ANOVA	Vehicle: 18 (10F / 8M) Captopril: 18 (10F / 8M)	F(1,32) = 0.1412 F(1,32) = 11.57 F(1,32) = 19.06	Interaction: P = 0.7096 Sex: P = 0.0018 Treatment: P = 0.0001	n/a	n/a
	B	Two-way ANOVA	Vehicle: 18 (10F / 8M) Captopril: 18 (10F / 8M)	F(1,32) = 0.3130 F(1,32) = 1.803 F(1,32) = 8.960	Interaction: P = 0.5798 Sex: P = 0.1888 Treatment: P = 0.0053	n/a	n/a
	C	Two-way ANOVA	Vehicle: 18 (10F / 8M) Captopril: 18 (10F / 8M)	F(1,32) = 1.265 F(1,32) = 5.529 F(1,32) = 10.07	Interaction: P = 0.2691 Sex: P = 0.0250 Treatment: P = 0.0033	n/a	n/a

Figure	Test	Sample Size	Statistic	P value	Follow-up Test	Post-hoc comparison, statistic, and P value
D	Two-way ANOVA	Vehicle: 18 (10F / 8M) Captopril: 18 (10F / 8M)	F(1,32) = 2.403 F(1,32) = 24.93 F(1,32) = 17.49	Interaction: P = 0.1309 Sex: P < 0.0001 Treatment: P = 0.0002	n/a	n/a
E	Two-way ANOVA	Vehicle: 18 (10F / 8M) Captopril: 18 (10F / 8M)	F(1,32) = 0.2750 F(1,32) = 0.1486 F(1,32) =2.610	Interaction: P = 0.6036 Sex: P = 0.7025 Treatment: P = 0.1160	n/a	n/a